Title

In vitro generation of antigen-specific, Class I MHC-null, cytotoxic T cells for Immunotherapy

Author

Chang, Patrick C

Publication Date

2022

Peer reviewed|Thesis/dissertation

UNIVERSITY OF CALIFORNIA

Los Angeles

In vitro generation of antigen-specific, Class I MHC-null, cytotoxic T cells for Immunotherapy

A dissertation submitted in partial satisfaction of the requirements for the degree

Doctor of Philosophy in Molecular Biology

by

Patrick C Chang

2022

ABSTRACT OF THE DISSERTATION

In vitro generation of antigen-specific, Class I MHC-null, cytotoxic T cells for Immunotherapy

by

Patrick C Chang

Doctor of Philosophy in Molecular Biology

University of California, Los Angeles

Professor Gay M. Crooks, Chair

While T cell-based immunotherapies using cells expressing antigen-specific receptors **(CARs or TCRs)** have produced promising clinical responses, current approaches are limited to autologous T cells due to the risk of graft-versus-host disease **(GvHD)** from allogeneic T cells through endogenous TCR expression and rejection through MHC incompatibility. Human pluripotent stem cells **(PSCs)** have the potential to address these challenges as they are an infinitely self-renewing source of hematopoietic cells, and are amenable to gene editing approaches to address alloreactivity; however, the two main barriers to using allogeneic T cells represent two critical components required for inducing positive selection in developing T cells. Mature, naïve T cell differentiation is dependent on signaling through TCR-MHC interactions to induce positive selection, and removal of either would effectively block this process. This dissertation

explores gene editing and T cell differentiation strategies that can circumvent the basic requirements for inducing positive selection to generate antigen-specific, Class I MHC-null, cytotoxic T cells using the *in vitro* “Artificial Thymic Organoid” system developed in our lab.

Chapter 2 focuses on preventing alloreactive TCRs development by ablating the recombination activating genes **(*RAG1*** and ***RAG2*)**, generating *RAG1*$^{-/-}$*RAG2*$^{-/-}$ double knockout **(DKO)** PSCs, responsible for endogenous TCR recombination. To support positive selection, edited PSCs were transduced to express a fully rearranged, Class I MHC-restricted 1G4 TCR **(DKO+TCR)**, and it was determined that positive selection hinged on endogenous expression of the 1G4 TCR’s cognate MHC.

Chapter 3 centers around artificially inducing positive selection in the absence of both endogenous TCRs and MHCs. To prevent T cell rejection, DKO+TCR PSCs were edited to knockout beta-2-microglobulin **(*B2M*)**, a critical subunit of Class I MHC heterodimers, to generate *RAG1*$^{-/-}$*RAG2*$^{-/-}$*B2M*$^{-/-}$ triple knockout PSCs with the 1G4 TCR **(TKO+TCR)**. In order to induce positive selection of antigen-specific, Class I MHC-null, mature, naïve T cells from TKO+TCR PSCs, the stromal component of the ATO system was engineered to provide the 1G4 TCR’s cognate MHC. Functional and transcriptional validation of TKO+TCR engineered T cells revealed a similar phenotype and cytokine release profile to unedited T cells, complete restriction of endogenous TCRs, and improved antigen-specific cytotoxicity *in vivo.*

The dissertation of Patrick C Chang is approved.

Donald Barry Kohn

Yvonne Chen

Lili Yang

April Pyle

Gay M. Crooks, Committee Chair

University of California, Los Angeles

2022

DEDICATION

To all my friends, family, and mentors who have supported me throughout this long and arduous journey called life (and graduate school)

TABLE OF CONTENTS

LIST OF FIGURES

Chapter 3 ***(Continued)***

List of Tables

Chapter 2

Chapter 3

ACKNOWLEDGEMENTS

First and foremost, I would like to acknowledge my mentor, Dr. Gay M. Crooks – I could not have reached this point without the constant guidance, support, and wisdom she has imparted to me along the way. As I take a step back to introspect about my time in her lab, I cannot stress how lucky I feel to have been given the opportunity to work in the wonderful, collaborative training environment that she has nurtured and curated over the years. I am especially grateful for all of the creativity she has inspired in me, and others, by instilling us with the freedom to voice and develop our ideas, and, most importantly, the resources to pursue them. Despite the constant barrage of administrative responsibilities and grant deadlines looming over the horizon, Dr. Crooks has always, effortlessly, found the time to ensure that each and every one of us received the proper care, attention, and insightful nudges to foster our development as researchers and inspire intellectual curiosity. As I am transitioning out of her lab, I will miss our meetings the most, where it was always a joy to discuss science and riff on about new ideas.

Additionally, I would like to thank the members of my doctoral, Drs. Donald Barry Kohn, Lili Yang, Yvonne Chen, and April Pyle for their constant support, expertise, and collective wisdom. While there were many bumps along the road, my project would not be where it is without all of your help along the way.

I would like to specially thank Drs. Donald Barry Kohn and Lili Yang for helping me build my foundation in gene editing and immunology, respectively, through my rotations with in their research groups. Additionally, I would like to acknowledge Drs. April Pyle, and Caroline Kuo, and Roger Hollis for all of their mentorship and guidance in all aspects related to gene editing.

As for the members of the Crooks Lab, I would also like to first acknowledge some of my mentors that have helped me navigate my journey here at UCLA. First, I would like to thank the senior researchers in the lab, Drs. Christopher Seet and Amélie Montel-Hagen, for their vast, combined wealth of immunological and general scientific knowledge. This project would not have been possible without their efforts to develop the ATO system. Working with the two of them over the years has been truly inspiring and they have been wonderful role models inside and outside of the research setting. While they're always on the run (literally, sometimes), they always find some time to stop for an enthusiastic chat about science and general happenings in the world.

I would also like to additional members of the Crooks Lab that have made this process fun and unforgettable. I would like to mention one member specifically, Judy Zhu, for all of her generosity, moral support, and insightful conversations we have had over the years. Judy always went above and beyond and was readily available to help with anything in and outside of the lab. I am indebted to Dr. Steven Tsai for all of the generous help and advice he has provided me. While clinic has kept him away from us, Steve is always one text or call away for moral support, and hot tea. Additionally, I would like to acknowledge Dr. Stephanie de Barros for of the wonderful conversations and help she has given me throughout my time in the Crooks Lab – especially all the help in the form of wonderful snacks from TJ's that she discovered, curated, and shared with me. Additionally, I would like to acknowledge Dr. Gloria Yiu for all of the cheerful conversations that could always brighten the mood, especially at the beginning of the COVID pandemic, and for bringing a little piece of home with her when she joined the lab – there's never a dull moment when we reminisce about Saratoga.

During my time in the Crooks Lab, I have had two mentees, and each of them went above and beyond all expectations. Chloe Towns was instrumental in getting this project off of the ground, and always a joy to mentor. I hope you achieve everything you have set out to accomplish, you certainly have the discipline and dedication to do so. Also, I would like to acknowledge Alex Sang Pil Yoo, who has been fun, to say the least, to mentor over the course of his PhD. In the short amount of time he has been in the lab, I have been consistently impressed by his development as a scientist and graduate student – I hope you realize that everything will be fine in the end, and I'm sure you will have a productive research career.

I would also like to mention the other members of the lab who have provided experimental and technical crucial to completing the work in this dissertation: Alexandre Zampieri, Xuegang Yuan, and Shawn Lopez; and all of the current and past members of the Crooks Lab who have been amazing to work, laugh, and eat with: Edward He, Suwen Li, Claire Engstrom, Julia Gensheimer, Rebecca Chan, and Jessica Lagosh.

Flow cytometry has been the bread and butter of my research, and much of this work would not have been possible without the generous help and support from the BSCRC Flow Cytometry core staff: Jessica Scholes, Felicia Codrea, and Jeff Calimlim.

I would also like to thank my funding sources: California Institute of Regenerative Medicine (CIRM), the Ruth L. Kirschstein National Research Service Award funded through the National Cancer Institute at the National Institutes of Health, and Pluto Immunotherapeutics, Inc.

To my family – I wouldn't be who I am today without all of you. Certainly, I wouldn't be here at this point without all of your incredible help and constant support. Thank you

for supporting me every step of the way along the way – even though I might not have deserved it, and sacrificing so much so that I could have the opportunity to pursue my dreams. I know you will always be there for me when I need it most. Most importantly, thank you for always helping me realize things will always be okay in the end – and whatever will be, will be.

To my friends – you are my family away from home. Thank you all for being my support system throughout this long and arduous journey, and all of the good times and fond memories we have shared. In the best, and even the worst, of times, I know I can always count on you all to brighten the day (and nights), and help me take a step back to recharge and refuel for the next challenging day.

Last, but not least, I would like to mention my mentors from UC San Diego who helped guide me down this path. I would like to thank Dr. Catriona Helen Macleod Jamieson, who assumed an enormous risk by taking an untrained, inexperienced student in the last year of his undergraduate studies, and Dr. Janine Low-Marchelli for all of her patient guidance and mentorship. I cannot begin to express the immense gratitude I have for both of these wonderful and inspiring scientists who gave me the chance to realize my dreams.

VITA

EDUCATION

University of California, Los Angeles — Los Angeles, CA
PhD Molecular Biology Interdepartmental Program — June 2022 (Expected)
Home Area: Cell and Developmental Biology, GPA 3.64/4.00
Principal Investigator: Dr. Gay Crooks, MBBS

University of California, San Diego — La Jolla, CA
MS Biological Sciences — August 2015
Principal Investigator: Dr. Catriona Jamieson, MD PhD
BS Physiology and Neuroscience — December 2013
BS Management Science *(Honors with Distinction)* — December 2013

HONORS AND AWARDS

2022	UCLA Jonsson Comprehensive Cancer Award, Poster Competition Award
2019-2022	NIH/NCI F31 Ruth L. Kirschstein National Research Service Award (F31CA239555)
2016	NSF Graduate Research Fellowship Program, Honorable Mention
2014	UCSD 6th Annual Biological Sciences Research Symposium, Best Poster
2013	UCSD Departmental Honors with Distinction, Economics
2011-2013	UCSD Revelle College Provost Honors

RESEARCH EXPERIENCE

Graduate Student Researcher — Los Angeles, CA
Cell and Developmental Biology, UCLA — June 2016 – June 2022
Principal Investigator: Dr. Gay Crooks, MBBS
Thesis: Engineering stem cell-derived T cells for Immunotherapy

- Engineering pluripotent stem cells using CRISPR/Cas9 to generate **antigen-restricted T cells** in the Artificial Thymic Organoid (ATO) for the development of an **off-the-shelf approach** to **adoptive cell transfer immunotherapy**
- Delineating the mechanism of **positive selection in human thymocytes** in the ATO system to **generate conventional lymphoid effectors** for immunotherapy applications
- **Functional validation** of engineered T cells through *in vitro* and *in vivo* assays, including **transcriptomic profiling** and **TCR repertoire analysis** through **single cell sequencing**
- Collaborate with researchers from the **Donald Kohn laboratory**, designed T cell differentiation assays to validate **lineage-specificity** of **novel gene therapy constructs** for treating rare pediatric lymphoid deficiencies
- Transcriptomic and epigenomic mapping of the distinct developmental stages during T cell maturation from patient and *in vitro*-derived samples
- Developing platform tool technology to identify **SARS-CoV2** T cell epitopes for vaccine development and specific T cell receptors for adoptive T cell immunotherapy

Graduate Student Researcher — La Jolla, CA
Department of Medicine, UCSD — September 2013 – August 2015
Principal Investigator: Dr. Catriona Jamieson, MD PhD
Thesis: The role of CTGF in chronic myeloid leukemia stem cell maintenance

- Investigated the role of an extracellular matrix protein in chronic myeloid leukemia (CML) disease progression, identifying a novel mechanism for increased survival and self-renewal

PUBLICATIONS

Chang PC, Zampieri A, Yuan XG, Yoo SP, Zhu YH, Towns CT, Tsai S, Montel-Hagen A, Seet CS, Crooks GM. "In vitro differentiation of antigen-specific, class I MHC-null cytotoxic T cells for Immunotherapy." 2022. (*Manuscript in preparation)*

Sun V, Sharpley M, Kaczor-Urbanowicz KE, **Chang PC**, Montel-Hagen A, Lopez S, Zampieri A, Zhu YH, C. De Barros S, Parekh C, Casero D, Banerje U, Crooks GM. "The metabolic landscape of thymic T cell development in vivo and in vitro." **Frontiers in Immunology,** 2021 July 28. (PMCID: PMC8355594)

Montel-Hagen A, Seet CS, Li S, Chick BY, **Chang PC**, Zhu YH, He C, Lopez S, Crooks GM. "Organoid-induced differentiation of conventional T cells from human pluripotent stem cells." ***Cell Stem Cell,*** 2019 March 7; 24(3):376-389. PMID: 30661959 (PMCID: PMC6687310)

ABSTRACTS

Chang PC, Zampieri A, Yuan XG, Yoo SP, Zhu YH, Towns CT, Tsai S, Montel-Hagen A, Seet CS, Crooks GM. "Engineering the in vitro organoid microenvironment for positive selection of human pluripotent stem cell-derived, class I MHC-null, antigen specific T cells". International Society for Stem Cell Research Annual Meeting (2022), San Francisco, CA.

- Selected for poster presentation, late breaking abstract*,* recipient of BSCRC travel award

Chang PC, Zampieri A, Yuan XG, Yoo SP, Zhu YH, Towns CT, Tsai S, Montel-Hagen A, Seet CS, Crooks GM. "Engineering the in vitro organoid microenvironment for positive selection of human pluripotent stem cell-derived, class I MHC-null, antigen specific T cells". UCLA Jonsson Comprehensive Cancer Center (JCCC) Annual Retreat (2022), Los Angeles, CA

- Recipient of poster competition award

Chang PC, Tsai S, Zhu YH, Towns C, Lopez S, Seet CS, Montel-Hagen A, Crooks GM. *"Towards engineered pluripotent stem cell-derived non-allogeneic, antigen-specific T cells".* European Society of Gene and Cell Therapy 27th Annual Congress (2019), Barcelona, Spain.

- Selected for poster presentation, late breaking abstract*.*

Chang PC, Low-Marchelli JM, Shahbandi A, Goff DJ, Jamieson CHM. *"Connective tissue Growth Factor Induces Anti-Apoptotic Factors in Chronic Myeloid Leukemia Stem Cells".* 56th American Society of Hematology Annual Meeting and Exposition (2014), San Francisco, CA.

- Selected for poster presentation, late breaking abstract*.*

Chang PC, Low-Marchelli JM, Shahbandi A, Goff DJ, Jamieson CHM. *"The Role of Extracellular Matrix Protein CTGF in Disease Progression of Blast Crisis Chronic Myelogenous Leukemia".* UCSD 6th Annual Biological Sciences Student Research Showcase (2014), La Jolla, CA.

- Recipient of Best Masters research award.

CHAPTER 1

Introduction

1.1 Human T cell lineage commitment in the thymus

T cells are critical components of the adaptive immune system that circulate and patrol the body, mobilizing in response to novel peptides presented by human major histocompatibility complex **(MHC)** proteins expressed by cells during viral infection or tumors with dysregulated gene transcription. While T cells can normally be found circulating in the hematopoietic system, their origins lie within the thymus, where they are differentiated from hematopoietic stem and progenitor cells **(HSPCs)** after migrating from their niches, most notably the bone marrow in adults.

Early T cell differentiation in the thymus begins when HSPCs encounter a microenvironment rich in Notch ligands, provided by cortical thymic epithelial cells **(cTECs)**, and interleukin-7 **(IL-7)** that activate transcriptional machinery and ultimately enforce T-lineage commitment[1–6]. While cTECs provide a variety of Notch ligands, studies in both human and mice have suggested that NOTCH1 activation by delta-like ligand 4 **(DLL4)** plays a crucial role in initiating T-lineage programs[6–8]. Upon engagement of the T-lineage committed pathway, HSPCs become T-lineage committed progenitors **(pro-T)** as they begin to upregulate the T cell associated marker, CD7, in addition to CD34[3].

After lineage specification, pro-T cells begin the complex transcriptionally and spatiotemporally regulated process of T cell differentiation as they transit through the cortex of the thymus. The beginning of this process is marked by the loss of surface CD34 expression, generating $CD34^{-}CD8^{-}CD4^{-}$ double negative **(DN)** precursors, and then

quickly followed by the upregulation of surface CD4, resulting in $CD34^{-}CD8^{-}CD4^{+}$ immature single positive CD4 precursors **(ISP4) (Figure 1.1)**[5,9]. During this transitional step, T cell precursors initiate the V(D)J recombination process, where the recombination activating genes 1 and 2 **(*RAG1*** and ***RAG2*)** begin to express and rearrange germline TCR Vβ loci for the generation of the diverse repertoire that is observed in the adaptive immune system[5,9,10].

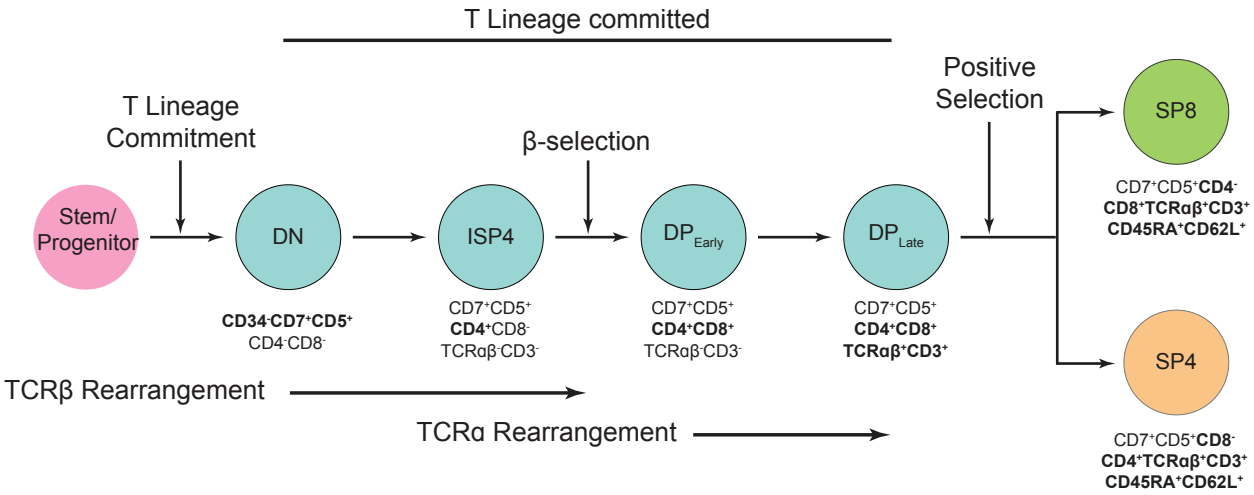

Figure 1.1 Human T cell Development
Key precursor stages are show with their surface markers with the stages and the approximate selection checkpoints shown. Abbreviations: “Double negative” **(DN)**, “Immature single positive CD4” **(ISP4)**, “Double positive” **(DP)**, “Mature, naïve single positive CD8” **(SP8)**, “Mature, naïve single positive CD4” **(SP4)**.

1.2 Germline TCR rearrangement in human T cell development

In cells that have not undergone T-lineage commitment, germline TCR loci are non-productive with a sequential array of variable **(V)**, diversity **(D)**, and joining **(J)** gene segments that prevent expression of functional TCR genes. The process by which mature T cells develop their diverse repertoire of productive TCRs is V(D)J recombination, which is facilitated through tight transcriptional regulation of the recombination activating genes 1 and 2 **(*RAG1*** and ***RAG2)*** genes in T-lineage committed cells[2,10].

The concerted process of V(D)J recombination begins with high expression of *RAG1* and *RAG2* during the early stages of lymphocyte development in order to prevent the process from occurring in other cell types. After *RAG1* and *RAG2* upregulation, they begin the V(D)J recombination process by detecting and binding conserved sequences found within the germline TCR loci, known as recombination signal sites **(RSSs)**, that flank each V, D, and J gene segment[10]. The resulting complex is able to remove large segments of V, D, and J genes by generating knicks in genomic DNA at these RSSs that result in double stranded breaks **(DSBs)**, which are subsequently repaired through non-homologous end joining **(NHEJ)** repair.

In pro-T cells, this process begins with D-to-J recombination and then followed by V-to-DJ recombination[5,10]. Through this process, the germline TCR loci undergo random recombination events to remove the extraneous V, D, J gene segments and that generate fully rearranged TCRs that are used to signal progenitor T **(pro-T)** cells to survive and differentiate further. Failure to generate a functional, rearranged TCR prevents signal transduction, resulting in further recombination or “death by neglect” where pro-T cells undergo apoptosis.

As this process is stochastic, V(D)J recombination is crucial for generating the diverse repertoires of randomly rearranged TCR loci that convey the broad response to foreign antigens by the adaptive immune system. Expression of functional *RAG1* and *RAG2* are essential for V(D)J recombination to occur in pro-T cells. The genes encoding *RAG1* and *RAG2* are located within a ~30KB sequence on chromosome 11 with their coding sequences found in one coding exon, largely unaffected by post-transcriptional splicing[11]. Studies have shown that mutations in either *RAG1* and *RAG2* that inhibit function led to significant reductions in functional TCR diversity altered repertoires, and even complete losses in mature T cells in severe cases. *RAG1* and *RAG2* knockouts have been well characterized in mice, resulting in complete losses of mature T lymphocytes and immunodeficiency[12,13]. While loss of function in *RAG* genes have functional benefits for disease modeling and therapeutic development, they are particularly deleterious in the clinical setting. Previous studies have shown that patients with severe combined immunodeficiency **(SCID)** and Omenn Syndrome **(OS)** exhibit a complete loss of mature T cells as a result of deletion or frameshift mutations in either *RAG1* or *RAG2*[10,14,15]. Together, these studies demonstrate the functional dependence of V(D)J recombination on both *RAG1* and *RAG2* for generating robust adaptive immune responses.

1.3 Positive selection of DP T cell precursors

TCR Vβ chains that have undergone productive rearrangement are expressed on the surface of developing T cells and complex with the invariant pre-TCRα, which is exclusively expressed during T cell development, and CD3 chains to form the pre-TCR complex for β-selection[16,17]. Signal transduction through the pre-TCR complex initiates β-selection, indicating to ISP4 T precursors that functional TCR Vβ rearrangement has occurred, licensing them to proceed through this checkpoint. Additionally, ISP4 progression through β-selection enforces allelic exclusion at the TCR Vβ locus, preventing additional recombination, and signals them to proliferate, survive, and differentiate to the $CD8^+CD4^+TCR\alpha\beta^-CD3^-$ early double positive **(DP_{Early})** stage of T cell development **(Figure 1.1)**[10,16–18].

At this stage of development, DP_{Early} precursors begin the process of endogenous TCR Vα rearrangement. Similar to TCR Vβ rearrangement, productive TCR Vα rearrangement in DP_{Early} cells is indicated by signaling through surface expression and signal transduction to the mature TCRαβ complex, which forms a pentameric complex with CD3 chains. After productive rearrangement of the TCR Vα locus, DP_{Early} T cells have progressed to the $CD8^+CD4^+TCR\alpha\beta^+CD3^+$ late double positive **(DP_{Late})** precursor stage, priming them for the next stage of development: positive selection.

Positive selection is the process through which DP_{Late} precursor T cells are signaled to survive and differentiate into mature, naïve T cells of either the $CD8^+$ or $CD4^+$ single positive lineages[19]. DP_{Late} precursors that have successfully rearranged both TCR Vα and Vβ chains interact with peptide-MHCs **(pMHCs)** presented by accessory cells in the thymus, which could include TECs or other antigen presenting cells. Low affinity,

“weak”, interactions between a functional TCRαβ and CD3 complex on DP_{Late} precursors and pMHCs signal them to survive and differentiate to the mature, naïve, single positive stage of T cell development[19,20]. Depending on the recognition of pMHCs presented by either Class I or Class II MHC, DP_{Late} precursors are signaled to either mature, naïve, single positive CD8 **(SP8)** or CD4 **(SP4)** T cells, respectively.

TCRs that produce high affinity, “strong”, interactions with pMHCs are recognized as self-reactive and are either eliminated in a process called “clonal deletion”, which prevents the development of alloreactive TCRs, or diverted towards intraepithelial **(IEL)** or regulatory **(T_{reg})** T cell lineages[19,21,22]. Alternatively, DP_{Late} precursors that fail to generate functional TCRs will be unable to interact with pMHCs and fated to undergo apoptosis through “death by neglect”.

1.4 *In vitro* generation of stem cell-derived human T cells

Early attempts to model T cell differentiation *in vitro* included fetal thymic organ cultures **(FTOCs)** and reaggregated thymic organ cultures **(RTOCs)**, which both required the use of primary tissues acquired from mice. FTOCs were generated with thymic fragments depleted of T cells from fetal mice seeded with HSPCs[23], while RTOCs utilized primary mouse thymic stroma and HSPCs[24,25]. While both methods were capable of generating mature T cells, these methods were limited by low efficiency, high variability, and the requirement for primary samples from large numbers of mice.

Following these attempts, it was demonstrated that the mouse bone marrow stromal cell line OP9, transduced with Notch ligand **(DLL1 or DLL4)** could be substituted for primary mouse thymic tissues in the presence of IL-7 and FLT3 ligand **(FLT3L)** in a 2D, monolayer culture system[26–28]. While the OP9 system supported T cell commitment from HSPCs, generation of DP precursors was inefficient and inconsistent. Consequently, the OP9 system generates limited amounts of DP_{Late} precursors that express surface TCRαβ and CD3.

Using the OP9 method, generation of mature, naïve, single positive T cells primarily depends on activation or agonist selection of DP precursors, most notably through anti-CD3/CD28 stimulation, which bypasses the normal requirement of TCR-pMHC interactions for positive selection. Attempts have been made to bypass this block in differentiation such as introducing a fully rearranged TCR through lentiviral transduction of HSPC[29], which increased the efficiency of DP precursor generation; however, despite co-expression of surface TCRαβ and CD3, spontaneous positive selection of DP T cell precursors did not occur. Generation of mature, naïve, single positive T cells was still

dependent on activation or agonist selection of DP T cell precursors, either through anti-CD3/CD28 stimulation or stimulation with an exogenous TCR-specific peptide.

More recently, cell-free derivative culture systems have been developed, which utilize synthetic beads that present DLL4 and/or additional factors to induce T cell development from both HSPC and pluripotent stem cell **(PSC)** inputs[30]. It was demonstrated that stromal-free systems were capable of inducing T-lineage specification, which is more amenable for good manufacturing practices **(GMP)** in therapeutic T cell generation; however, spontaneous positive selection of mature, naïve T cells remained ever elusive, and positive election of DP T cell precursors was still dependent on agonist or activation induced maturation. Collectively, these observations from 2D OP9 and bead-based systems indicate that other factors may be required to spontaneously induce positive selection, especially through stochastic TCR-pMHC interactions.

1.5 The Artificial Thymic Organoid system

More recently, members from our group developed a novel 3D *in vitro*, serum-free "Artificial Thymic Organoid" **(ATO)** system that induces highly efficient and reproducible production of mature naïve T cells from HSPCs ($CD34^+CD3^-$ or $CD34^+CD38^-Lin^-$) purified from multiple sources, including cord blood, bone marrow, and mobilized peripheral blood[31]. In this method, purified HSPCs are aggregated with the murine bone marrow stromal cell line MS5 transduced to express human Notch ligands DLL1 or DLL4, creating 3D cell pellets on filters, which create an air-fluid interface **(Figure 1.2A)**. The medium surrounding the filters consists of RPMI with B27 supplement **(RB27)**, ascorbic acid, rhIL-7, and rhFLT3L (FLT3 ligand) **(Figure 1.2B)**. Over the course of 10-12 weeks in the ATO, HSPCs undergo orderly T-lineage commitment and differentiation to DP_{Late} precursors that undergo spontaneous positive selection to generate mature, naïve, single positive T cells without the need for activation or agonist selection of DP precursors.

Since its inception, the ATO system has also been adapted to generate mature, naïve, single positive T cells from human PSCs, replacing HSPCs which are a finite primary human source[32]. While T cell differentiation can be directly induced from undifferentiated PSCs, it was shown that T cell production is more consistent and efficient when cultures are initiated with mesoderm derivatives of PSCs, which are referred to as human "embryonic mesodermal progenitors" **(EMPs) (Figure 1.2C)**.

Using one of our previously published protocols, EMPs are generated from PSCs through a 3.5-day mesoderm induction protocol using XVIVO15 and human growth factors (rhActivin-A, rhBMP4, rhVEGF, rhbFGF) **(Figure 1.2D)**[33]. Then, purified $CD326^-CD56^+$ EMPs are aggregated with MS5-hDLL4 into 3D aggregates for two weeks of

hematopoietic induction in EGM2 medium, hematopoietic cytokines (rhSCF, rhFLT3L, rhTPO), and a TGF-β inhibitor (SB-43152) **(Figure 1.2D**). T cell induction occurs in the same aggregates for an additional 5-7 weeks by simply changing to RB27 media supplemented with rhSCF, rhIL-7 and FLT3L. By week 5, mature, naïve, single positive T cells comprise ~90% of the cells, indicating that DP precursors had efficiently underwent spontaneous positive selection.

Additionally, it was demonstrated that the ATO system can be engineered to generate antigen-restricted SP8 T cells from multiple stem cell sources[31,32]. PSCs or HSPCs were transduced with lentivirus to express a fully rearranged TCR under a constitutive promoter and then differentiated into DP precursors that spontaneously underwent positive selection into mature, naïve SP8 T cells, without the need for activation or agonist selection. TCR-engineered SP8 T cells were functionally validated and exhibited antigen-specific cytotoxicity *in vitro* and *in vivo*[31,32].

Regardless of stem cell source, the ATO system efficiently generates mature, naïve, single positive T cells *in vitro*, qualitatively improving on previous 2D monolayer systems, which do not support spontaneous positive selection of DP precursors[26,27]. Furthermore, the ATO system can differentiate functional, chimeric antigen receptor **(CAR)** T cells in addition to antigen-specific, mature, naïve T cells from engineered PSCs[32,34,35].

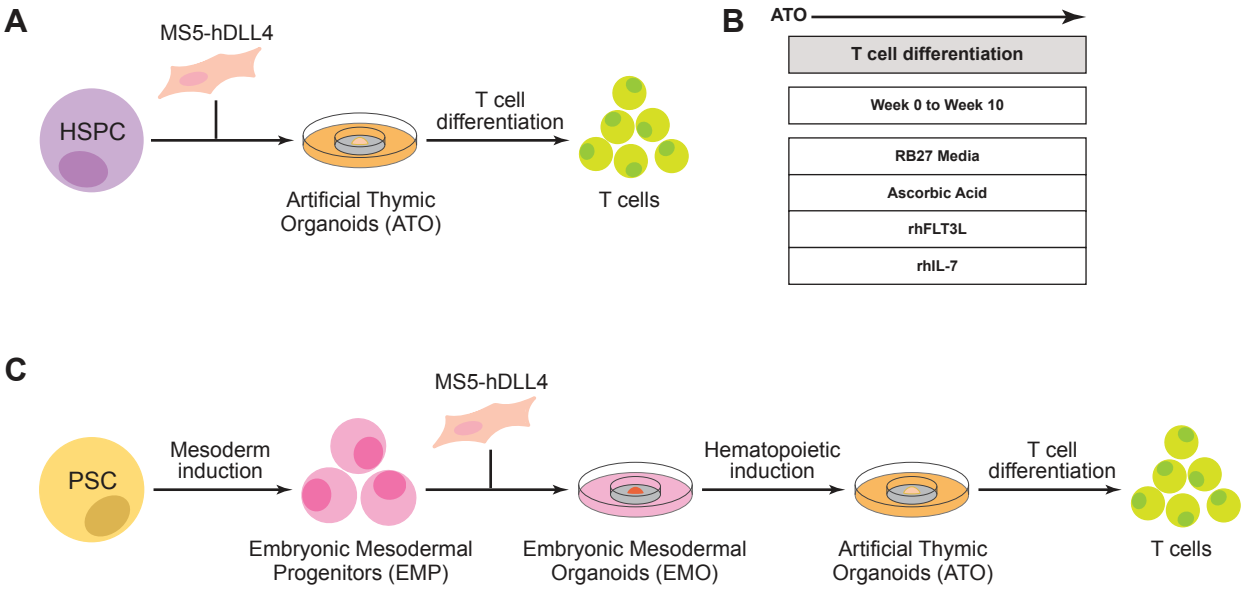

D

PSC → EMO → ATO

Mesoderm Induction			Hematopoietic Induction		T cell differentiation
Day -17	Day -16	Day -15	Day -14 to -7	Day -6 to 0	Week 0 to Week 7
XVIVO15	XVIVO15	XVIVO15	EGM2	EGM2	RB27 Media
rhBMP4	rhBMP4	rhBMP4	SB Blocker	SB Blocker	Ascorbic Acid
rhVEGF	rhVEGF	rhVEGF		rhSCF	rhSCF
rhFGF	rhFGF	rhFGF		rhFLT3L	rhFLT3L
rhActivinA				rhTPO	rhIL-7

Figure 1.2 *In vitro* generation of stem cell-derived T cells with the artificial thymic organoid
(A-B) Schematic of the protocol used to generate mature, naïve T cells in the artificial thymic organoid (ATO) from HSPCs **(A),** and the medium used for differentiation **(B). (C)** Schematic of the protocol used for generating ATOs from PSCs. **(D)** Medium change schedule for differentiating mature, naïve T cells from PSCs. After 3.5 days of mesoderm induction (days -17 to -15), EMPs areharvested and aggregated with MS5-hDLL4 in embryonic mesodermal organoids (EMOs) for 2 weeks in hematopoietic induction media (days -14 to 0). At day 1, the ATO phase, T cell differentiation is initiated within the existing organoids by changing to T cell differentiation medium.

1.6 Engineered T cells for Immunotherapy

Cell-based immunotherapies in which autologous T cells have been engineered to express chimeric antigen receptors **(CARs)** and antigen-specific T cell receptors **(TCRs)** have produced promising clinical responses in patients with otherwise treatment-refractory diseases[36,37]. While both methods are promising, CARs are more prevalent in the clinic as they can be engineered to target surface antigens irrespective of HLA type, and are synthetically designed to respond more potently to cognate antigens. Despite being HLA-restricted, TCRs have their individual benefits as their MHC restriction allows them to target both surface and intracellular tumor antigens, significantly increasing the number of individually targetable sequences for engineered adoptive cell therapies **(ACTs).**

Despite producing curative results, accessibility and widespread adoption of engineered ACTs, including CAR-T and TCR-T, has been limited by the complex and costly manufacturing processes for delivering patient specific treatments. Currently, autologous engineered T cell products rely on both adequate patient lymphocyte counts as well as a disease prognosis which permits a delay in treatment while T cells are manufactured[38–40]. In addition, clinical responses are uneven, at least in part because of the variability of the T cell composition of each patient product[41,42].

Current applications of CAR-T and TCR-T rely on genetic modification and *ex vivo* expansion of mature, circulating T cells, which poses several limitations to physiological activity after re-infusion. Additionally, in TCR-T, mispairing between exogenously transduced and endogenous TCR chains could potentially lead to reduction of antigen-specific reactivity as well as alloreactivity[43,44]. Furthermore, alloreactivity imparted by

endogenous HLA expression has restricted these approaches to the use of autologous T cells, limiting widespread adoption as treatments are inherently personal.

One strategy to overcome the limited duration of responses from exhausted peripheral blood T cells is to transplant autologous, self-renewing hematopoietic stem cells **(HSCs)** modified to express CARs or TCRs; however, this approach is still patient-specific and requires pre-transplant conditioning to allow HSC engraftment[45]. The efficacy of this approach also assumes that the patient's thymic function would be sufficient for physiological T cell production from HSCs, which might not be the case for older or heavily treated patients[46]. Thus, a broad application of this strategy is problematic due to the limited capacity to manufacture products for patients with uncommon HLA types, in addition to ineligibility for patients with reduced immune cell outputs[37,44].

To overcome some of these constraints, development of an "off-the-shelf" engineered T cell product has garnered increasing interest; however, the requirement for an allogeneic source with this approach presents two barriers: donor T cell mediated alloreactivity, which could potentially cause graft versus host disease (GvHD), and host-mediated rejection of HLA-mismatched allogeneic donor cells.

While manipulation of these allogeneic mechanisms via gene editing of healthy donor peripheral blood T cells has been shown to be feasible[39,45], current techniques do not guarantee complete ablation of endogenous TCRs, and the process of gene editing carries the risk of genomic translocations and deleterious off-target events. Therefore, there is a need to identify self-renewing sources of engineered T cells that allow for the identification and expansion of suitable clones after multiple cycles of gene editing.

Due to their self-renewing capacity, human pluripotent stem cells **(PSCs)** are especially amenable to gene editing and clonal selection. The use of PSCs, however, presents an additional hurdle, due to the complex *in vitro* process of hematopoietic and T cell differentiation that must follow genetic manipulation. The two main barriers to using allogeneic engineered T cells, alloreactive TCRs and HLA-mismatching, represent the two critical components required to generate TCR-pMHC interactions during DP T precursor positive selection. While activation or agonist selection of DP T cell precursors can overcome this limitation, engineered cells may be terminally differentiated and phenotypically exhausted as a result of this process. Furthermore, mature, naïve T cells have been implicated in conveying superior antitumor immunity persistence[47,48], underscoring the need to improve *in vitro* strategies for generating phenotypically naïve, stem cell-derived T cells for immunotherapy.

As the generation of alloreactive TCRs is a major hurdle in developing “off-the-shelf” approaches to immunotherapy, it is logical to remove the primary mechanism for generating endogenous TCRs in pro-T cells. While the introduction of an exogenous TCR may be sufficient for rescuing T cell maturation, removal of both *RAG1* and *RAG2* has not been previously characterized, and may severely impact T cell differentiation and positive selection. In Chapter 2 of this dissertation, I describe our work on delineating the effect of ablating *RAG1* and *RAG2* in PSCs on T cell differentiation using the ATO system.

Another barrier to generating “off-the-shelf” therapy approaches to immunotherapy is HLA-restriction of T cells, which could induce GvHD after transfusion. Positive selection is dependent on low affinity TCR-pMHC interactions to signal survival, proliferation, and differentiation of DP T cell precursors to mature, naïve, single positive T cells. Therefore,

removal of MHCs in PSCs would effectively block positive selection in developing DP T precursors, which is dependent on pMHC interactions. In Chapter 3 of this dissertation, I describe our efforts to circumvent this requirement using the accessory cells of the ATO system to induce positive selection of mature, naïve, single, positive T cells in the absence of endogenously expressed MHC and TCR rearrangement machinery in PSC-derived cells.

CHAPTER 2

Delineating the T cell differentiation potential of *RAG1*$^{-/-}$*RAG2*$^{-/-}$ double knockout pluripotent stem cells *in vitro*

2.1 Introduction

The self-renewal capacity of human PSCs allows the development of a standardized source for engineered T cells. Gene-edited clones can be selected based on lack of CRISPR/Cas9 off-target cutting, optimal T cell production and cytotoxicity and other functional features, and then qualified for clinical use and indefinitely expanded. However, two main issues arise with transplanting allogeneic, PSC-derived T cells for adoptive cell therapies **(ACTs)**: alloreactive T cells, which could result from the random rearrangement of TCRs during T cell development; and host rejection of allogeneic T cells due to mismatching in human major histocompatibility complexes **(MHCs)**, which could lead to graft versus host disease **(GvHD)** and rejection of engineered cells. To address the first of these two issues, Chapter 2 centers on removing the endogenous V(D)J recombination machinery in PSCs to prevent the development of alloreactive TCRs.

During normal thymopoiesis, the recombination activating genes 1 and 2 **(*RAG1*** and ***RAG2*)** are responsible for coordinating the V(D)J recombination process of germline TCR loci to produce the diverse repertoire of mature TCRs observed in mature T cells, crucial for the broad response of the adaptive immune system to foreign antigens[2,10]. Previous studies in patients with severe combined immunodeficiency **(SCID)** and Omenn Syndrome **(OS)** have shown that deletion or frameshift mutations in either *RAG1* or *RAG2* lead to significant defects in TCR rearrangement[10,14,15]. Consequently, patients exhibit

significant or complete losses in mature T cells and adaptive immune responses, similar to immunodeficient mouse models that have been developed through *RAG1* or *RAG2* knockouts[12,13].

CRISPR/Cas9 gene editing will be used to simultaneously ablate both *RAG1* and *RAG2* in the NIH-approved HLA-A*0201^{pos} H1[49] and HLA-A*0201^{neg} ESI017[50] PSC lines to eliminate endogenous TCR rearrangement, preventing the generation of alloreactive TCRs during T cell differentiation. Edited PSCs will be cloned and selected based on bi-allelic excision of both genes, and then T cell differentiation potential of *RAG1*$^{-/-}$*RAG2*$^{-/-}$ double knockout **(DKO)** PSCs will be characterized using the *in vitro* "Artificial Thymic Organoid" **(ATO)**, which induces orderly differentiation of T cells and spontaneous positive selection of DP T cell precursors from PSCs[32].

As positive selection is dependent on TCR interactions with peptide-MHC **(pMHC)** complexes, mature, naïve T cell differentiation in the absence of both *RAG1* and *RAG2* is expected to be blocked. To generate antigen-restricted, mature, naïve T cells, an exogenous TCR transgene will be introduced into DKO PSCs to support positive selection in the absence of endogenously rearranged TCRs. For these studies, the fully rearranged HLA-A*0201-restricted 1G4 TCR **(1G4 TCR**, hereafter**)**, which recognizes the NYESO$_{157-165}$ tumor-associated peptide, will be expressed in DKO PSCs through lentiviral transduction[51,52]. Restoration of positive selection in DKO PSCs with the 1G4 TCR **(DKO+TCR**, hereafter**)** will be functionally characterized by the generation of mature, naïve, single positive CD8 **(SP8,** hereafter**)** in the ATO system. As positive selection is dependent on cognate MHC expression, *in vitro* positive selection of antigen-restricted, mature, naïve SP8 T cells will be predicated on cognate MHC-TCR interactions.

2.2 Results

2.2.1 *RAG1/RAG2* knockout is achieved through a complete gene ablation strategy in PSCs.

CRISPR/Cas9 guide RNAs **(gRNAs)** were targeted near the start codons of *RAG1* and *RAG2*, which are located in close proximity on Chromosome 11. 5 gRNAs were chosen for each gene based on optimal on- and off-target efficiency *in silico*, yielding 2 gRNAs after *in vitro* validation of on-target activity using previously published methods **(Figure 2.1A-D)**[53–55]. Off-target activity was screened using the GUIDE-seq method, yielding 1 gRNA with high on- and no detectable off-target activity for each gene **(Figure 2.1E-F)**.

As *RAG1* and *RAG2* are conveniently located within a ~30KB region, a gene ablation knockout strategy was employed for generating clonal *RAG1*$^{-/-}$*RAG2*$^{-/-}$ double knockout **(DKO)** PSC lines from the H1 (HLA-A*0201^{pos}) and ESI017 (HLA-A*0201^{-}) parent PSC lines **(Figure 2.1G)**. Single cell clones were plated at low density and propagated before diagnostic PCRs were performed to confirm bi-allelic ablation of *RAG1* and *RAG2* **(Figure 2.1H)**. First, primers were directed towards a sequence within the excised genomic fragment to confirm the coding sequences of *RAG1* and *RAG2* were deleted from the genome **(Figure 2.1G-H)**. Then, a second set of PCRs were performed to confirm proper chromosomal end joining after CRISPR/Cas9 gene editing **(Figure 2.1G-H)**. Additionally, PCR products from the second set were Sanger sequenced to confirm the new chromosomal junction and identify successfully edited clones **(Figure**

2.1I). Frequency of clones with bi-allelic knockout of *RAG1* and *RAG2* was increased by ~1 log-fold with the inclusion of a HDR template spanning the predicted junction of *RAG1-RAG2* after gene excision **(Figure 2.1J)**. Following sequence validation, DKO PSCs were expanded to confirm growth and morphology were unchanged from their parent lines, and determined to be karyotypically normal.

2.2.2 *RAG1/RAG2* double knockout prevents TCR expression but blocks PSC T cell maturation

Following generation and validation of single cell clones, DKO PSCs were differentiated towards the T cell lineage using our previously developed protocol for generating T cells from PSCs, the "Artificial Thymic Organoid" (ATO) system[32] **(Figure 2.2A)**. Unedited (wildtype, hereafter **WT**) PSCs proceeded through development normally, upregulating surface TCR and CD3, and underwent positive selection predominantly towards the $CD8^+$ T cell lineage **(Figures 2.2B-C and 2.3A-B).**

Differentiation of both DKO PSC lines proceeded normally into the T-lineage committed phase ($CD45^+CD5^+CD7^+$) **(Figure 2.4A-B);** however, DKO PSC-derived T cells did not express surface TCR throughout the entire course of differentiation, confirming a functional loss of endogenously rearranged TCR chains (**Figure 2.2B**). While there was an initial burst of innate-like $CD8\alpha^+$ cells ($CD45^+CD5^+CD7^+CD8\alpha^+$ $TCR\alpha\beta^-CD3^-$), differentiation of DKO PSCs proceeded no further than the double positive stage **(DP**, $CD45^+CD5^+CD7^+CD8\alpha^+CD4^+$) of T cell development, indicating a failure to undergo positive selection because of the absence of TCR expression **(Figures 2.2C and 2.4A-B)**.

DKO cultures peaked at 3 weeks with a dramatic decrease in DP over the remainder of differentiation, indicating death-by-neglect (**Figures 2.2C-D, and 2.4A-B**). Together, the differentiation profile of DKO PSCs demonstrates that *RAG1-RAG2* deletion halts conventional T cell development at the DP T precursor stage, while having no observable effect on the early stages of T cell commitment.

2.2.3 Rescue of positive selection through transgenic TCR expression in DKO PSCs is MHC-restricted

We next investigated whether lentiviral expression of a single exogenous TCR could overcome the halt in differentiation seen in the DKO lines and restore positive selection. The WT and DKO clones of H1 (HLA-A*0201^{pos}*)* and ESI017 (HLA-A*0201^{neg}*)* PSCs were transduced with a lentiviral vector encoding the TCRα and TCR Vβ chains of the 1G4 HLA-A*0201-restricted TCR specific for the tumor-associated NYESO$_{157\text{-}165}$ peptide (hereafter, **WT+TCR** or **DKO+TCR PSCs**)[51,52]. Following transduction and enrichment for transduced cells by flow cytometry, WT+TCR and DKO+TCR PSCs were expanded to confirm growth and morphology were unchanged from their parent lines, and determined to be karyotypically normal.

Lentiviral transduction of the 1G4 TCR in both H1 and ESI017 DKO PSC lines produced high level expression of the transgene in all resulting T cells (**Figure 2.5A**). Expression of the transgenic TCR did not impair differentiation from either WT+TCR PSC lines, with robust production of mature, naïve, single positive CD8+ T cells (SP8), regardless of MHC-expression (**Figures 2.5B and 2.6A**).

In contrast, when 1G4 TCR was expressed in DKO lines, only the HLA-A*0201^{pos} line (H1) generated SP8 T cells; the HLA-A*0201^{neg} (ESI017) line did not proceed beyond the DP stage (**Figure 2.5B and 2.6A**), and cultures were dominated by CD4^{-}CD8^{-} (DN) cells and were not sustained past 3 weeks (**Figures 2.5B-C**). Thus, in the absence of endogenously rearranged TCRs, positive selection only occurred in T cells that expressed the cognate MHC to which the transgenic TCR was restricted, demonstrating that "self-selection" occurs during T cell differentiation.

Positively selected SP8s generated from H1 DKO+TCR PSCs displayed a conventional CD8αβ^{+} phenotype and naïve T cell markers (CD8α^{+}CD8β^{+}CD45RO^{-} CD45RA^{+}CD62L^{+}) (**Figures 2.5D and 2.6A**). Overall percentage and cell yield per ATO aggregate of SP8s, however, were markedly lower in comparison to the WT line, suggesting that rescue of positive selection was inefficient with the exogenous TCR in a RAG-deficient setting (**Figure 2.5E**).

A

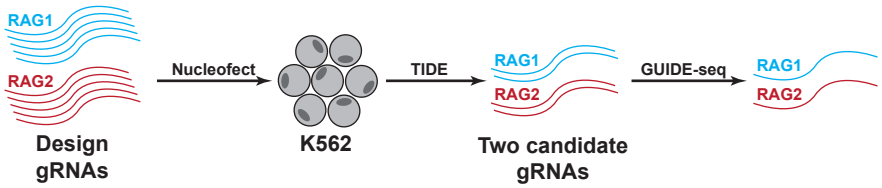

B

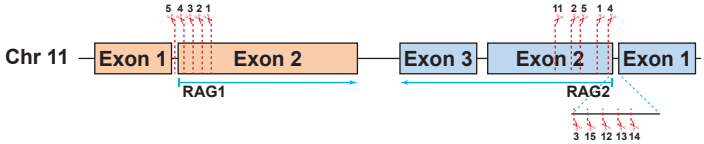

C

RAG1 (gRNA #)	gRNA sequence (PAM sequence included)	Specifitcity (*in silico* score)	Efficiency (*in silico* score)	INDEL % (*in vitro* cutting)
1	TCTTTTCAAAGGATCTCACCCGG	98.29	51.06	6.20%
2	TGGGTGCTGAATTTCATCTGGGG	94.06	59.37	2.95%
3	GCAGAACTGAGTCCCAAGGTGGG	89.51	56.28	1.40%
4	AACTGAGTCCCAAGGTGGGTGGG	87.91	65.83	21.95%
5	CTCAGGTACCTCAGCCAGCATGG	85.08	65.35	4.15%

D

RAG2 (gRNA #)	gRNA sequence (PAM sequence included)	Specifitcity (*in silico* score)	Efficiency (*in silico* score)	INDEL % (*in vitro* cutting)
1	AACATAGCCTTAATTCAGCCAGG	67.17	50.34	15.25%
2	CCAGATGGAAAACTCCAGTGGGG	60.77	75.26	27.05%
3	TGCAGAGACATAGTTTCTGATGG	55.51	56.54	6.55%
4	AGAAACTATGTCTCTGCAGATGG	52.37	53.80	13.35%
5	AAATTCATCAGTGAGAAGCCTGG	50.13	58.51	27.70%
11	CAAGTGGCTGGGTAGCGAAGAGG	82.60	71.70	18.43%
12	CCTAGGGAGCATATAGTCCGTGG	91.40	59.80	52.45%
13	TGTGAATAAAGACTAGCCGAAGG	85.90	68.20	21.25%
14	TGTCGGGCAAACCGCTACCCTGG	94.70	58.00	38.95%
15	CAGTCCCACTGCAAGCGTGTGGG	84.50	63.00	14.68%

E

RAG1 CRISPR #1

RAG1 CRISPR #4

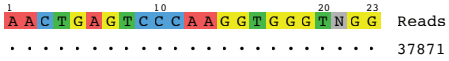

F

RAG2 CRISPR #2

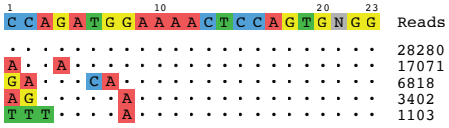

RAG2 CRISPR #5

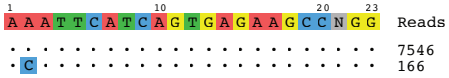

RAG2 CRISPR #12

RAG2 CRISPR #14

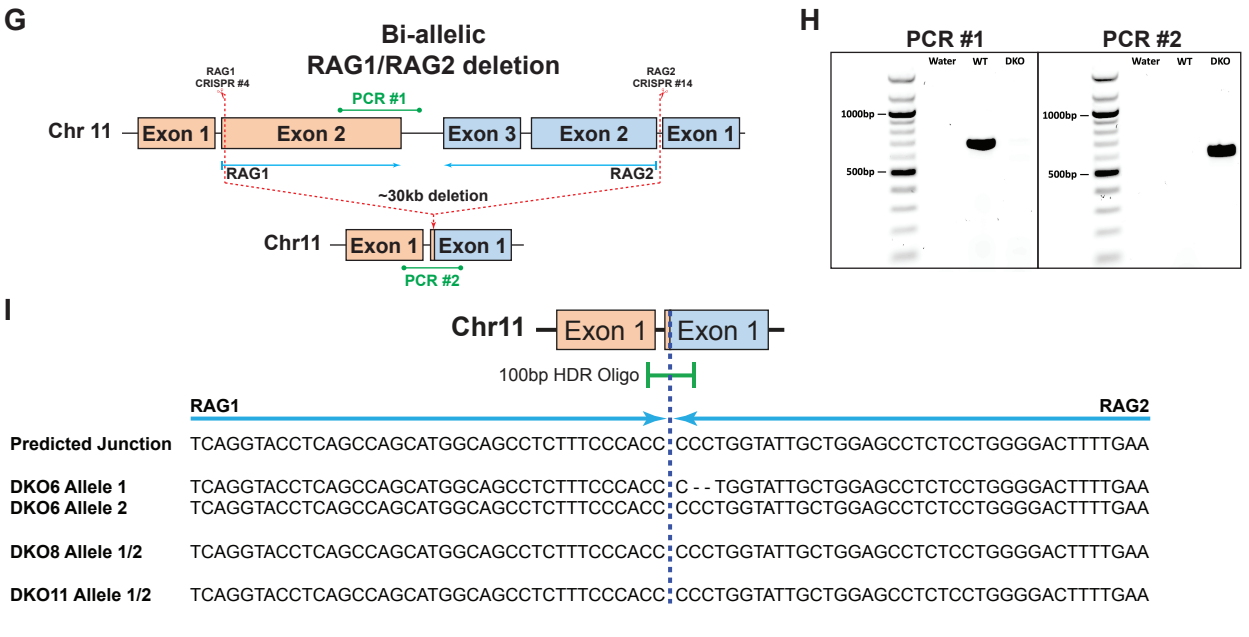

J

Bi-allelic Knockout Cloning Efficiency			
Method	**Clones Screened**	**Clones Identified**	**% Efficiency**
NHEJ	127	1	0.78%
HDR	72	6	**8.33%**

Figure 2.1 Strategy for CRISPR/Cas9 gene excision of *RAG1* and *RAG2* to generate double knockout PSCs

(A) Schematic of the screening process for selecting 1 gRNA candidate for each gene, *RAG1* and *RAG2*, with high on-target and low-off target activity in vitro. **(B)** Schematic of the region on Chromosome 11 containing the coding sequences of *RAG1* and *RAG2*. gRNAs were designed to target sites around the start of the coding sequences for both genes, which are located in Exon 2. **(C)** Summary of gRNA (black) and PAM (red) sequences and predicted on- and off-target scores for gRNAs targeting *RAG1* **(C)** and *RAG2* **(D)** in silico (scored on a scale of 100). On-target activity in K562 cells is shown as the percentages of insertion deletion mutations (INDEL %) calculated via Sanger Sequencing (TIDE). Additional gRNAs for *RAG2* were assayed due to detectable off-target activity with the original set. **(E-F)** Off-target gRNA activity analysis via the GUIDE-seq method for *RAG1* **(F)** and *RAG2* **(F)**. On-target reads are represented by ".", and off-target reads are denoted by their mismatched bases. **(G)** Design of the gene ablation strategy of the *RAG1-RAG2* locus in PSCs using *RAG1* gRNA #4 and *RAG2* gRNA #14. PCR primers, as shown, were designed to detect bi-allelic deletion of *RAG1* and *RAG2*. **(H)** Representative diagnostic PCR amplifications of the region on Chromosome 11 encoding for *RAG1* and *RAG2*. (Left) PCR primers were designed to amplify a 693bp segment of DNA found within the excised region on Chromosome 11 (PCR #1). Removal of both alleles from the genome is indicated by a loss of banding. (Right) PCR primers were designed to amplify the entire ~30KB region excised by CRISPR/Cas9 gene editing. PSC clones with at least one allele of *RAG1/RAG2* excised displayed a 608bp band, signifying proper rejoining of the chromosomal ends. **(I)** Sanger sequencing of the predicted repair site in representative DKO PSC clones were deconvoluted using the CRISP-ID method. **(J)** Cloning efficiency of *RAG1*$^{-/-}$/*RAG2*$^{-/-}$ double knockout (DKO) PSCs through non-homologous end joining (NHEJ) or homology directed repair (HDR) using a 100bp single stranded DNA donor template.

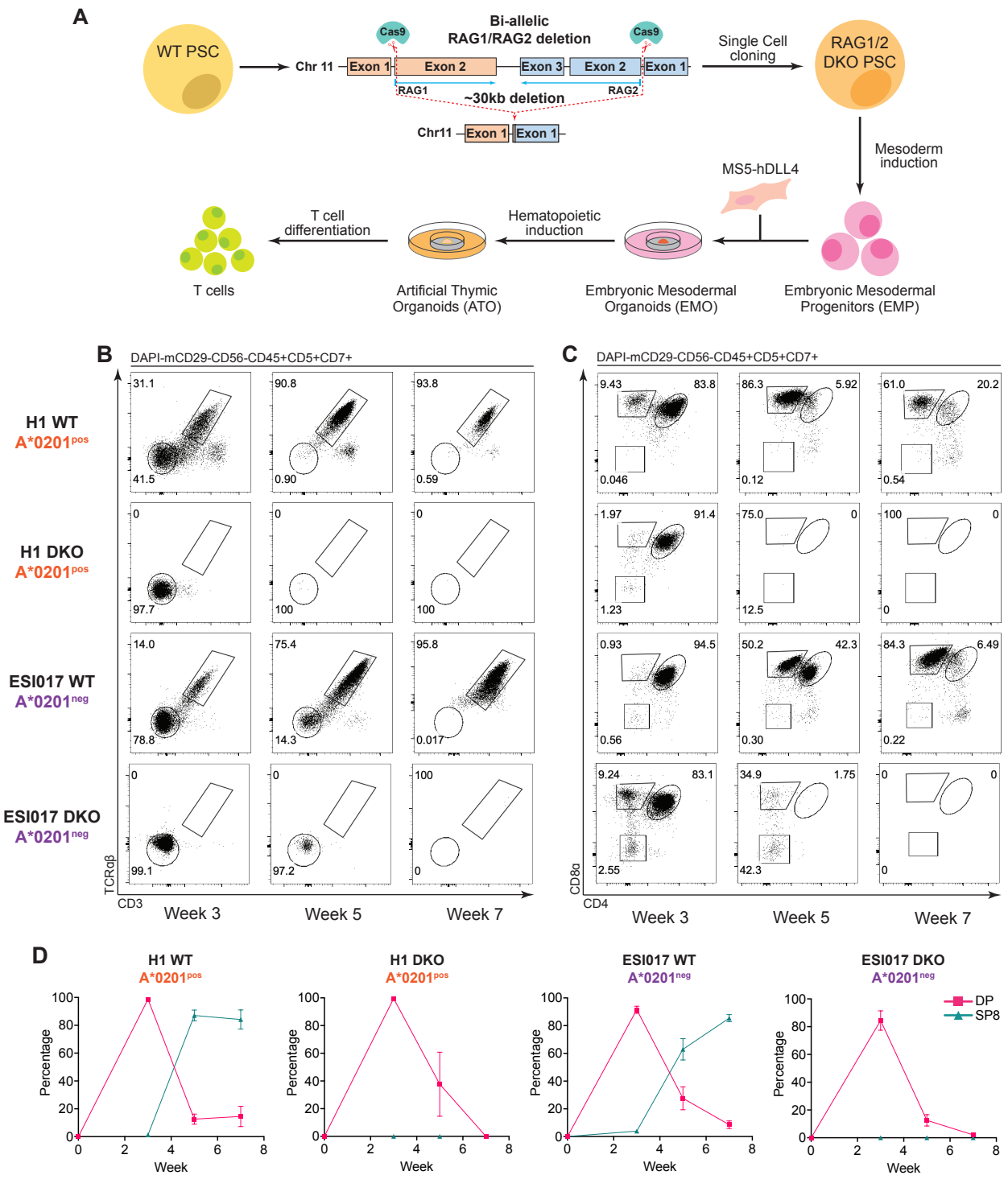
A
WT PSC
Chr 11
Exon 1
Exon 2
Exon 3
Exon 2
Exon 1
Cas9
Cas9
Bi-allelic
RAG1/RAG2 deletion
RAG1
RAG2
~30kb deletion
Chr11
Exon 1
Exon 1
Single Cell
cloning
RAG1/2
DKO PSC
Mesoderm
induction
MS5-hDLL4
T cell
differentiation
Hematopoietic
induction
T cells
Artificial Thymic
Organoids (ATO)
Embryonic Mesodermal
Organoids (EMO)
Embryonic Mesodermal
Progenitors (EMP)
B
DAPI-mCD29-CD56-CD45+CD5+CD7+
H1 WT
A*0201pos
H1 DKO
A*0201pos
ESI017 WT
A*0201neg
ESI017 DKO
A*0201neg
TCRαβ
CD3
Week 3
Week 5
Week 7
C
DAPI-mCD29-CD56-CD45+CD5+CD7+
CD8α
CD4
Week 3
Week 5
Week 7
D
H1 WT
A*0201pos
H1 DKO
A*0201pos
ESI017 WT
A*0201neg
ESI017 DKO
A*0201neg
Percentage
Week
DP
SP8

Figure 2.2 *RAG1/RAG2* double knockout halts T cell development at the double positive stage of T cell maturation

(A) Schematic for generating clonal *RAG1/RAG2* double knockout (DKO) PSCs, and then differentiation in the artificial thymic organoid (ATO) system. **(B)** Representative flow cytometry analysis of ATOs generated from unedited (WT) and *RAG1/RAG2* deleted (DKO) PSCs from the H1 (A*0201^{pos}) and ESI017 (A*0201^{neg}) parent lines. Surface expression of TCRαβ and CD3 from T lineage-committed cells are shown at the indicated time points. Gating indicated above panels. **(C)** Kinetics of CD8α and CD4 expressing on T lineage-committed cells from WT and DKO PSCs differentiated in the ATO system shown at the indicated time points. Gating indicated above panels. **(D)** Frequency of precursor and mature T cell populations at the indicated time points (mean ± SEM, n=3 independent experiments). Frequency of populations from gates shown in (C), defined as: double positive (DP, CD8α^{+}CD4^{+}) and single positive CD8 (SP8, CD8α^{+}CD4^{-}TCRαβ^{+}CD3^{+})

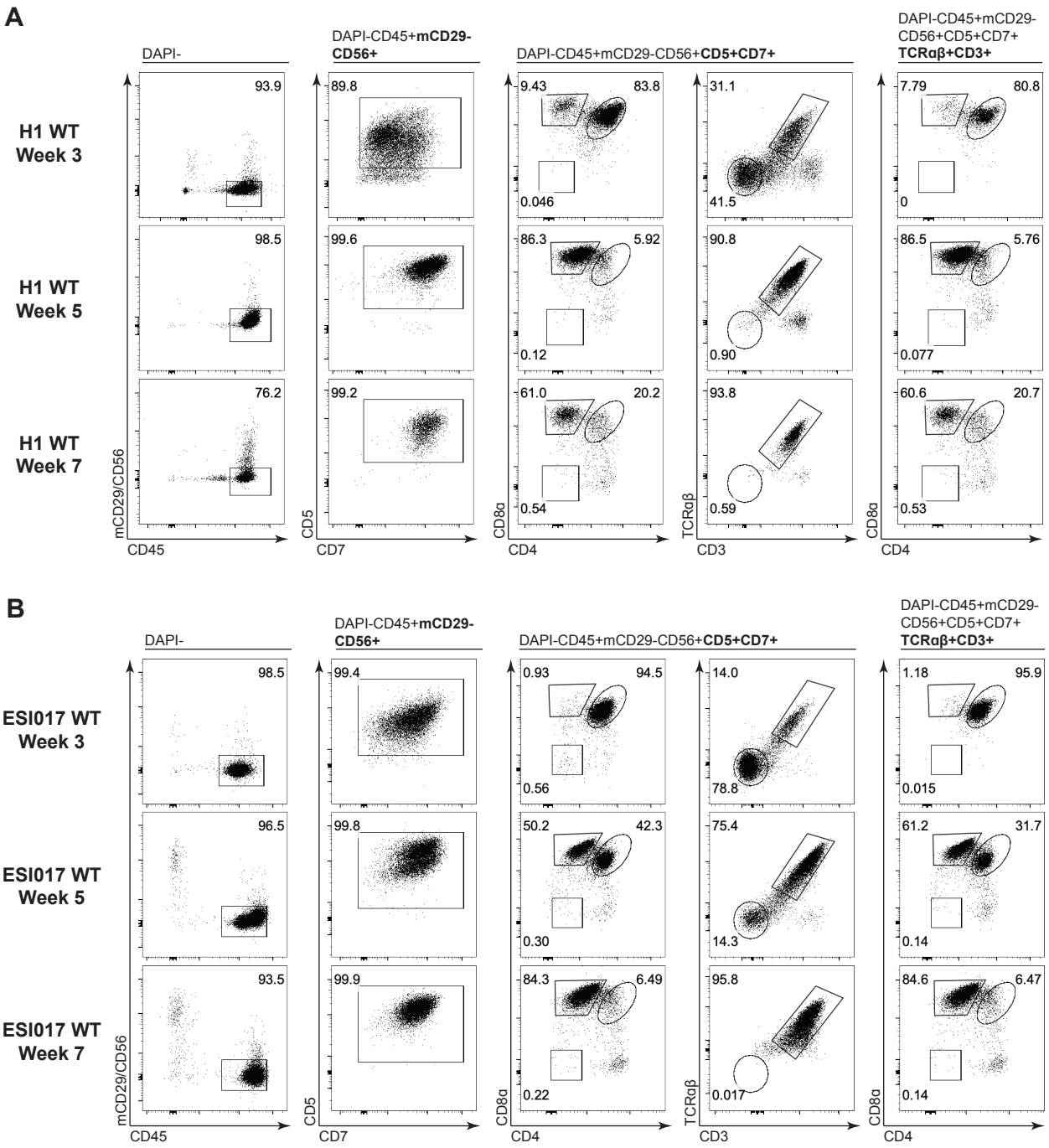

Figure 2.3 Differentiation kinetics of WT and DKO PSCs in the ATO system
(A-B) Representative flow cytometry plots of the gating strategy used to track the progress of T cell differentiation from H1 WT PSCs **(A)** and ESI017 WT PSCs **(B)** in the ATO system at the indicated time points.

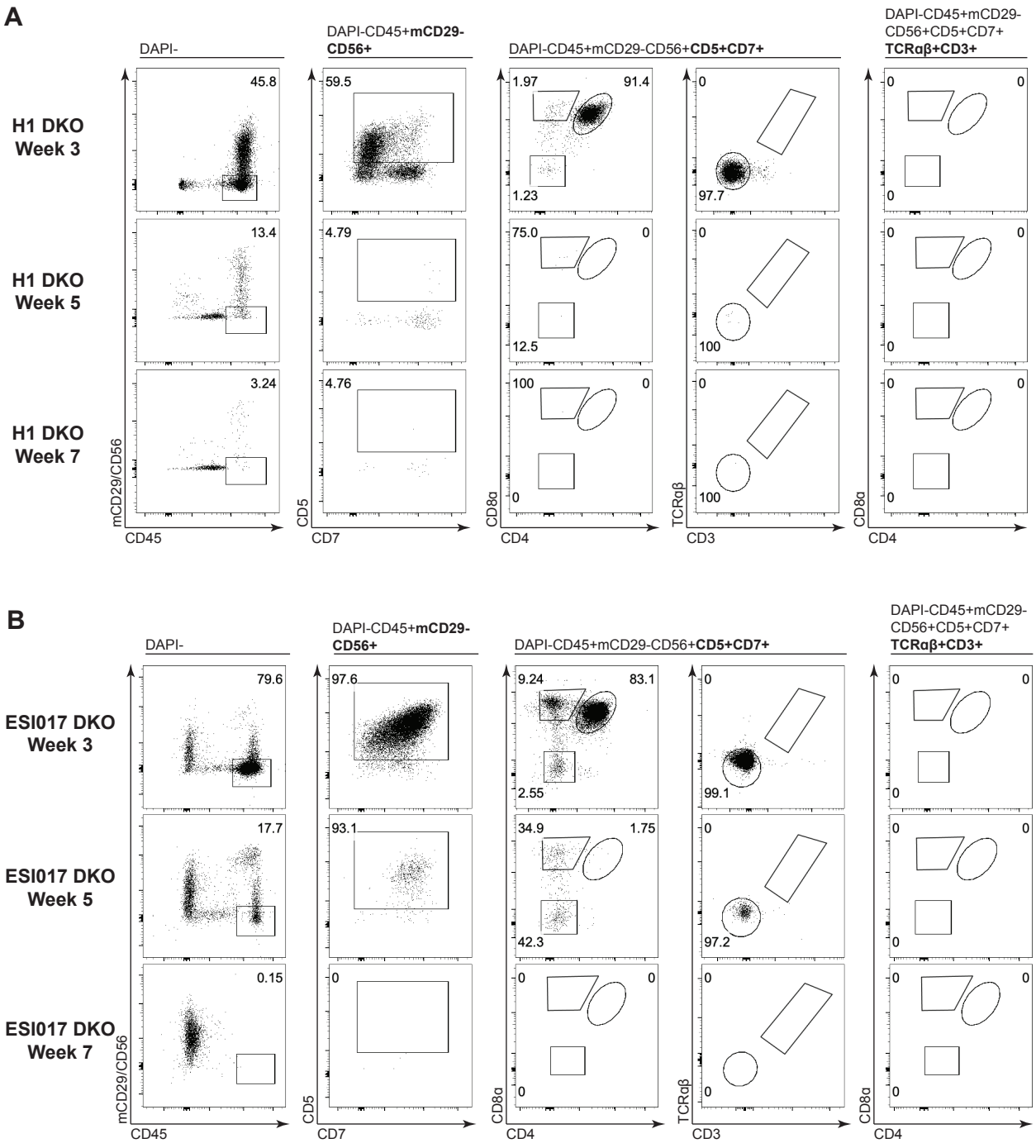

Figure 2.4 Differentiation kinetics of DKO PSCs in the ATO system
(A-B) Representative flow cytometry plots of the gating strategy used to track the progress of T cell differentiation from H1 DKO PSCs **(A)** and ESI017 DKO PSCs **(B)** in the ATO system at the indicated time points.

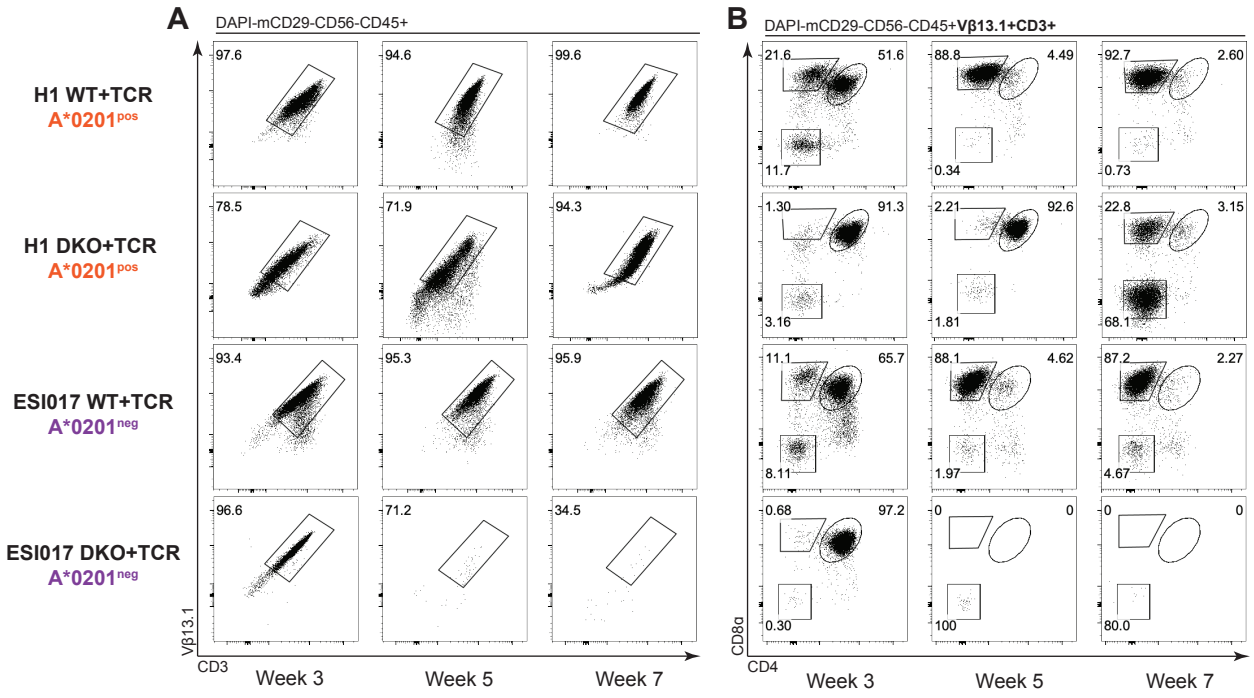
A
DAPI-mCD29-CD56-CD45+
H1 WT+TCR
A*0201pos
H1 DKO+TCR
A*0201pos
ESI017 WT+TCR
A*0201neg
ESI017 DKO+TCR
A*0201neg
97.6
94.6
99.6
78.5
71.9
94.3
93.4
95.3
95.9
96.6
71.2
34.5
Vβ13.1
CD3
Week 3
Week 5
Week 7
B
DAPI-mCD29-CD56-CD45+Vβ13.1+CD3+
21.6
51.6
11.7
88.8
4.49
0.34
92.7
2.60
0.73
1.30
91.3
3.16
2.21
92.6
1.81
22.8
3.15
68.1
11.1
65.7
8.11
88.1
4.62
1.97
87.2
2.27
4.67
0.68
97.2
0.30
0
0
100
0
0
80.0
CD8α
CD4
Week 3
Week 5
Week 7

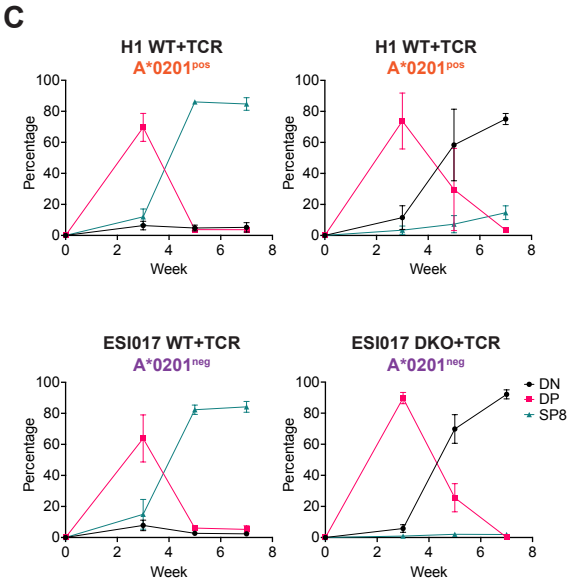
C
H1 WT+TCR
A*0201pos
H1 WT+TCR
A*0201pos
ESI017 WT+TCR
A*0201neg
ESI017 DKO+TCR
A*0201neg
Percentage
Week
DN
DP
SP8

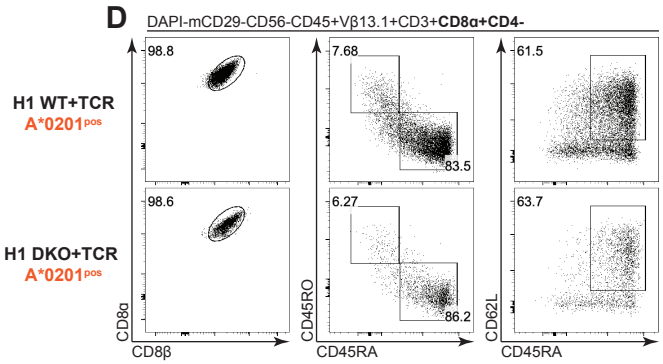
D
DAPI-mCD29-CD56-CD45+Vβ13.1+CD3+CD8α+CD4-
H1 WT+TCR
A*0201pos
H1 DKO+TCR
A*0201pos
98.8
7.68
83.5
61.5
98.6
6.27
86.2
63.7
CD8α
CD8β
CD45RO
CD45RA
CD62L
CD45RA

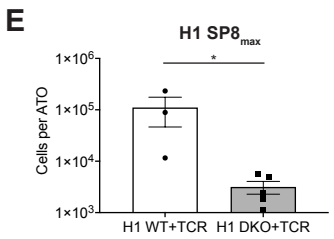
E
H1 SP8max
Cells per ATO
H1 WT+TCR
H1 DKO+TCR

Figure 2.5 1G4 TCR rescue of *RAG1/RAG2* DKO PSC T cell differentiation is MHC-restricted
(A-B) Representative flow cytometry analysis of WT and *RAG1/RAG2* deleted (DKO) PSCs from both parent lines, H1 (A*0201^{pos}) and ESI017 (A*0201^{neg}), stably transduced to express the HLA-A*0201-restricted 1G4 TCR (WT+TCR and DKO+TCR). Surface expression of Vβ13.1 and CD3 (gated as shown) during ATO differentiation of PSC-derived cells at the indicated time points **(A)**. Differentiation kinetics of 1G4 TCR-expressing T cells based on CD8α and CD4 expression at the indicated time points of ATO differentiation (gated as shown) **(B)**. **(C)** Frequency of precursor and mature T cell populations, from gates shown in (B) at the indicated time points (mean ± SEM; H1, n=3; ESI017, n=4 independent experiments, gated as shown). Populations defined as: double negative (DN, CD8α$^-$CD4$^-$), double positive (DP, CD8α$^+$CD4$^+$), single positive CD8 (SP8, CD8α$^+$CD4$^-$CD8β$^+$). **(D)** At 7 weeks of T cell differentiation, ATO-derived H1 WT+TCR and DKO+TCR SP8 T cells (gated as shown) were analyzed for maturation markers of conventional T cells as shown. **(E)** Maximum SP8 T cell output per ATO aggregate, calculated from every analysis point during T cell differentiation. Mean ± SEM (*$p < 0.05$) are shown for each group (n=3 independent experiments for H1 WT+TCR and n=5 for H1 DKO+TCR).

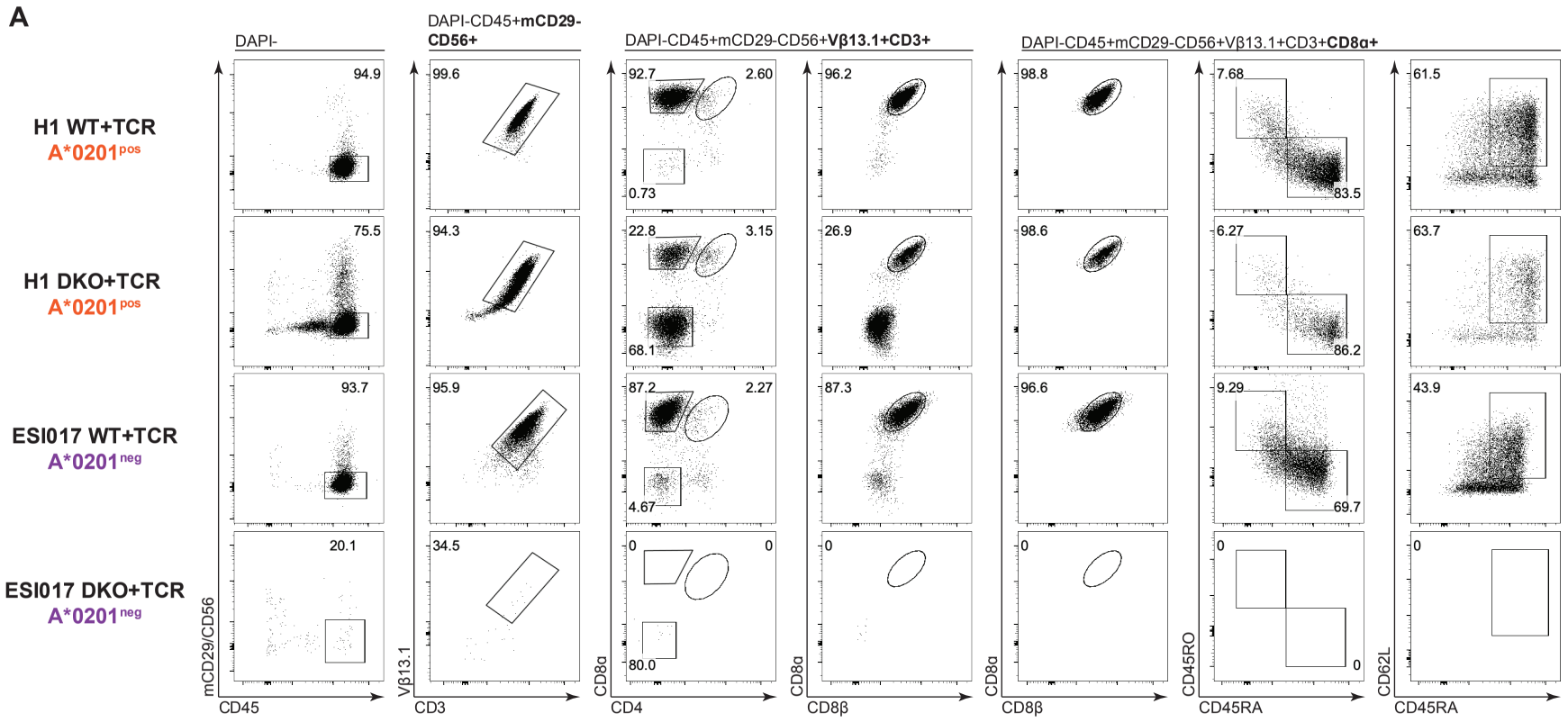
A
H1 WT+TCR
A*0201pos
H1 DKO+TCR
A*0201pos
ESI017 WT+TCR
A*0201neg
ESI017 DKO+TCR
A*0201neg
DAPI-
DAPI-CD45+mCD29-CD56+
DAPI-CD45+mCD29-CD56+Vβ13.1+CD3+
DAPI-CD45+mCD29-CD56+Vβ13.1+CD3+CD8α+
94.9
75.5
93.7
20.1
99.6
94.3
95.9
34.5
92.7
2.60
0.73
22.8
3.15
68.1
87.2
2.27
4.67
0
0
80.0
96.2
26.9
87.3
0
98.8
98.6
96.6
0
7.68
83.5
6.27
86.2
9.29
69.7
0
0
61.5
63.7
43.9
0
mCD29/CD56
CD45
Vβ13.1
CD3
CD8α
CD4
CD8α
CD8β
CD8α
CD8β
CD45RO
CD45RA
CD62L
CD45RA

Figure 2.6 Gating strategy for the analysis of mature, naïve SP8 T cells from PSCs transduced with the 1G4 TCR in the ATO system

(A) WT and RAG1/RAG2 DKO PSCs from both parent PSC lines, H1 (A*0201^{pos}) and ESI017 (A*0201^{neg}) were transduced to express the HLA-A*0201-restricted 1G4 TCR recognizing the NYESO$_{157-165}$ peptide, generating the WT+TCR and DKO+TCR lines. Representative flow cytometry analysis of maturation markers for conventional T cell from WT+TCR and DKO+TCR ATOs, harvested after 7 weeks of T cell differentiation.

2.3 Discussion

Here, we demonstrate the spontaneous positive selection of DP T precursors in the absence of endogenous TCR rearrangement machinery from gene edited PSCs *in vitro*. Generation of antigen-restricted, mature, naïve SP8 T cells from *RAG1*$^{-/-}$*RAG2*$^{-/-}$ DKO+TCR PSCs is dependent on the MHC-restriction of the exogenous 1G4 TCR, as only H1 (HLA-A*0201^{pos}), but not ESI017 (HLA-A*0201^{neg}), PSC-derived DP T precursors spontaneously underwent positive selection to generate SP8 T cells with a naïve, conventional ($CD3^+TCR\alpha\beta^+CD8\alpha^+CD8\beta^+CD45RO^-CD45RA^+CD62L^+$) phenotype without the need for activation or agonist-mediated selection.

RAG1-RAG2 deletion did not result in observable functional defects on T-lineage specification, as DKO and DKO+TCR PSCs efficiently differentiated into DP T precursors. While T cells have been generated in *RAG*-deficient backgrounds, these studies did not employ a complete gene ablation strategy for one or both proteins at that the same time[56,57]. Simple knockout strategies may be insufficient in preventing all endogenous TCR recombination, as clinical studies of *RAG* proteins have shown that residual activity can be retained despite truncation or frameshift mutations[35,58,59]. Furthermore, while simple knockout of either *RAG* protein may be sufficient in preventing alloreactive TCR generation during activation or antigen-mediated T cell maturation, residual activity from either protein could be especially permissive to endogenous TCR recombination during positive selection, as it is a rate-limiting, stochastic step.

Interestingly, ESI017 (HLA-A*0201^{neg}) WT+TCR PSCs escaped the MHC-restriction of the 1G4 TCR, efficiently generating conventional, mature, naïve SP8 T cells. ESI017 WT+TCR PSC-derived SP8 T cells were enriched for surface expression of the

exogenous TCR Vβ chain, shown by Vβ13.1 antibody staining, indicating successful expression of the fully rearranged TCR at the surface. TCR Vβ repertoire analysis in SP8 T cells was not performed through sequencing or antibody staining, as it has been well characterized in previous studies, from other groups and ours, that expression of fully rearranged TCRβ chains induces allelic exclusion of endogenous TCRβ loci during T cell development from stem cells[17,18,31,32,60].

Allelic exclusion of the endogenous TCRα, however, has not been well characterized and only assumed to occur based on observations with the TCRβ locus. As antibody panels are not readily available, TCR Vα repertoire analysis has only been enabled through recently developed high-throughput sequencing techniques. One study demonstrated that allelic exclusion of TCR Vα is not observed when T cells are differentiated from T-iPSCs, which possess fully rearranged TCR chains, and *RAG2* knockout non-T-iPSCs transduced with an exogenous TCR[57].

While we did not study endogenous TCR Vα repertoires in *RAG*-competent PSCs transduced with exogenous TCRs, we can infer that SP8 T cells generated from ESI017 (HLA-A*0201^{neg}) WT+TCR PSCs could have escaped the 1G4 TCR's MHC-restriction through endogenous TCRα rearrangements. As our exogenous TCR contained human elements, mispairing between exogenous TCRβ and stochastically rearranged endogenous TCRα chains could provide a mechanism for escaping the 1G4 TCR's MHC restriction, broadening the repertoire of peptides and MHC capable of generating positive selection signals. The studies presented in Chapter 3 of this dissertation will address this hypothesis through single cell sequencing of TCR Vα and Vβ repertoires.

In the absence of endogenously rearranged TCRs, transduction of DKO PSCs with the exogenous 1G4 TCR restored surface presentation of TCRαβ and CD3; however, spontaneous positive selection of DP T precursors was MHC-restricted. Only cultures initiated with H1 DKO+TCR PSCs that expressed the 1G4 TCR's cognate MHC, HLA-A*0201, achieved positive selection. Efficiency of SP8 T cell generation and from H1 DKO+TCR PSCs was lower and cultures were notably increased in TCR-expressing DN cells; however, we believe that the reduction in positive selection efficiency is indicative of the antigen-specific nature of DKO+TCR DP precursors, which significantly limits the range of interactable pMHCs for positive selection.

In this Chapter, we demonstrate that spontaneous positive selection of antigen-specific SP8 T cells from DKO+TCR PSCs, after complete genomic ablation of both *RAG1* and *RAG2*, is restricted to the cognate MHC of the exogenous 1G4 TCR. Furthermore, spontaneous positive selection is blocked in the absence of cognate MHC, indicating that positive selection relies on TCR and cognate pMHC presentation from PSC-derived cells within the ATO system, at least in the context of ablating both *RAG* genes[32].

While improvements in T cell outputs have yet to be addressed, we have demonstrated that antigen-restricted, mature, naïve SP8 T cells can be generated *in vitro* without the need for activated or agonist selection of DP T precursors. Together, these results demonstrate that it is feasible to generate PSC-derived T cells in the absence of all TCR rearrangement machinery, addressing the critical issue of allogeneic TCR production in stem cell-derived T cell products, which could be applied towards "off-the-shelf" approaches to ACT immunotherapy.

2.4 Materials and Methods

Cell Lines

The MS5-hDLL4 cell line was generated in our lab as previously described[32]. Briefly, MS5 cells[61] were transduced with a lentiviral vector encoding full-length human *DLL4*. The highest 5% DLL4-expressing cells were isolated by FACS using an anti-DLL4 antibody and passaged in DMEM with 10% fetal bovine serum (FBS). Stable expression was confirmed by flow cytometry for DLL4 expression after several weeks of culture, as well as qRT-PCR and DNA sequencing.

Lentiviral vectors packaging

The full-length coding sequences of human DLL4, human HLA-A*0201, human B2M, and human ICAM1 were synthesized (Integrated DNA Technologies, Skokie, IL) and cloned into third-generation lentiviral vector backbone pCCL-c-MNDU3 (gift from Dr. Donald Kohn, UCLA).

The codon optimized TCR Vα and Vβ (including Vβ13.1) chains of a TCR specific for HLA-A*0201/NYESO1$_{157\text{-}165}$ (derived from the 1G4 TCR[51])is previously described[52] (gift from Dr. Antoni Ribas, UCLA). TCR coding sequences and the mTagBFP2 fluorescent protein[62], all separated by furin-SGSG-2A linkers, were subcloned into the third-generation pCCL lentiviral vector downstream of the ubiquitin C (UBC) promoter and intron 1.

Packaging and concentration of lentivirus particles were performed as previously described[31]. Briefly, 293T cells (ATCC) were co-transfected with a lentiviral vector plasmid, pCMV-DR8.9, and pCAGGS-VSVG using TransIT 293T (Mirus Bio, Madison,

WI) for 17 hours followed by treatment with 20 mM sodium butyrate for 8 hours, followed by generation of cell supernatants in serum-free UltraCulture for 48 hours. Supernatants were concentrated by ultrafiltration using Amicon Ultra-15 100K filters (EMD Millipore, Billerica, MA) at 4000 x g for 40 minutes at 4C and stored as aliquots at -80C.

Human pluripotent cell lines

The human pluripotent stem cell (PSC) lines[49] (WiCell, Cat. WA01) and ESI017[50] (ESI BIO, Cat. ES-700), were maintained and expanded on Matrigel-coated 6-well plates (Growth Factor reduced Matrigel matrix, BD Biosciences, Cat. 356231) in mTeSR™ Plus complete medium (mTeSR™ Plus Basal Medium + 5X Supplement, Stem Cell Technologies, Cat. 100-0276). Culture medium was changed daily. After reaching ~70% confluency, PSC cultures were dissociated with TrypLE™ Express (GIBCO Life Technologies, Cat. 12604-013) and seeded in single cell suspension at a density of 2 x 10^5 cells/well of a Matrigel-coated 6-well plate in mTeSR™ Plus complete medium and ROCK inhibitor Y-27632 dihydrochloride (10μM) (Tocris, Cat. 1254), which was removed from culture medium after 1 day.

Design and validation of CRISPR/Cas9 guide RNAs

Using published algorithms found on the Benchling web tool (https://benchling.com), 5 guide RNAs (gRNAs) with optimal *in silico* predicted on- and off-target scores (out of 100) were designed to target sequences near the start of *RAG1, RAG2,* and *B2M*[53–55,63–65]*.* On-target efficiency was assayed *in vitro* at each target locus

by nucleofection of gRNA expressing pX459 plasmid (Zhang Lab, MIT; Addgene, Cat. 62988) into K562 erythroleukemia cells (ATCC, Cat. CCL-243).

Genomic DNA (gDNA) was harvest from nucleofected cells, and flanking regions of *RAG1* and *RAG2,* cleavage sites were amplified via PCR. Products were purified and on-target CRISPR/Cas9 cutting efficiency was determined by Sanger sequencing of the PCR products. Using the Tracking of Insertion or Deletion mutations (INDELs) by Decomposition (TIDE) tool[66], the percentage of edited cells was calculated based on the INDELs produced as a result of double stranded breaks from CRISPR/Cas9.

For each gene target, the 2 gRNA candidates with the highest on-target *in vitro* cutting activity were chosen for off-target cleavage activity *in vitro* via the genome-wide, unbiased identification of DSBs enabled by sequencing (GUIDE-seq)[67].1 gRNA with high on- and low off-target cutting activity was chosen for each target gene to proceed with editing in PSC lines.

Gene editing of human pluripotent stem cell lines

CRISPR/Cas9 gene editing of PSCs was performed with ribonucleoprotein complexes[68,69] (RNPs) of purified spCas9-NLS (QB3 MacroLab, UC Berkeley, Berkeley, CA) and custom synthesized small guide RNAs (gRNAs) (Synthego, Mountain View, CA). spCas9-NLS and gRNAs were stored at -80C prior to use for gene editing of PSCs.

Briefly, PSCs were allowed to grow in wells of a Matrigel-coated 6-well plate until reaching ~70% confluency before being dissociated with TrypLE™ Express (GIBCO Life Technologies, Cat. 12604-013) and resuspended in single cell solution. Prior to nucleofection, 60pmol spCas9 and individual 84pmol gRNA were complexed together at

a ratio of 1pmol spCas9:1.4pmol gRNA for 15m at room temperature. PSCs were resuspended at a concentration of 2 x 10^5 cells in 14µL of P4 Primary Cell Nucleofector® Solution (P4 Primary Cell 4D-Nucleofector™ X Kit S, Lonza, Cat. V4XP-4032).

For single gRNA reactions, fully complexed RNPs (60pmol spCas9:84pmol gRNA) were added to resuspended cells and the volume was brought up to 20µL using P4 Primary Cell Nucleofector® Solution. For dual gRNA reactions, RNPs were complexed individually and then added (2 x 60pmol spCas9 total) into the cell suspension with a custom-synthesized single stranded oligo donor template (ssODN, 100bp, resuspended at 100µM) (Ultramer® DNA Oligo, Integrated DNA Technologies, Skokie, IA) to a final concentration of 3µM in solution. 20µL of combined PSC, RNP, and/or ssODN solutions were added into individual wells of the Lonza 16-well Nucleocuvette® Strip (Lonza). Nucleofection was performed on the Lonza 4D-Nucleofector® Core and X Unit (Lonza, Cat. AAF1003B and AAF-1003X) using pulse and frequency code CB-150. Cells were allowed to rest in the cuvette for 10m before transferring into 1.5mL mTeSR™ Plus and ROCK inhibitor Y-27632 dihydrochloride (10µM), and then plated in 1 well of a Matrigel-coated 12-well plate. Culture medium was changed daily, and ROCK inhibitor Y-27632 dihydrochloride (10µM) was removed from medium after 48hr. Edited PSCs were allowed to reach ~70% confluency before being expanded for single cell cloning and cryopreservation.

Knockout of *RAG1* and *RAG2* in both H1 and ESI017 parent lines was achieved using a gene ablation strategy that excised the ~30KB region on Chromosome 11 in which their coding regions were located using the *RAG1* CRISPR #4 and *RAG2* CRISPR #14 gRNAs **(Figure 2.1C-D),** and a 100bp ssODN HDR template (5'-TTTTCATTGTTCTC

AGGTACCTCAGCCAGCATGGCAGCCTCTTTCCCACCCCCTGGTATTGCTGGAGCC

TCTCCTGGGGACTTTTGAACAGGTGACCCGA-3') **(Figure 2.1G)**.

Table 2.1. List of primers for genotyping *RAG* genes

Primer Name	Sequence (5'-3')	Sequence Amplified (length)
RAG PCR #1 FWD	tgtatactgggacccttggggag	RAG1 Exon 2 (693bp)
RAG PCR #2 FWD	agaattcccacagatgcggcagag	RAG1 Exon 2 (693bp)
RAG PCR #2 FWD	tgtatactgggacccttggggag	RAG1-RAG2 Junction (608bp)
RAG PCR #2 REV	gtcacggcttttgtaacctcgg	RAG1-RAG2 Junction (608bp)

Single cell cloning of edited human pluripotent stem cell lines

Single cell cloning was achieved with low density plating of expanded, edited PSCs as previously described[53]. Briefly, expanded, edited PSCs were dissociated into single cell solution with TrypLE™ Express (GIBCO Life Technologies, Cat. 12604-013) and then plated in Matrigel-coated 10cm dishes at a density of 0.5-1 x 10^4 cells/plate in mTeSR™ Plus complete culture medium with ROCK inhibitor Y-27632 dihydrochloride (10μM). Culture medium was changed daily, and ROCK inhibitor Y-27632 dihydrochloride (10μM) was removed from medium after 48hr. After colony formation, 24-48 individual colonies were scraped with a 200μL "P200" pipette tip under a microscope, and then transferred into individual wells of a Matrigel-coated 12-well plate with mTeSR™ Plus culture medium. Once cells reached 60-80% confluency, cells were passaged via scraping for expansion and genotyping PCRs to determine bi-allelic knockout of edited genes. Clones with bi-allelic knockouts were expanded, cleaned for differentiation and then genotyped once again before cryopreservation and karyotyping.

Transduction of human pluripotent stem cell lines

NYESO TCR-transduced PSC lines were generated by transduction of unedited or knockout H1 or ESI017 PSCs with a lentiviral vector encoding the 1G4 TCR (Class I

MHC-restricted NYESO1 specific TCR, described below) and the fluorescent marker mTagBFP2. Briefly, PSCs were dissociated into single cell suspension and plated at a density of 2 x 10^5 cells/well of a Matrigel-coated 6-well plate in mTeSR™ Plus culture medium with ROCK inhibitor Y27632 dihydrochloride (10μM). The following day, culture medium was changed to 1mL of mTeSR™, and concentrated lentiviral supernatant was added directly into the wells. Medium was changed each day until cells reached ~70% confluency, when cells were dissociated with TypLE™ Express (GIBCO Life Technologies, Cat. 12604-013) and purified via FACS sorting using the following phenotype: TRA1-81$^+$mTagBFP2$^+$. Isolated cells were returned to culture on Matrigel-coated 6-well plates and mTeSR™ Plus culture medium for expansion and cryopreservation.

Generation and isolation of human embryonic mesodermal progenitors (EMPs)

Mesodermal commitment was induced as previously described[32,33,70] with certain optimizations. Briefly, PSCs were maintained as single-cell cultures on Matrigel-coated 6-well plates in mTeSR™ Plus complete medium. PSCs were harvested as single cell suspension after TrypLE™ Express (GIBCO Life Technologies Ref 12604-013) treatment for 6 minutes at 37C, washed, and counted. Cells were resuspended directly in X-VIVO15 medium (Lonza, Cat. 04-418Q) supplemented with rhActivin A (10ng/mL) (R&D Systems, Cat. 338-AC-0101), rhBMP4 (10ng/mL) (R&D Systems, Cat. 314-BP-010), rhVEGF (10ng/mL) (R&D Systems, Cat. 298-VS-005), rhFGF (10ng/mL) (R&D Systems, Cat. 233-FB-025), and ROCK inhibitor Y-27632 dihydrochloride (10μM) (Tocris, Cat. 1254). Cells were plated on Matrigel coated 6-well plates at 3.3 x 10^6 cells per well in 3mL. Media was

then changed daily with X-VIVO 15 supplemented with rhBMP4 (10ng/mL), rhVEGF (10ng/mL), and rhFGF (10ng/mL). At day 3.5, cells were washed 3 times with PBS and incubated with Accutase (Innovative Cell Technologies, Cat. AT-104), 1mL per well for 10m at 37C. Cells were harvested by dilution with MACS buffer (PBS, 0.5% bovine serum albumin, 2mM EDTA) followed by depletion of $CD326^+$ (EPCAM) cells by magnetic cell sorting (MACS) using CD326 (EPCAM) MicroBeads (Miltenyi, Auburn, CA, Cat. 130-061-101). In addition, EMPs derived from *RAG1*$^{-/-}$*RAG2*$^{-/-}$*B2M*$^{-/-}$ triple knockout (TKO) PSCs were stained with PE-conjugated B2M antibody and then depleted of $B2M^+$ cells by MACS using Anti-PE MicroBeads (Miltenyi, Auburn, CA, Cat. 130-048-801).

Human pluripotent stem cell-derived EMO and ATO cultures

EMOs and ATOs were generated as previously described[32]. Briefly, sequential generation of EMOs and then ATOs was accomplished in 3D aggregates through changing media **(Figure 1.2 C-D**). EMOs were established by aggregating purified EMPs with MS5-hDLL4 cell. MS5-hDLL4 cells were harvested by trypsinization and resuspended in hematopoietic induction media comprised of EGM2 (Lonza, Cat. CC-4176) supplemented with ROCK inhibitor Y-27632 dihydrochloride (10μM) (Tocris Bioscience, Cat. 1254) and TGF-bRI inhibitor SB-431542 ("SB Blocker") (10μM) (Tocris Bioscience, Cat. 1614). At Day -14, 5 x 10^5 MS5-hDLL4 cells were combined with 5 x 10^4 (H1) or 1 x 10^5 (ESI017) purified EMPs per ATO in 1.5mL Eppendorf tubes and centrifugated at 300 x g for 5m at 4C in a swinging bucket centrifuge.

Multiple (up to 180) EMOs were prepared per tube. Supernatants were carefully removed and the cell pellet was resuspended by brief vortexing and resuspended in

hematopoietic induction medium at a volume of 5mL per EMO. 3 EMOs were individually plated (5μL/EMO) on a 0.4mm Millicell transwell insert (EMD Millipore, Billerica, MA, Cat. PIMC0R5G50) and then placed in a 6-well plate containing 1mL of hematopoietic induction medium per well. Medium was changed every 2-3 days for 1 week with medium composed of EGM2 with SB Blocker (10mM). At Day 7, medium was changed to EGM2 + SB Blocker (10mM) with the hematopoietic cytokines, rhTPO 5ng/mL (R&D Systems, Cat. 288-TPN-025), rhFLT3L 5ng/mL (R&D Systems, Cat. 308-FK-025), and rhSCF 50ng/mL (R&D Systems, Cat. 255-SC-200). This medium was changed every 2-3 days for an additional 7 days. At Day 0, ATOs were initiated by simply changing the medium to “RB27” (described above) supplemented with 10ng/mL rhSCF, 5ng/mL rhFLT3L, and 5ng/mL rhIL-7 (R&D Systems, Cat. 207-IL-200). Medium was changed completely every 3-4 days.

Isolation of ATO-derived T cells

ATOs were harvested by adding MACS buffer (PBS, 0.5% bovine serum albumin, 2mM EDTA) to each filter, briefly disaggregating the ATO by pipetting with a 1mL “P1000” pipette, and then passed through a 50μm nylon strainer. For bulk-scale collection of ATOs, aggregates were harvested in a similar fashion; however, up to 150 aggregates were collected in a well filled with MACS buffer and then transferred onto a 50μm nylon filter, where aggregates were physically dissociated on top of the filter using the back end of a sterile 1mL syringe. After dissociation, the filter was washed with MACS buffer, and cell mixtures were centrifuged at 300 x g for 5m at 4C in a swinging bucket centrifuge.

Flow cytometry and antibodies

Staining for flow cytometry was performed in PBS with 0.5% BSA and 2mM EDTA for 15m at 4°C in the dark. TruStain FcX (Biolegend, San Diego, CA) was added to all samples for 5m prior to antibody staining. Tetramer staining with the PE-conjugated HLA-A*0201/NYESO1$_{157-165}$ tetramer (MBL International, Woburn, MA) at a 1:50 final dilution at room temperature for 20m prior to additional antibody staining for 15m at 4°C. DAPI was added to all samples prior to analysis.

Analysis was performed on a BD LSRII Fortessa, and FACS sorting on FACSARIA or FACSARIA-H instruments (BD Biosciences, San Jose, CA) at the UCLA Broad Stem Cell Research Center Flow Cytometry Core. For all analyses (except intracellular staining), DAPI+ cells were gated out, and doublets were removed through FSC-H vs. FSC-W and SSC-H vs SSC-W gating. Anti-human antibody clones for surface and intracellular staining were obtained from Biolegend (San Diego, CA): CD3 (UCHT1), CD4 (RPA-T4), CD5 (UCHT2), CD7 (CD7-6B7), CD8α (SK1), CD25 (BC96), CD27 (O323), CD28 (CD28.2), CD326 (EPCAM) (Clone 9C4), CD34 (581), CD45 (HI30), CD45RA (HI100), CD45RO (UCHL1), CD56 (HCD56), CD62L (DREG-56), CD107α (H4A3), B2M (2M2), CCR7 (G043H7), HLA-ABC (W6/32), IFNγ (4S.B3), IL-2 (MQ1-17H12), TCRαβ (IP26), TNFα (MAb11), Vβ13.1 (H131), 4-1BB (clone 4B4-1); and Miltenyi (San Jose, CA): CD8β (clone REA715). Anti-mouse CD29 (clone HMb1-1) was obtained from Biolegend (San Diego, CA). Flow cytometry data were analyzed with FlowJo software (Tree Star Inc.).

Quantification and Statistical Analysis

In all figures, n represents independent experiments and data are represented as mean ± standard error of the mean (SEM) as indicated. For all figures, statistical analysis was performed using GraphPad Prism software and p-values were calculated from the Wilcoxon rank sum test (Mann-Whitney U Test). The p-values are directly indicated on the figure, above the corresponding graphs. *$p < 0.05$; **$p < 0.01$; and ***$p < 0.001$ were considered statistically significant.

CHAPTER 3

Engineering the *in vitro* organoid microenvironment for positive selection of pluripotent stem cell-derived, antigen-specific, Class I MHC-null, cytotoxic T cells

3.1 Introduction

As previously mentioned, two main issues that arise with transplanting allogeneic, human pluripotent stem cell **(PSC)**-derived T cells for adoptive cell therapies **(ACTs)** are: alloreactive TCRs, which could result from randomly rearranged TCRs during T cell differentiation; and host rejection of allogeneic T cells due to mismatching human major histocompatibility complexes **(MHCs),** which could lead to GvHD and rejection of engineered, allogeneic cells. Chapter 3 addresses both of these logistical hurdles in developing PSC-derived, engineered allogeneic T cells for ACT; specifically, in the context of generating antigen-specific, Class I MHC-null, mature, naïve T cells *in vitro* from gene-edited PSCs.

Class I MHCs are expressed as heterodimers of human leukocyte antigen **(*HLA*)** proteins and the invariant light beta-2-microglobulin **(*B2M*)** on all cells, allowing the immune system to identify foreign antigens. Mismatches between Class I MHC heterodimers lead to Class I-mediated rejection by T cells from the host immune system, which would be particularly problematic for transplanting allogeneic T cells during ACT. Previous studies have demonstrated that CRISPR/Cas9-mediated knockout of *B2M* is sufficient in preventing ectopic Class I MHC expression[56,71]. Therefore, to generate a

Class I MHC-null phenotype in PSCs, *B2M* will be targeted for CRISPR/Cas9 gene editing in PSCs.

As Class I MHC proteins are expressed on the surface of PSCs, polyclonal knockouts can be enriched through flow cytometry. Class I MHC knockout in PSCs will employ a CRISPR/Cas9 gene editing strategy to generate double stranded breaks **(DSBs)** at the beginning of the *B2M* coding sequence, resulting in insertion deletion mutations **(INDELs)** from non-homologous end joining **(NHEJ)** DNA repair[63].

To generate antigen-specific, Class I MHC-null, mature, naïve T cells from PSCs, the recombination activating genes 1 and 2 **(*RAG1*** and ***RAG2*)** will also have to be removed. In Chapter 2 of this dissertation, clonal *RAG1*$^{-/-}$*RAG2*$^{-/-}$ double knockout **(DKO)** PSCs were generated from the ESI017 (HLA-A*0201^{neg}) parent line. After expansion and validation, DKO PSC clones were transduced to express the fully rearranged HLA-A*0201-restricted 1G4 TCR **(1G4 TCR**, hereafter**)** that recognizes the tumor associated tumor associated NYESO$_{157\text{-}165}$ peptide **(DKO+TCR,** hereafter**).** DKO+TCR PSCs from Chapter 2 will be used for CRISPR/Cas9 gene editing to generate polyclonal *RAG1*$^{-/-}$ *RAG2*$^{-/-}$*B2M*$^{-/-}$ triple knockout PSCs **(TKO+TCR,** hereafter**)**.

In Chapter 2, it was determined that positive selection of antigen-specific, mature, naïve, single positive CD8 T cells **(SP8**, hereafter**)** from DKO+TCR PSCs is dependent on cognate MHC expression. Due to its polyclonal nature, TKO+TCR PSCs will be exclusively generated from DKO+TCR PSCs derived from the HLA-A*0201^{neg} ESI017 parent PSC line as an additional control for inefficient gene editing or purification by flow cytometry[50].

As positive selection is dependent on TCR interactions with peptide-MHC **(pMHC)**, T cell differentiation is expected to be blocked at the DP T precursor stage in the absence of human Class I MHC. Positive selection of DP T precursor cells will be dependent on accessory, non-PSC-derived, cells expressing pMHCs during T cell differentiation. As the "Artificial Thymic Organoid" **(ATO)** system uses the murine MS5 bone marrow stromal cell line transduced to express the Notch ligand, delta-like ligand 4 **(*hDLL4*)**, to induce orderly T-lineage commitment and differentiation from PSCs *in vitro*, these accessory cells could be modified to express human Class I MHCs and present pMHCs for positive selection[32].

While the murine MS5 cell line is not human-derived, studies have demonstrated that endogenously processed murine peptides can induce positive selection of human stem cell-derived antigen-specific T cells in transplantation studies with transgenic mice expressing human MHC[18,72]. In this Chapter, we will determine if these observations can be recapitulated to induce positive selection of DP T cell precursors *in vitro*. Generation of antigen-specific, Class I MHC-null, mature, naïve SP8 T cells from TKO+TCR PSCs will be dependent on TCR-pMHC interactions between human DP T cell precursors and engineered murine MS5 stroma.

3.2 Results

3.2.1 Generation of Class I MHC-null PSCs via *hB2M* knockout in DKO PSCs

As surface expression of Class I MHC is dependent on dimerization with *beta-2-microglobulin* **(*B2M*)**, CRISPR/Cas9 gRNAs were designed to target the beginning of the *B2M* coding sequence to generate insertion deletion mutations **(Figures 3.1A-E)**. The optimal guide was used remove all Class I MHC expression in ESI017 DKO+TCR PSCs producing so-called triple knockout **(TKO)** PSCs **(Figure 3.1F).** Edited cells were isolated by flow cytometry based on a Class I MHC-null phenotype (HLA-A,B,C^{-}B2M^{-}) **(Figure 3.1F)**, yielding ESI017 RAG1$^{-/-}$RAG2$^{-/-}$B2M$^{-/-}$ TKO PSC lines **(TKO+TCR**, hereafter**)**. Fully edited TKO+TCR PSCs were expanded to confirm growth and morphology were unchanged from the parent ESI017 line, and determined to be karyotypically normal.

3.2.2 Engineering the organoid microenvironment to support positive selection of Class I MHC-null TKO PSCs

As Class I MHC molecules were ablated in TKO+TCR PSCs, positive selection could not be achieved through transgenic TCR expression alone. Therefore, to provide a positive selection signal for developing DP T precursors from TKO+TCR PSCs, the MS5-hDLL4 line (**hDLL4**, hereafter) was transduced to express the cognate MHC for the 1G4 TCR, HLA-A*0201 with or without human beta-2-microglobulin **(*hB2M*)**, generating the hDLL4-A*0201-hB2M **("hDLL4-A02B")** and hDLL4-A*0201 **("hDLL4-A02")** lines, respectively. To support positive selection, a subset of the hDLL4-A02B stroma was transduced to also express the extracellular matrix factor, intercellular adhesion molecule

1 **(ICAM**), which has been shown to increase signaling strength through TCR and survival of T cells by interacting with lymphocyte function-associated antigen 1 **(*LFA-1*)**[73–75]. The resulting hDLL4-A*0201-hB2M-ICAM stroma is hereafter referred to as **hDLL4-A02BI**.

Differentiation of WT+TCR PSCs was induced in the ATO using either standard hDLL4 or hDLL4-A02BI stroma, and progressed normally through development (**Figures 3.2A-B, 3.3A, and 3.4A)**, generating mature, naïve, antigen-specific SP8 T cells regardless of stromal conditions in the ATO **(Figure 3.2B)**. In contrast, development of T cells from TKO+TCR PSCs was halted at the DP stage of development under normal hDLL4 and hDLL4-A02 stromal conditions (**Figure 3.2B)**. However, DP T precursors generated from TKO+TCR PSCs were able to undergo positive selection to SP8 T cells in stromal conditions that expressed both HLA-A*0201 and *hB2M* (**Figures 3.2B, 3.5A, and 3.6A)**. Similarly, positive selection was also induced in HLA-A*0201^{neg} DKO+TCR DP T precursors in ATOs aggregated with hDLL4-A02B stroma **(Figure 3.S1A-B)**.

Interestingly, inclusion of ICAM in hDLL4-A02BI stroma did not impact the percentage of SP8 T cells in ATO cultures **(Figure 3.6A-B)**; however, the maximum output of SP8 T cells, measured over the course of differentiation, was significantly increased **(Figure 3.6C).** TKO+TCR SP8 T cells reached peak enrichment in organoid cultures after 6 weeks of T cell differentiation **(Figure 3.2C)**, and displayed a conventional, mature, naïve phenotype **(Figures 3.2D and 3.5A)**. In the absence of any Class I MHC, TKO+TCR-derived DP T precursors in ATO cultures decreased rapidly **(Figures 3.2C and 3.6B)**, similar to previous experiments with HLA-A*0201^{neg} DKO+TCR PSCs (**Figures 2.5B-C**).

Despite improved output from TKO+TCR PSCs with hDLL4-A02BI stroma, maximum SP8 T cell yield was still reduced in comparison to WT+TCR PSC-derived cultures **(Figure 3.2E)**. Similar to what we observed with DKO+TCR PSCs **(Figures 3.S1, and 2.5E)**, we hypothesized that this reduction could be due to mispairing between endogenous and exogenous TCR chains in WT+TCR SP8 T cells; such mispairing would be expected to be beneficial for positive selection by broadening the range of TCR-pMHC interactions capable of inducing positive selection. Furthermore, evidence of TCR mispairing is supported by the fact that the WT+TCR PSC line in these experiments is derived from the ESI017 parent PSC line, which does not express the cognate MHC of the 1G4 TCR, HLA-A*0201.

3.2.3 Allelic exclusion of endogenous TCR loci is complete in TKO+TCR, but not WT+TCR PSCs

To investigate the mechanism of MHC-restriction escape, TCR sequencing was performed on SP8 T cells generated from WT, WT+TCR, and TKO+TCR PSCs. SP8 T cells were isolated and sequenced using the 10X Genomics platform to detect exogenous and endogenous TCR Vα and Vβ chains at single-cell resolution. Sequencing results revealed that a significant portion of WT+TCR SP8 T cells, >65%, expressed endogenously rearranged TCRs in addition to the exogenous 1G4 TCR **(Figure 3.7A)**.

In addition to the exogenous TCR transgene, endogenously rearranged TCR Vα chains were detected in 65.86 ± 5.26% (mean ± SD) of WT+TCR SP8 T cells generated using hDLL4 stroma (n=2, 9492 cells total), and 65.62 ± 3.70% of cells generated with hDLL4-A02BI stroma (n=3, 11818 cells total). Similar to WT SP8 T cells, a diverse TCR

Vα repertoire was observed **(Figure 3.7B)**, indicating (as expected) that the exogenous TCR transgene was ineffective in suppressing endogenous TCR Vα rearrangement during T cell development, much like with previously reported observations obtained through activation-induced maturation of DP T cell precursors[57]

Interestingly, in addition to the exogenous 1G4 TCR, endogenously rearranged TCR Vβ chains were also detected in 16.78 ± 7.11% of WT+TCR SP8 T cells generated with hDLL4 stroma and 12.23 ± 3.26% of SP8 T cells generated with hDLL4-A02BI stroma **(Figure 3.7A)**. Typically, allelic exclusion of endogenous TCR Vβ loci is observed when an exogenous TCR is expressed prior to V(D)J recombination; however, these results indicate that allelic exclusion of the endogenous TCR Vβ was not absolute, at least in the context of *in vitro* PSC-differentiation of T cells **(Figure 3.7A)**[18,60]. While only a minority of T cells co-expressed endogenous TCR Vβ in addition to the exogenous TCR **(Figure 3.7A)**, they expressed a broad TCR Vβ repertoire similar to unedited cells **(Figure 3.7C)**. As expected, TKO+TCR SP8 T cells showed 100% contribution from the transgenic 1G4 TCR, confirming that *RAG1-RAG2* deletion prevented endogenous TCR rearrangement (n=3, 13874 cells total) **(Figure 3.7A-C)**.

Together, these experiments support the idea that reduction in selection efficiency and output of SP8 T cells from TKO+TCR PSCs may be due to the absence of mispairing events between exogenously and endogenously rearranged TCRs, resulting in limited opportunities for productive TCR-MHC interactions. Furthermore, combined with the previous observation that selection of DKO+TCR PSCs was HLA-A*0201-restricted **(Figures 2.5A-B, and 2.6A)**, these results demonstrate that ESI017 WT+TCR PSCs can escape HLA-A*0201-restriction of the exogenous 1G4 TCR through *RAG*-induced

endogenous TCR recombination. In summary, these experiments demonstrate that the ATO system can be engineered to induce positive selection of DP T precursors artificially in the absence of endogenous TCR and MHC expression.

3.2.4 Functional characterization of Class I MHC-null, antigen-specific SP8 T cells

WT+TCR and TKO+TCR SP8 T cells were isolated from ATO cultures and expanded with K562 artificial antigen-presenting cells **(aAPCs)** expressing the cognate antigen (NYESO) prior to functional assays. Similar to WT+TCR SP8 T cells, TKO+TCR SP8 T cells showed polyfunctional production of IFNγ, TNFα, and CD107a mobilization in response to stimulation with aAPCs expressing the cognate antigen (NYESO) but not irrelevant (MART1) peptide (**Figure 3.8A**); IL-2 expression was minimal. Overnight stimulation with cognate antigen demonstrated that TKO+TCR SP8 T cells upregulated surface CD25 and 4-1BB (**Figure 3.8B)** and underwent antigen-specific proliferation over 5 days after stimulation **(Figure 3.8C)**.

Complementary with the finding that WT+TCR expressed mismatched TCR chains **(Figure 3.7A-C)**, staining with the tetramer for the 1G4 TCR revealed that ~60% of WT+TCR SP8 T cells had mispaired TCRs at the surface, despite uniform expression of the transgenic Vβ13.1 TCR chain **(Figure 3.8D).** In contrast, TKO+TCR SP8 T cells retained a 1:1 ratio of 1G4 TCR tetramer and transgenic Vβ13.1 staining **(Figure 3.8D)**, and downregulated surface TCR in response to cognate antigen **(Figure 3.8E)**. Expanded TKO+TCR T cells also displayed potent antigen-specific cytotoxicity *in vitro* against K562 expressing NYESO but not MART1 pMHC at an effector-to-target ratio as low as 1:32 (**Figure 3.8F**). TKO+TCR SP8 T cells were able to undergo robust expansion, reaching

>250-fold expansion over 5 cycles of antigen-specific activation in the presence of IL-7 and IL-2 **(Figure 3.8G)**.

TKO+TCR and WT+TCR SP8 T cells were subjected to one freeze-thaw cycle and remained functional as they could be further expanded with K562 aAPCs expressing the cognate antigen (NYESO)**.** Following expansion, frozen SP8 T cells were used for *in vivo* tumor challenge in immune deficient (NOD-Scid-Gamma, NSG) mice intravenously (I.V.) engrafted with luciferase-expressing NALM6 tumor cells expressing the cognate antigen as a single chain trimer **(Figure 3.9A)**. Engraftment of NALM6 tumor was confirmed by imaging, before mice were stratified into groups (n=9) based on average bioluminescence readings **(Figure 3.9B)**. After stratification, SP8 T cells were injected retro-orbitally with the addition of IL-2 (10,000 IU/mouse) and dosed interperitoneally (I.P.). Monitoring of tumor progression was performed by imaging (2x / week), and I.P. IL-2 dosing continued throughout the course of the experiment (10,000 IU/mouse/dose) **(Figure 3.9B).** At the conclusion of the experiment, TKO+TCR SP8 T cells demonstrated significantly improved tumor control compared to mice that either received PBS with no T cells, or WT+TCR SP8 T cells **(Figure 3.9B-C)**.

A

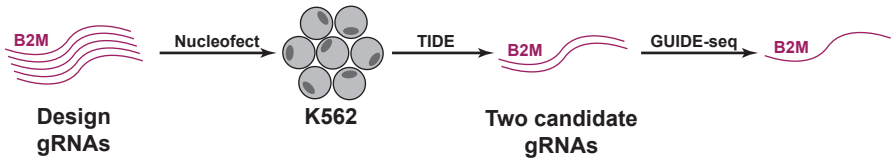

1 gRNA:
High on-target activity,
No off-target activity detected

B

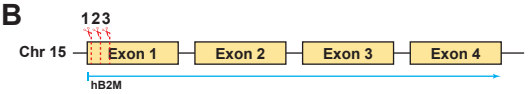

C

B2M (gRNA #)	gRNA sequence (PAM sequence included)	Specificity (*in silico* score)	Efficiency (*in silico* score)	INDEL % (*in vitro*, Plasmid)
1	TATAAGTGGAGGCGTCGCGCTGG	98.29	51.06	25.30%
2	GGCCGAGATGTCTCGCTCCGTGG	94.06	59.37	57.35%
3	GAGTAGCGCGAGCACAGCTAAGG	89.51	56.28	45.40%

D

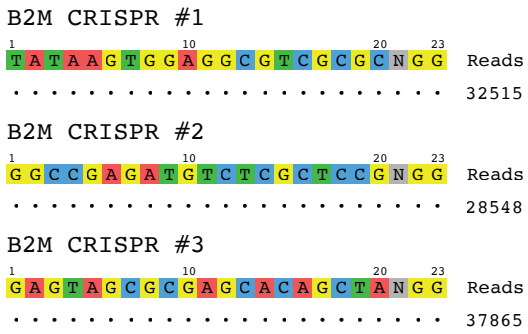

E

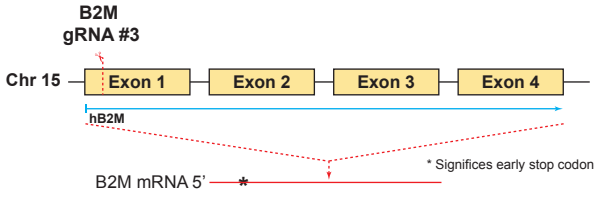

F

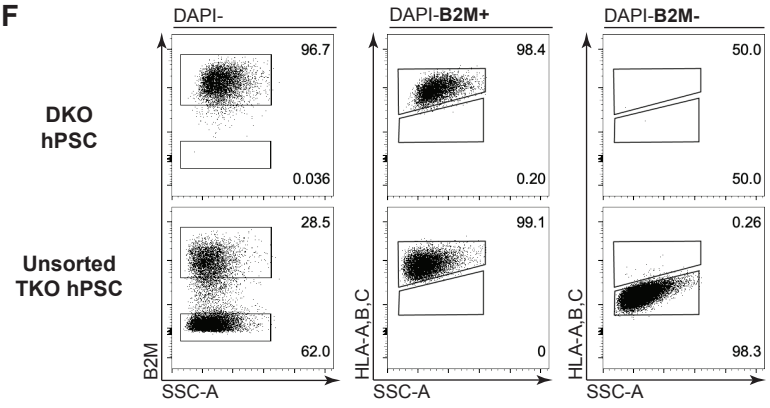

Figure 3.1 Generation of polyclonal *B2M* knockout PSCs by INDEL generation
(A) Schematic of the screening process for selecting 1 gRNA candidate for *B2M* with high on-target and low-off target activity in vitro. **(B)** Schematic of the region on Chromosome 11 containing the coding sequence of *B2M* where gRNAs were designed to target sites near the start of the coding sequence. **(C)** Summary of gRNA (black) and PAM (red) sequences and predicted on- and off-target scores for gRNAs targeting *B2M* . On-target activity in K562 cells is shown as the percentages of insertion deletion mutations (INDEL %) calculated via Sanger Sequencing (TIDE). **(D)** Off-target gRNA activity analysis via the GUIDE-seq method. On-target reads are represented by ".", and off-target reads are denoted by their mismatched bases. **(E)** Design of the gene knockout strategy of B2M in PSCs using *B2M* gRNA #3. As surface expression of Class I MHC is dependent on dimerization with B2M, INDELs that resulted in early stop codons would be sufficient for generating knockouts that can be purified through FACS sorting. **(F)** Sorting strategy for purifying Class I MHC-null PSCs by flow cytometry. Phenotype of knockout PSCs are shown with HLA-A,B,C and B2M staining.

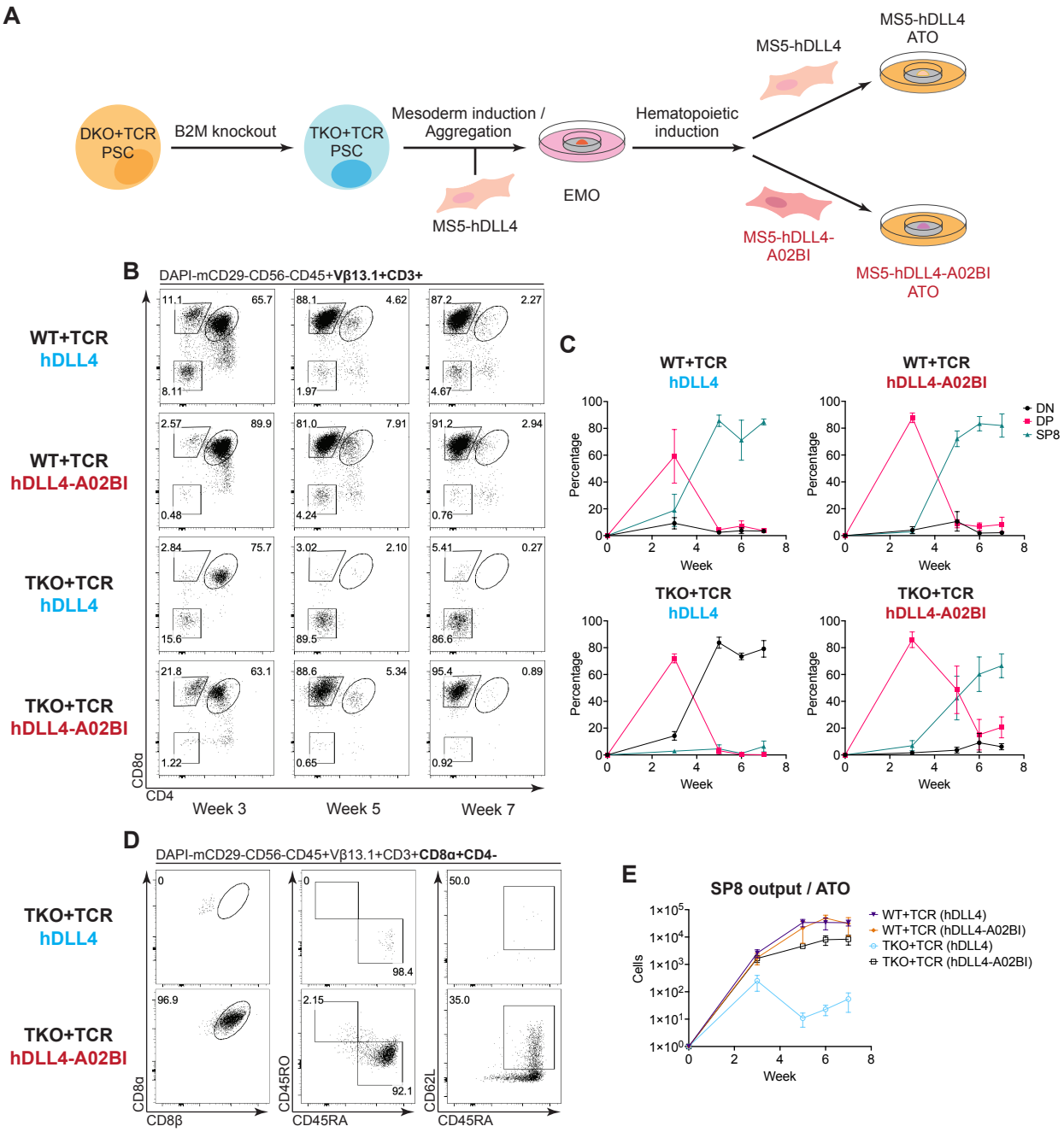
A
DKO+TCR PSC
B2M knockout
TKO+TCR PSC
Mesoderm induction / Aggregation
MS5-hDLL4
EMO
Hematopoietic induction
MS5-hDLL4
MS5-hDLL4 ATO
MS5-hDLL4-A02BI
MS5-hDLL4-A02BI ATO
B
DAPI-mCD29-CD56-CD45+Vβ13.1+CD3+
WT+TCR hDLL4
WT+TCR hDLL4-A02BI
TKO+TCR hDLL4
TKO+TCR hDLL4-A02BI
CD8α
CD4
Week 3
Week 5
Week 7
C
WT+TCR hDLL4
WT+TCR hDLL4-A02BI
TKO+TCR hDLL4
TKO+TCR hDLL4-A02BI
Percentage
Week
DN
DP
SP8
D
DAPI-mCD29-CD56-CD45+Vβ13.1+CD3+CD8α+CD4-
TKO+TCR hDLL4
TKO+TCR hDLL4-A02BI
CD8α
CD8β
CD45RO
CD45RA
CD62L
CD45RA
E
SP8 output / ATO
Cells
Week
WT+TCR (hDLL4)
WT+TCR (hDLL4-A02BI)
TKO+TCR (hDLL4)
TKO+TCR (hDLL4-A02BI)

Figure 3.2 Engineering the ATO system to express HLA-A*0201 rescues differentiation of 1G4 TCR-transduced *RAG1/RAG2/B2M* triple knockout PSCs

(A) Schematic of the process for generating TKO+TCR PSCs. ESI017 DKO+TCR PSC clones were gene-edited to knockout *B2M* and then FACS-purified to generate the polyclonal ESI017 TKO+TCR line. Following hematopoietic induction, EMOs were harvested and then aggregated with either MS5-hDLL4 (hDLL4) or MS5-hDLL4-A0201-hB2M-ICAM (hDLL4-A02BI) stroma for ATO T cell differentiation. **(B)** Differentiation kinetics of WT+TCR and TKO+TCR T cells with MS5- hDLL4 or hDLL4-A02BI at the indicated time points of ATO differentiation, using gates as shown. **(C)** Frequency of precursor and mature T cell populations, from gating shown in (B) at the indicated time points (mean ± SEM; n=3 independent experiments for WT+TCR and n=4 for TKO+TCR). Populations defined as: double negative (DN, $CD8\alpha^{-}CD4^{-}$), double positive (DP, $CD8\alpha^{+}CD4^{+}$), single positive CD8 (SP8, $CD8\alpha^{+}CD4^{-}CD8\beta^{+}$). **(D)** At 7 weeks of T cell differentiation, TKO+TCR PSC-derived SP8 T cells were analyzed for maturation markers of conventional T cells. **(E)** Number of WT+TCR and TKO+TCR SP8 T cells per ATO aggregate with hDLL4 or hDLL4-A02BI (mean ± SEM, n=3 independent experiments for WT+TCR, and n=4 for TKO+TCR conditions)

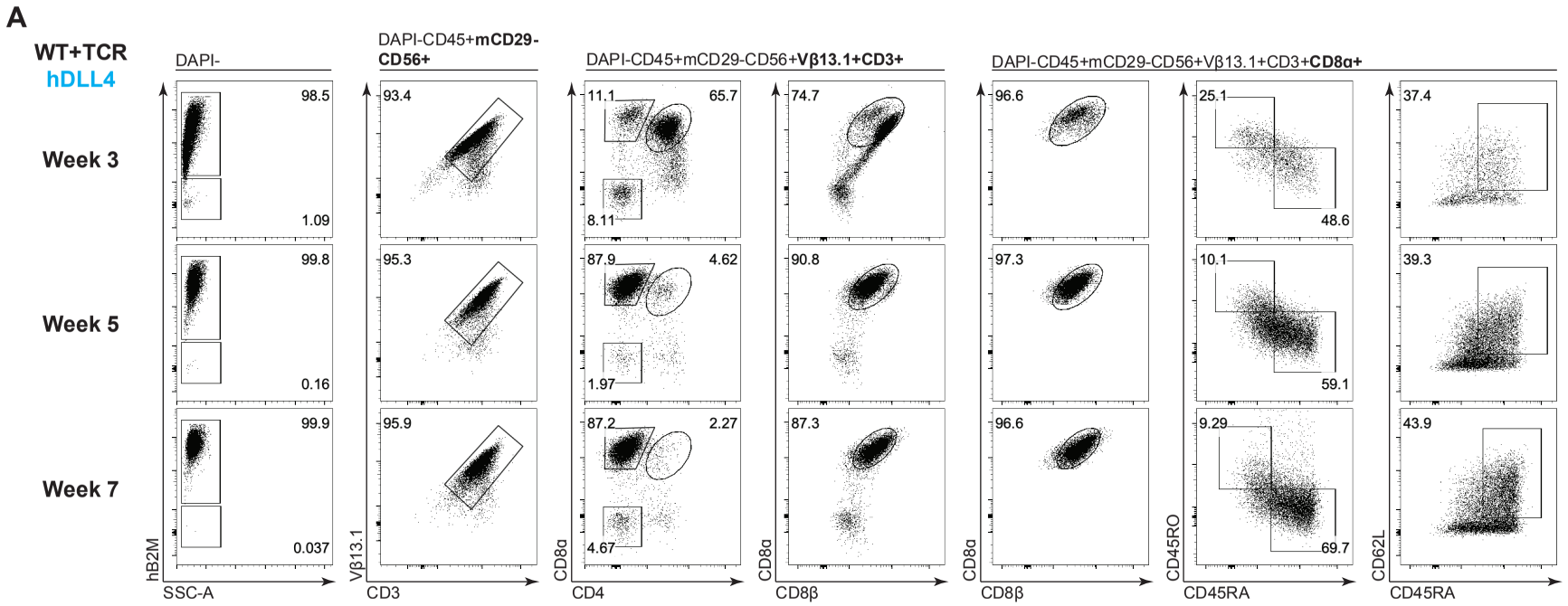
A
WT+TCR
hDLL4
Week 3
Week 5
Week 7
DAPI-
DAPI-CD45+mCD29-CD56+
DAPI-CD45+mCD29-CD56+Vβ13.1+CD3+
DAPI-CD45+mCD29-CD56+Vβ13.1+CD3+CD8α+
98.5
1.09
99.8
0.16
99.9
0.037
93.4
95.3
95.9
11.1
65.7
8.11
87.9
4.62
1.97
87.2
2.27
4.67
74.7
90.8
87.3
96.6
97.3
96.6
25.1
48.6
10.1
59.1
9.29
69.7
37.4
39.3
43.9
hB2M
SSC-A
Vβ13.1
CD3
CD8α
CD4
CD8α
CD8β
CD8α
CD8β
CD45RO
CD45RA
CD62L
CD45RA

Figure 3.3 Differentiation kinetics and gating strategy of WT+TCR PSCs with MS5-hDLL4 stroma in the ATO system

(A) At the indicated time points during T cell differentiation, representative flow cytometry analysis (n=3) of maturation markers for conventional T cells from ATOs aggregated with ESI017 WT+TCR PSCs and MS5-hDLL4 stroma.

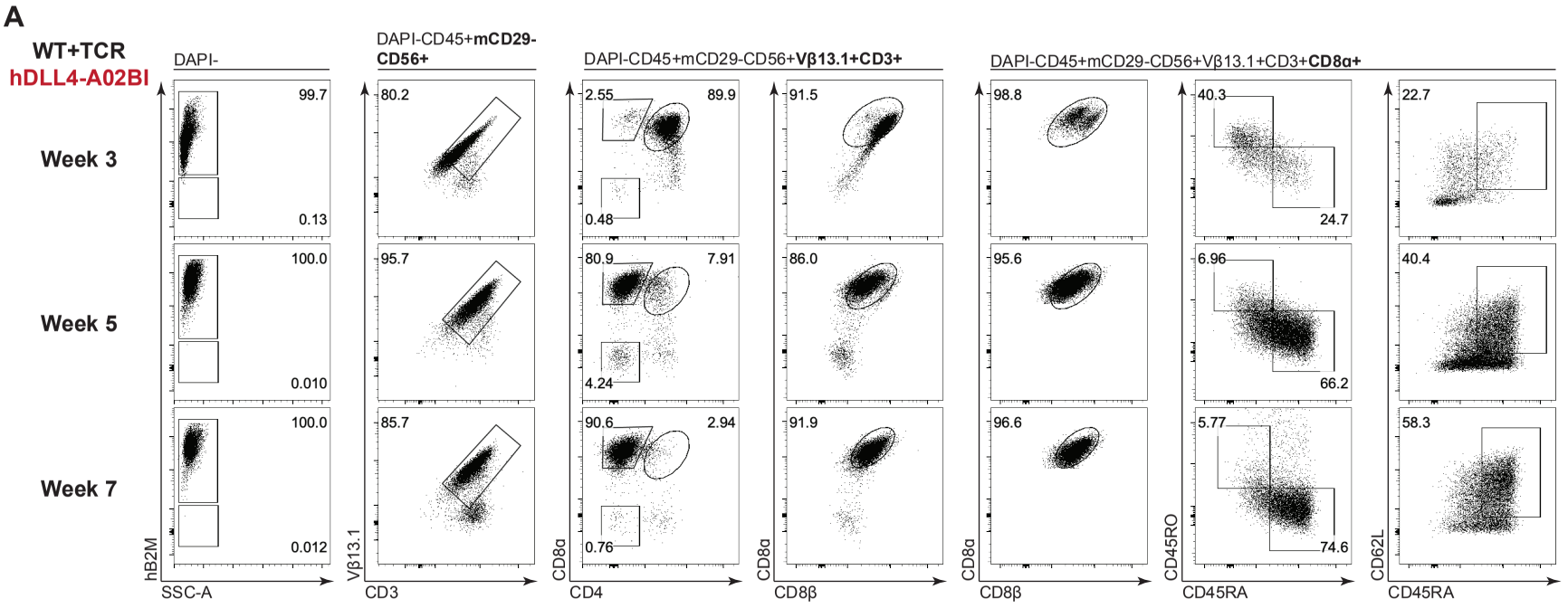
A
WT+TCR
hDLL4-A02BI
Week 3
Week 5
Week 7
DAPI-
DAPI-CD45+mCD29-CD56+
DAPI-CD45+mCD29-CD56+Vβ13.1+CD3+
DAPI-CD45+mCD29-CD56+Vβ13.1+CD3+CD8α+
99.7
0.13
100.0
0.010
100.0
0.012
hB2M
SSC-A
80.2
95.7
85.7
Vβ13.1
CD3
2.55
89.9
0.48
80.9
7.91
4.24
90.6
2.94
0.76
CD8α
CD4
91.5
86.0
91.9
CD8α
CD8β
98.8
95.6
96.6
CD8α
CD8β
40.3
24.7
6.96
66.2
5.77
74.6
CD45RO
CD45RA
22.7
40.4
58.3
CD62L
CD45RA

Figure 3.4 Differentiation kinetics and gating strategy for WT+TCR PSCs with MS5-hDLL4-A02BI stroma in the ATO system

(A) At the indicated time points during T cell differentiation, representative flow cytometry analysis (n=3) of maturation markers for conventional T cells from ATOs aggregated with ESI017 WT+TCR PSCs and MS5-hDLL4-A02BI stroma.

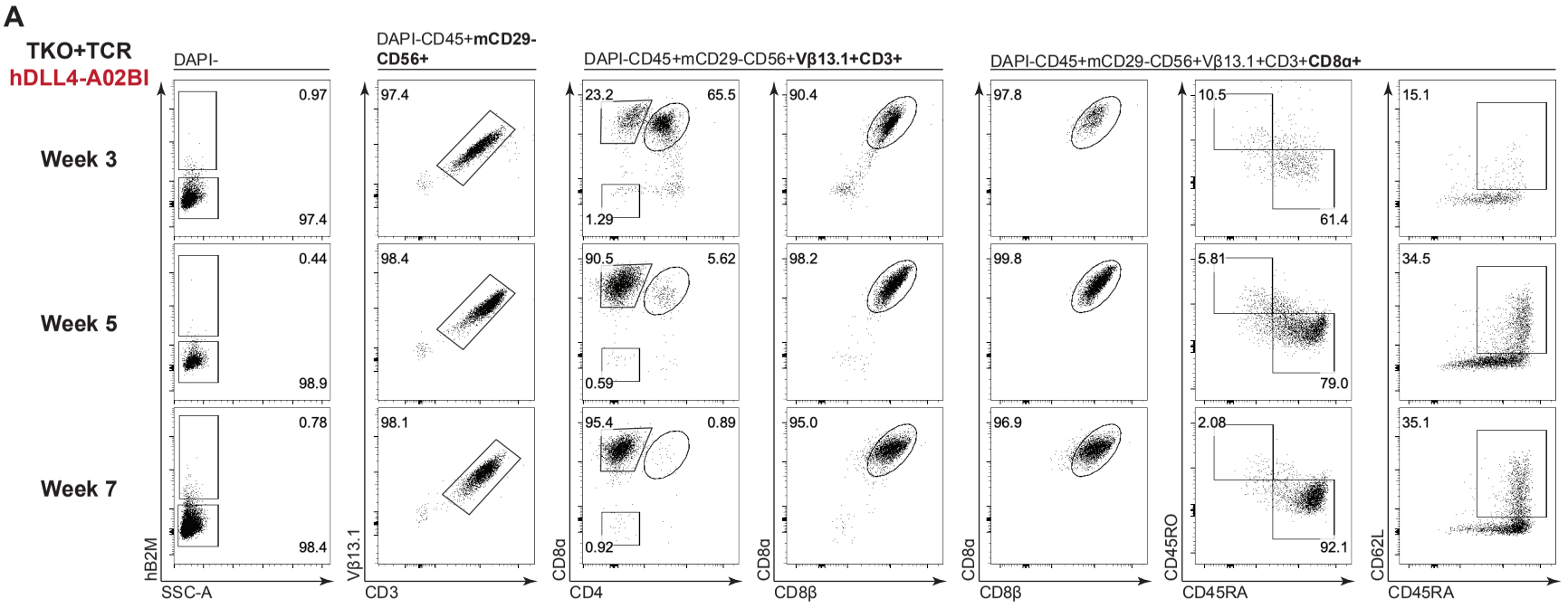
A
TKO+TCR
hDLL4-A02BI
Week 3
Week 5
Week 7
DAPI-
DAPI-CD45+mCD29-CD56+
DAPI-CD45+mCD29-CD56+Vβ13.1+CD3+
DAPI-CD45+mCD29-CD56+Vβ13.1+CD3+CD8α+
0.97
97.4
0.44
98.9
0.78
98.4
97.4
98.4
98.1
23.2
65.5
1.29
90.5
5.62
0.59
95.4
0.89
0.92
90.4
98.2
95.0
97.8
99.8
96.9
10.5
61.4
5.81
79.0
2.08
92.1
15.1
34.5
35.1
hB2M
SSC-A
Vβ13.1
CD3
CD8α
CD4
CD8α
CD8β
CD8α
CD8β
CD45RO
CD45RA
CD62L
CD45RA

Figure 3.5 Differentiation kinetics and gating strategy for TKO+TCR PSCs with MS5-hDLL4-A02BI stroma in the ATO system

(A) At the indicated time points during T cell differentiation, representative flow cytometry analysis (n=4) of maturation markers for conventional T cells from ATOs aggregated with ESI017 TKO+TCR PSCs and MS5-hDLL4-A02BI stroma.

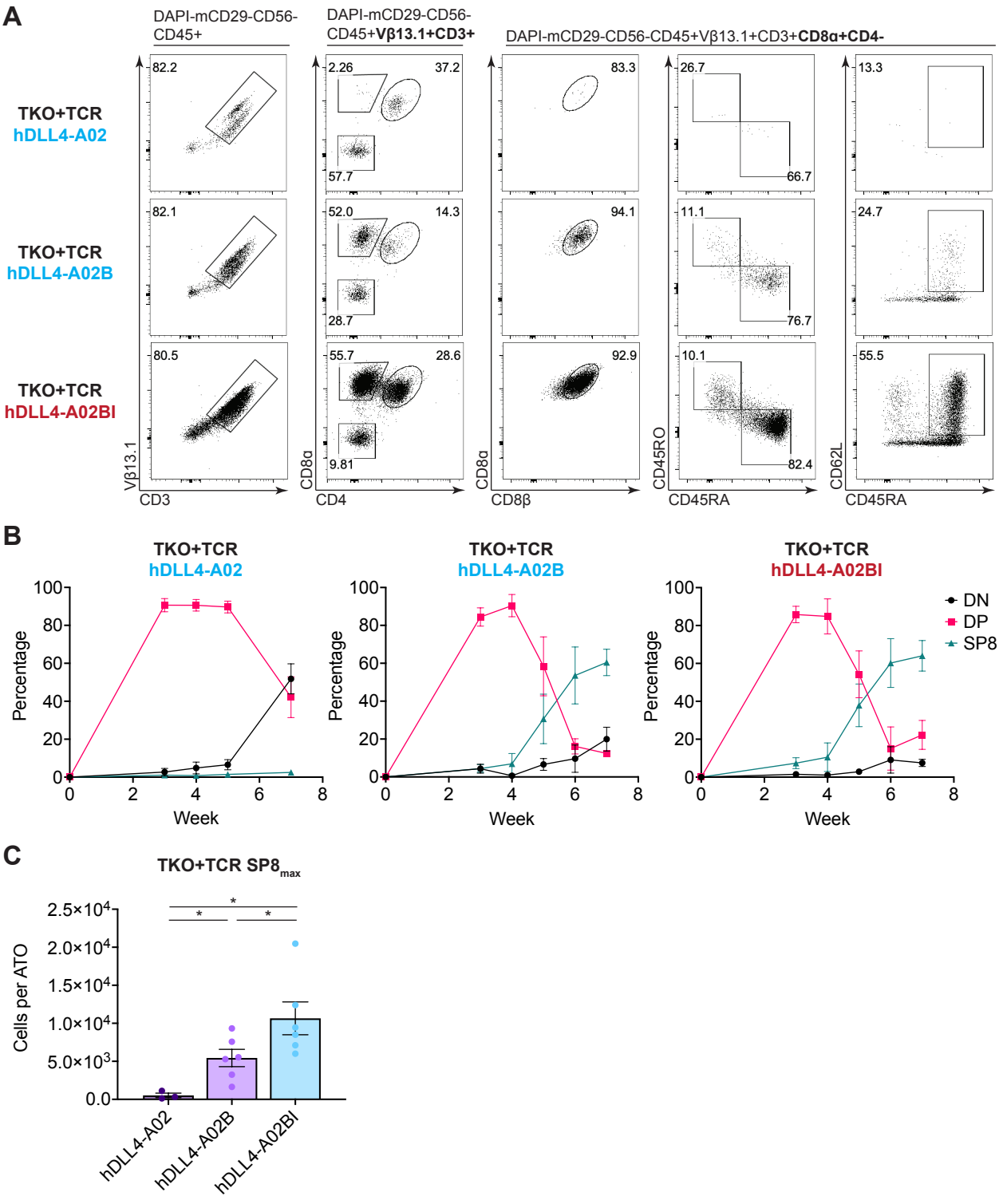
A
DAPI-mCD29-CD56-CD45+
DAPI-mCD29-CD56-CD45+Vβ13.1+CD3+
DAPI-mCD29-CD56-CD45+Vβ13.1+CD3+CD8α+CD4-
TKO+TCR hDLL4-A02
TKO+TCR hDLL4-A02B
TKO+TCR hDLL4-A02BI
82.2
2.26
37.2
57.7
83.3
26.7
66.7
13.3
82.1
52.0
14.3
28.7
94.1
11.1
76.7
24.7
80.5
55.7
28.6
9.81
92.9
10.1
82.4
55.5
Vβ13.1
CD3
CD8α
CD4
CD8α
CD8β
CD45RO
CD45RA
CD62L
CD45RA
B
TKO+TCR hDLL4-A02
TKO+TCR hDLL4-A02B
TKO+TCR hDLL4-A02BI
Percentage
Week
DN
DP
SP8
C
TKO+TCR SP8max
Cells per ATO
2.5×10^4
2.0×10^4
1.5×10^4
1.0×10^4
5.0×10^3
0.0
hDLL4-A02
hDLL4-A02B
hDLL4-A02BI

Figure 3.6 Generation of Class I MHC-null, positively selected, antigen-specific SP8 T cells from TKO+TCR PSCs is dependent on *hB2M* transduction in MS5-hDLL4-A*0201 stromal cells, and improved by the addition of *ICAM*

(A) Representative flow cytometry plots from ESI017 TKO PSCs transduced with the HLA-A*0201-restricted 1G4 TCR recognizing the $NYESO1_{157-165}$ peptide (TKO+TCR), and differentiated 7 weeks in the ATO system with the following stromal conditions: MS5-hDLL4-A*0201(hDLL4-A02), MS5-hDLL4-A*0201-hB2M (hDLL4-A02B), MS5-hDLL4-A*0201-hB2M-ICAM1 (hDLL4-A02BI). After 7 weeks of T cell differentiation, TKO+TCR PSC-derived ATOs were analyzed for maturation markers of conventional T cells. **(B)** Frequency of T cell phenotypes (i.e., double negative (DN), double positive (DP), and SP8 T cells) over seven weeks of differentiation with specialized stroma (n=3 independent experiments for hDLL4-A02, and n=6 for both hDLL4-A02B and hDLL4-A02BI). **(C)** Maximum output of SP8 T cells produced from TKO+TCR PSCs (shown as cells per ATO organoid) with each ATO stromal condition, calculated from every analysis point during T cell differentiation. Mean ± SEM (*$p<0.05$) are shown for each stromal condition (n=3 for hDLL4-A02, n=6 for both hDLL4-A02B and hDLL4-A02BI).

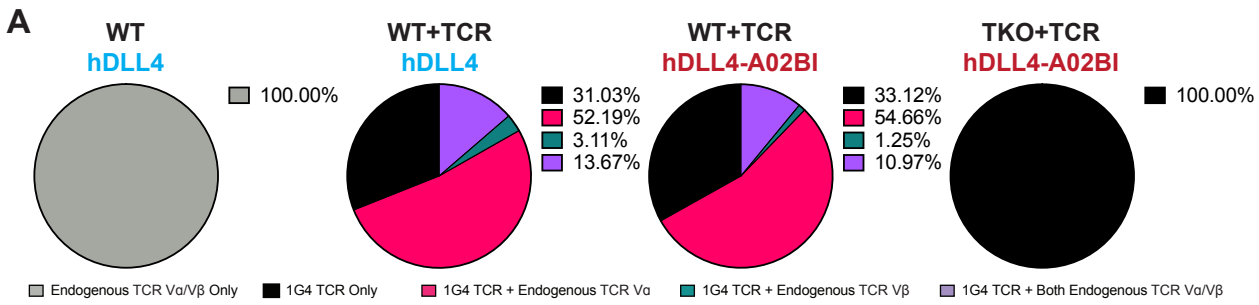
A
WT
hDLL4
100.00%
WT+TCR
hDLL4
31.03%
52.19%
3.11%
13.67%
WT+TCR
hDLL4-A02BI
33.12%
54.66%
1.25%
10.97%
TKO+TCR
hDLL4-A02BI
100.00%
Endogenous TCR Vα/Vβ Only
1G4 TCR Only
1G4 TCR + Endogenous TCR Vα
1G4 TCR + Endogenous TCR Vβ
1G4 TCR + Both Endogenous TCR Vα/Vβ

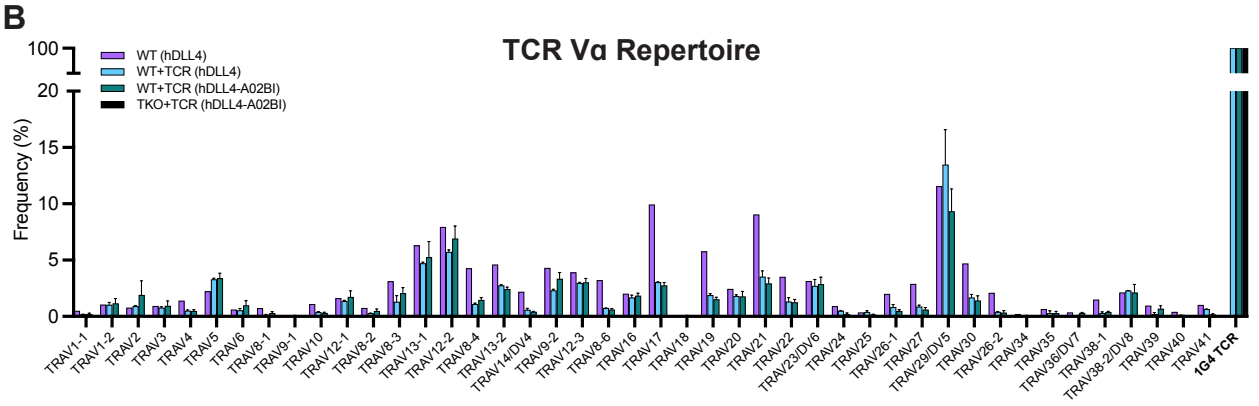
B
TCR Vα Repertoire
WT (hDLL4)
WT+TCR (hDLL4)
WT+TCR (hDLL4-A02BI)
TKO+TCR (hDLL4-A02BI)
Frequency (%)
100
20
15
10
5
0
TRAV1-1
TRAV1-2
TRAV2
TRAV3
TRAV4
TRAV5
TRAV6
TRAV8-1
TRAV9-1
TRAV10
TRAV12-1
TRAV8-2
TRAV8-3
TRAV13-1
TRAV12-2
TRAV8-4
TRAV13-2
TRAV14/DV4
TRAV9-2
TRAV12-3
TRAV8-6
TRAV16
TRAV17
TRAV18
TRAV19
TRAV20
TRAV21
TRAV22
TRAV23/DV6
TRAV24
TRAV25
TRAV26-1
TRAV27
TRAV29/DV5
TRAV30
TRAV26-2
TRAV34
TRAV35
TRAV36/DV7
TRAV38-1
TRAV38-2/DV8
TRAV39
TRAV40
TRAV41
1G4 TCR

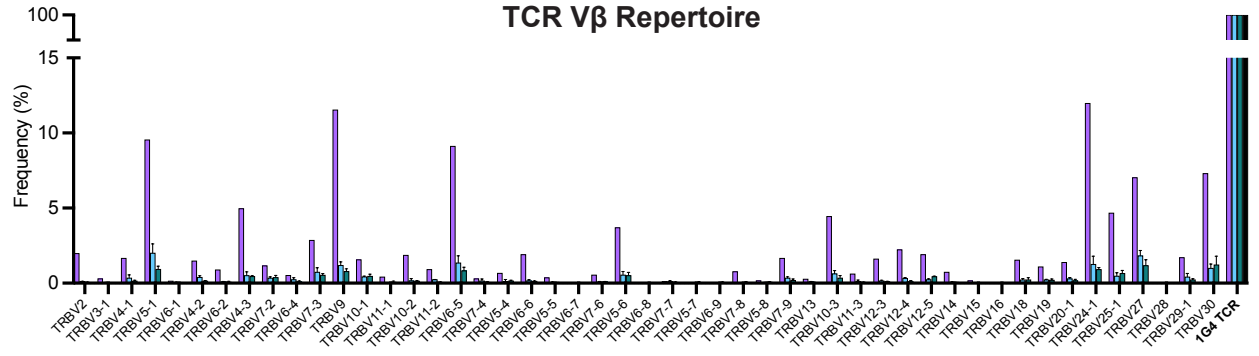
C
TCR Vβ Repertoire
Frequency (%)
100
15
10
5
0
TRBV2
TRBV3-1
TRBV4-1
TRBV5-1
TRBV6-1
TRBV4-2
TRBV6-2
TRBV4-3
TRBV7-2
TRBV6-4
TRBV7-3
TRBV9
TRBV10-1
TRBV11-1
TRBV10-2
TRBV11-2
TRBV6-5
TRBV7-4
TRBV5-4
TRBV6-6
TRBV5-5
TRBV6-7
TRBV7-6
TRBV5-6
TRBV6-8
TRBV7-7
TRBV5-7
TRBV6-9
TRBV7-8
TRBV5-8
TRBV7-9
TRBV13
TRBV10-3
TRBV11-3
TRBV12-3
TRBV12-4
TRBV12-5
TRBV14
TRBV15
TRBV16
TRBV18
TRBV19
TRBV20-1
TRBV24-1
TRBV25-1
TRBV27
TRBV28
TRBV29-1
TRBV30
1G4 TCR

Figure 3.7 Allelic exclusion of endogenous TCR chains by an exogenous TCR is incomplete in RAG1/RAG2¬-competent WT PSCs

(A) After 6 weeks of T cell differentiation, mature naïve SP8 T cells were isolated for TCR repertoire analysis at single cell resolution from the following ATO conditions: WT PSCs and hDLL4 stroma (n=1), WT+TCR PSCs and hDLL4 stroma (n=2), WT+TCR PSCs and hDLL4-A02BI stroma (n=3), TKO+TCR PSCs and hDLL4-A02BI stroma (n=3). Pie charts demonstrating the ratios of barcoded cells that expressed full contigs of only endogenous TCR Vα/Vβ chains (gray), only 1G4 TCR chains (black), 1G4 TCR and endogenous TCR Vα chains (pink), 1G4 TCR and endogenous TCR Vβ chains (green), and 1G4 TCR and both endogenous TCR Vα/Vβ chains (purple). **(B-C)** TCR Vα **(B)** and TCR Vβ diversity **(C)** from mature, naïve SP8 T cells isolated for TCR repertoire analysis at single cell resolution. WT PSCs and hDLL4 stroma (purple, n=1, 4021 cells total), WT+TCR PSCs and hDLL4 stroma (blue, n=2, 9492 cells total), WT+TCR PSCs and hDLL4-A02BI stroma (green, n=3, 11818 cells total), TKO+TCR PSCs and hDLL4-A02BI stroma (black, n=3, 13874 cells total).

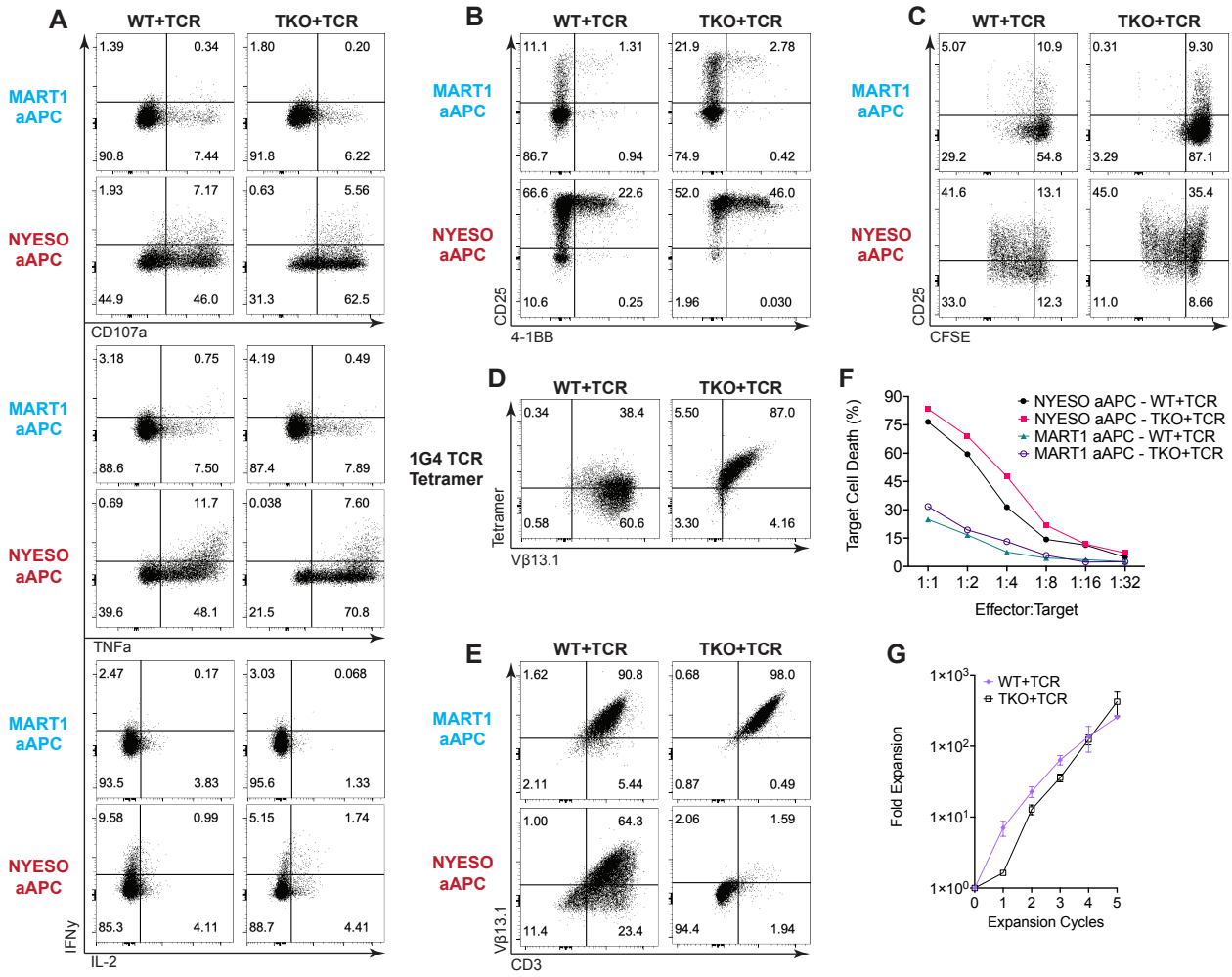
A
WT+TCR
TKO+TCR
MART1 aAPC
NYESO aAPC
1.39
0.34
90.8
7.44
1.80
0.20
91.8
6.22
1.93
7.17
44.9
46.0
0.63
5.56
31.3
62.5
CD107a
3.18
0.75
88.6
7.50
4.19
0.49
87.4
7.89
0.69
11.7
39.6
48.1
0.038
7.60
21.5
70.8
TNFa
2.47
0.17
93.5
3.83
3.03
0.068
95.6
1.33
9.58
0.99
85.3
4.11
5.15
1.74
88.7
4.41
IFNy
IL-2
B
WT+TCR
TKO+TCR
MART1 aAPC
NYESO aAPC
11.1
1.31
86.7
0.94
21.9
2.78
74.9
0.42
66.6
22.6
10.6
0.25
52.0
46.0
1.96
0.030
CD25
4-1BB
C
WT+TCR
TKO+TCR
MART1 aAPC
NYESO aAPC
5.07
10.9
29.2
54.8
0.31
9.30
3.29
87.1
41.6
13.1
33.0
12.3
45.0
35.4
11.0
8.66
CD25
CFSE
D
WT+TCR
TKO+TCR
1G4 TCR Tetramer
0.34
38.4
0.58
60.6
5.50
87.0
3.30
4.16
Tetramer
Vβ13.1
E
WT+TCR
TKO+TCR
MART1 aAPC
NYESO aAPC
1.62
90.8
2.11
5.44
0.68
98.0
0.87
0.49
1.00
64.3
11.4
23.4
2.06
1.59
94.4
1.94
Vβ13.1
CD3
F
NYESO aAPC - WT+TCR
NYESO aAPC - TKO+TCR
MART1 aAPC - WT+TCR
MART1 aAPC - TKO+TCR
Target Cell Death (%)
90
75
60
45
30
15
0
1:1
1:2
1:4
1:8
1:16
1:32
Effector:Target
G
WT+TCR
TKO+TCR
Fold Expansion
1×10^3
1×10^2
1×10^1
1×10^0
0
1
2
3
4
5
Expansion Cycles

Figure 3.8 Functional characterization of TKO+TCR PSC-derived, antigen-specific T cells *in vitro*
(A) WT+TCR and TKO+TCR (1G4 TCR) SP8 T cells were isolated from week 6 ATOs generated with hDLL4-A02BI stroma and expanded with K562 artificial antigen-presenting cells (aAPCs) expressing the cognate antigen (NYESO), IL-2, and IL-7 prior to in vitro functional assays. After 7 days, cytokine production and CD107a upregulation were assayed in response to K562 aAPCs presenting irrelevant (MART1) or cognate (NYESO) antigen as a single chain trimer. Data are representative of 3 independent experiments. **(B)** Upregulation of activation markers CD25 and 4-1BB on WT+TCR and TKO+TCR SP8 T cells in response to MART1 or NYESO aAPCs for 24hrs. **(C)** Proliferation (as measured by CFSE) of WT+TCR and TKO+TCR SP8 T cells in response to MART1 or NYESO aAPCs for 5 days. **(D)** Staining with the tetramer specific for 1G4 TCR and the Vβ13.1 chain of 1G4 TCR on WT+TCR and TKO+TCR SP8 T cells, 6 days post-expansion with NYESO aAPCs. **(E)** Downregulation of transgenic 1G4 TCR (measured by Vβ13.1) and CD3 on WT+TCR and TKO+TCR SP8 T cells in response to culture with MART1 or NYESO aAPCs for 24hrs. **(F)** In vitro cytotoxicity of WT+TCR and TKO+TCR SP8 T cells against MART1 or NYESO aAPCs. Cell killing is shown as the percentage of target cells positive for Apotracker™ Green binding at 6hrs, at the indicated effector to target cell ratios. **(G)** Post-ATO expansion of WT+TCR and TKO+TCR SP8 T cells in response to cognate NYESO aAPCs, IL-2, and IL-7 (mean ± SEM shown; data are representative of 2 independent experiments).

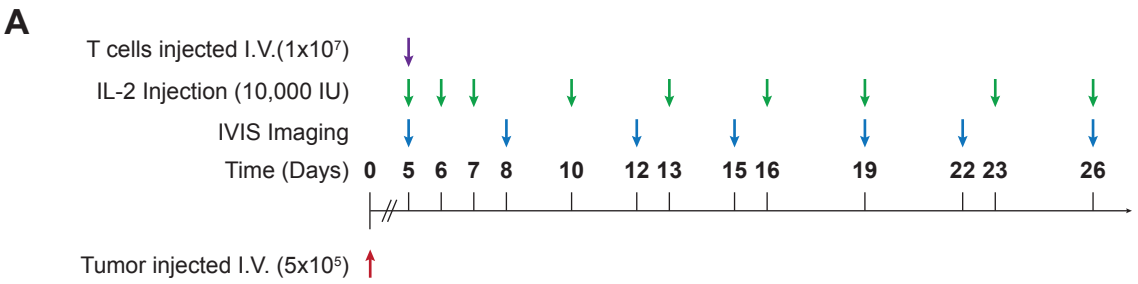
A
T cells injected I.V.(1x10⁷)
IL-2 Injection (10,000 IU)
IVIS Imaging
Time (Days) 0 5 6 7 8 10 12 13 15 16 19 22 23 26
Tumor injected I.V. (5x10⁵)

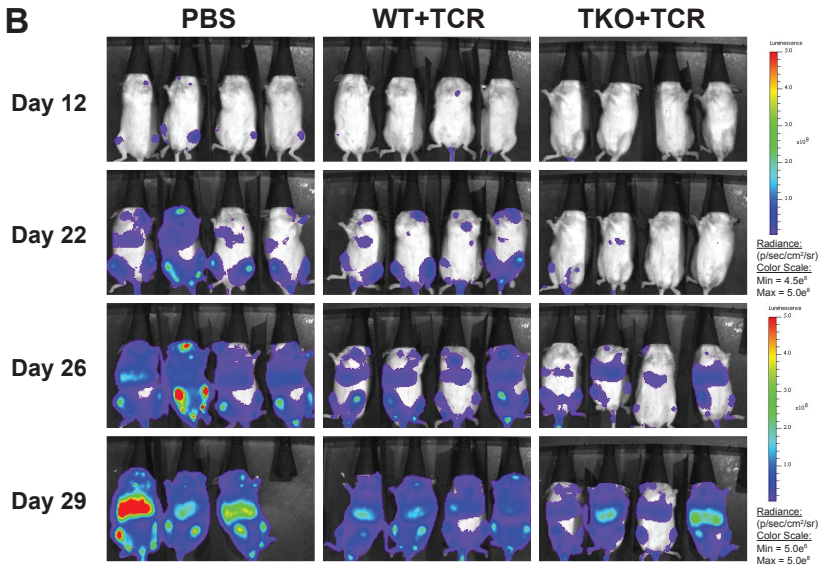
B
PBS
WT+TCR
TKO+TCR
Day 12
Day 22
Day 26
Day 29
Radiance: (p/sec/cm²/sr)
Color Scale:
Min = 4.5e⁶
Max = 5.0e⁶
Radiance: (p/sec/cm²/sr)
Color Scale:
Min = 5.0e⁶
Max = 5.0e⁶

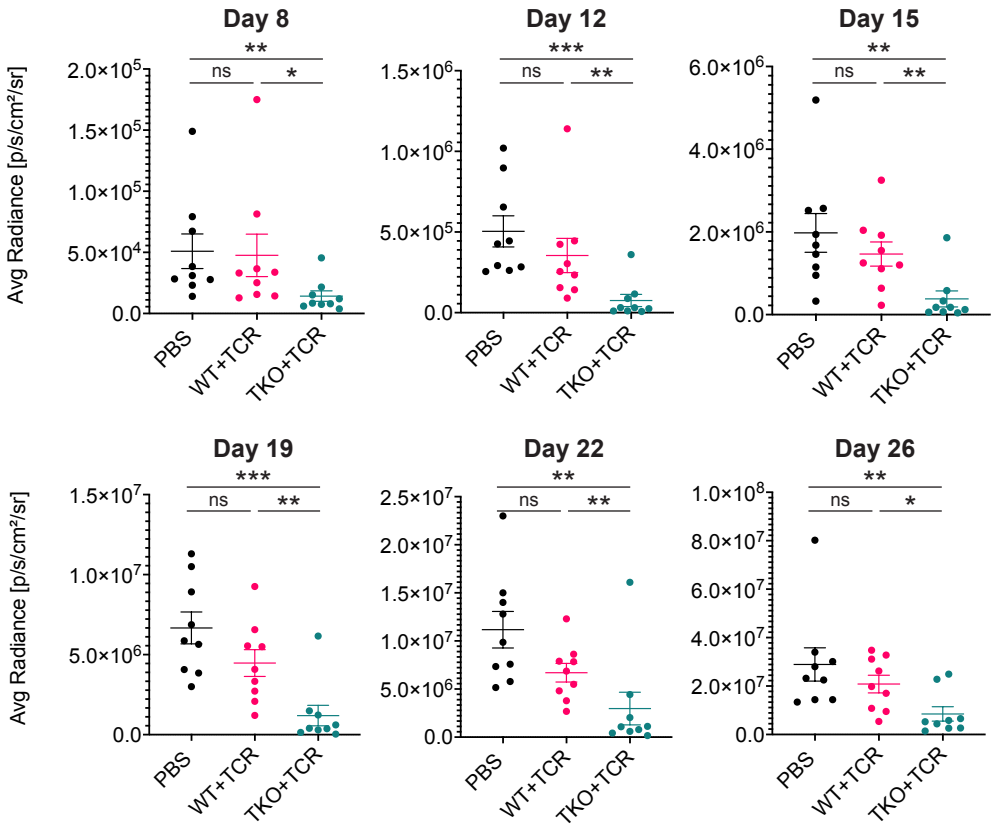
C
Day 8
Day 12
Day 15
Day 19
Day 22
Day 26
Avg Radiance [p/s/cm²/sr]
ns
*
**
***
PBS
WT+TCR
TKO+TCR

Figure 3.9 *In vivo* function of 1G4 TCR-expressing, Class I MHC-null, *RAG1/RAG2*-null SP8 T cells
(A) Experimental design of in vivo tumor challenge in NSG mice intravenously (I.V.) engrafted with NALM6 tumor cells (5 x 10^5 per mouse) expressing the cognate NYESO peptide-MHC as a single chain trimer and firefly luciferase. 5 days after tumor engraftment, mice were injected I.V. with PBS, WT+TCR SP8 T cells (1 x 10^7/mouse), or TKO+TCR SP8 T cells (1 x 10^7 per mouse). Tumor bioluminescence was measured every 3-4 days; IL-2 (10,000 IU per dose) was administered on the indicated days. **(B)** Representative imaging of mice from each treatment group (PBS, WT+TCR, or TKO+TCR). **(C)** In vivo imaging of tumor growth in each treatment group. Mean ± SEM (*$p < 0.05$; **$p < 0.01$; and ***$p < 0.001$) for each group is shown (n=9, all groups).

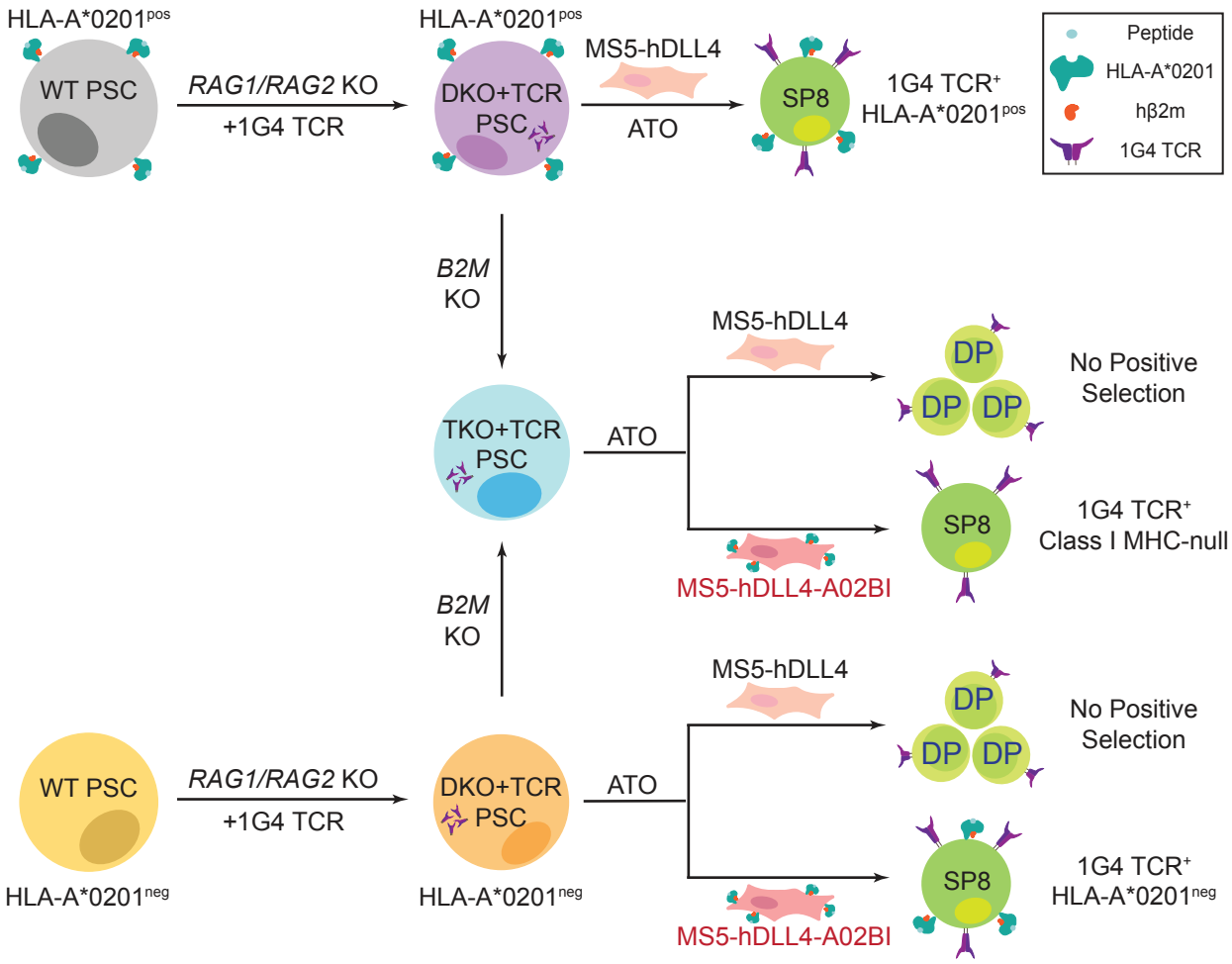

Figure 3.10 Graphical summary of DKO+TCR and TKO+TCR PSC generation, and T cell differentiation outcomes after differentiation in the ATO system

HLA-A*0201^{pos} and HLA-A*0201^{neg} and WT PSCs were CRISPR/Cas9 gene edited to ablate both *RAG1* and *RAG2,* and then transduced to express the exogenous, fully rearranged 1G4 TCR, generating the DKO+TCR PSC lines. Spontaneous positive selection of DP T precursors to generate mature, naïve SP8 T cell in ATOs initiated with HLA-A*0201^{pos} DKO+TCR PSCs. In the absence of cognate MHC expression on PSC-derived cells (HLA-A*0201^{neg} DKO+TCR and TKO+TCR), positive selection of HLA-A*0201^{neg} DKO+TCR and Class I MHC-null TKO+TCR DP T precursors could be induced through cognate MHC expression in MS5-hDLL4 cells (MS5-hDLL4-A02B or MS5-hDLL4-A02BI).

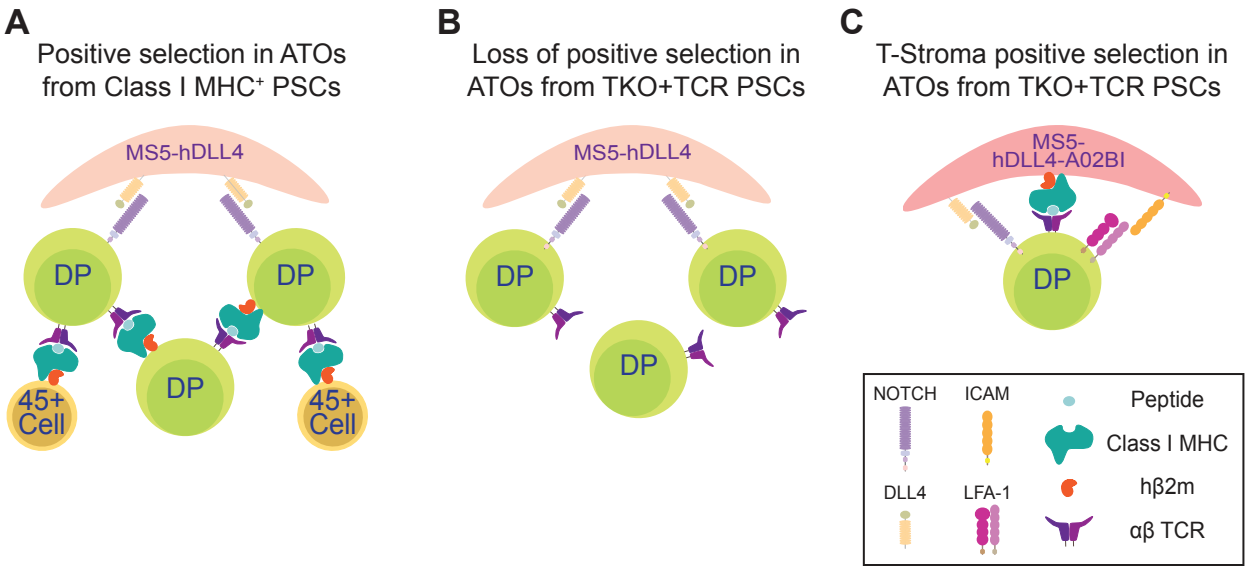

Figure 3.11 Proposed mechanisms of DP T precursor positive selection through interactions with accessory cells within the ATO system

(A) In ATOs aggregated with MS5-hDLL4 stroma and Class I MHC$^+$ PSCs, (WT, WT+TCR, DKO+TCR PSCs), DP T precursors and other Class I MHC-expressing PSC-derived CD45$^+$ cells to induce positive selection through surface expressed TCRαβ chains. Spontaneous positive selection, regardless of an exogenous TCR's MHC-restriction, occurs in RAG-competent PSC lines (WT, WT+TCR). Spontaneous positive selection of DKO+TCR DP T cells will only occur in the presence of the exogenous TCR's cognate MHC. **(B)** When alloreactive mechanisms are removed in TKO+TCR PSCs, positive selection signal cannot be induced due to the absence of Class I pMHCs. **(C)** In the final model, positive selection can be induced in TKO+TCR DP T precursors through T-stroma interactions with MS5-hDLL4 cells transduced to express cognate MHC, and T cell output can also be enhanced with the addition of co-factors such as ICAM (hDLL4-A02BI).

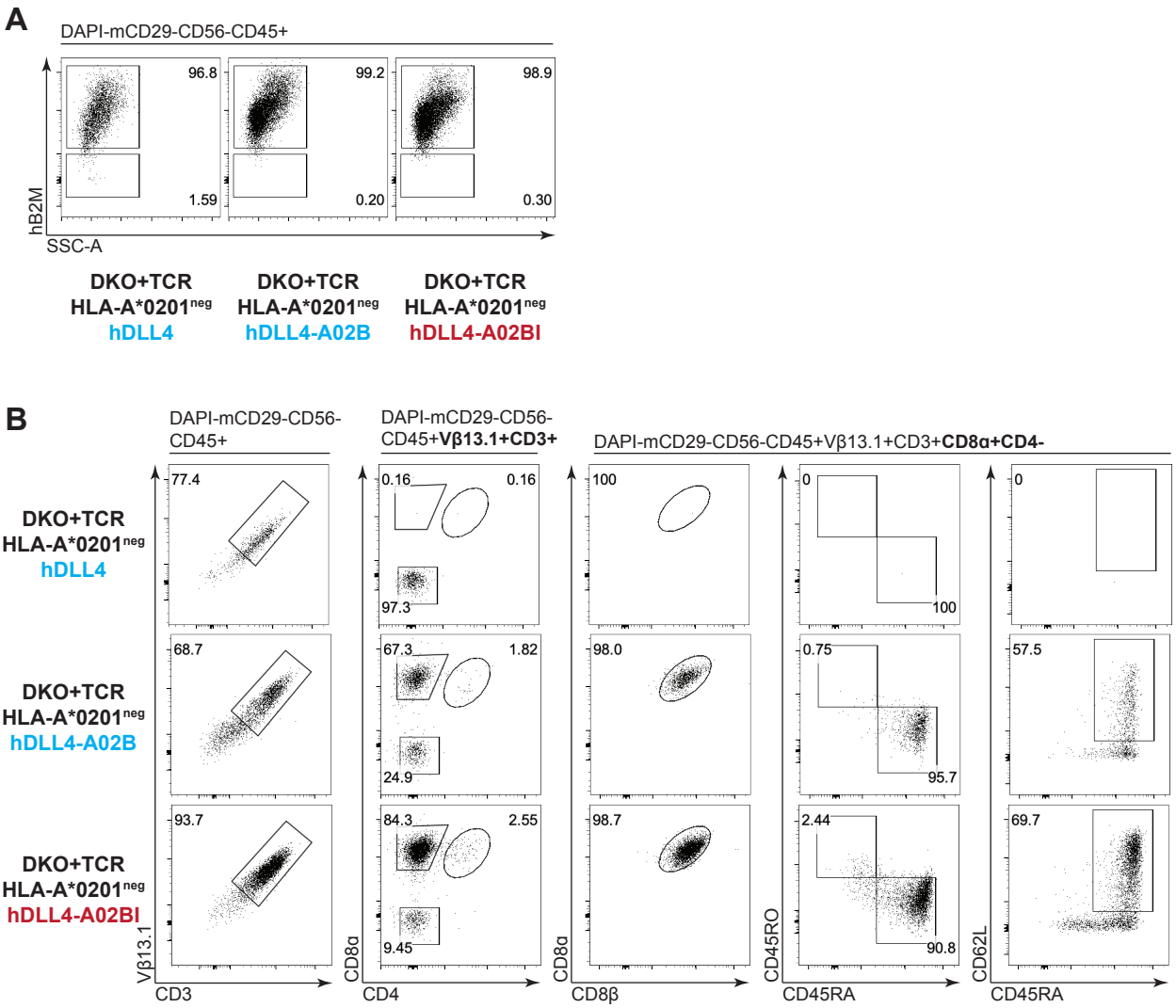

Figure 3.S1 Inclusion of HLA-A*0201 and hB2M in MS5-hDLL4 stroma induces positive selection in HLA-A*0201^{neg} ESI017 DKO+TCR PSCs

(A-B) Representative flow cytometry plots from ESI017 DKO PSCs transduced with the HLA-A*0201-restricted 1G4 TCR recognizing the NYESO1$_{157-165}$ peptide (DKO+TCR), and differentiated in the ATO system with the following stromal conditions: MS5-hDLL4 (hDLL4), MS5-hDLL4-A*0201-hB2M (hDLL4- A02B), and MS5-hDLL4-A*0201-hB2M-ICAM1 (hDLL4-A02BI). After 3 weeks of T cell differentiation, DKO+TCR PSC-derived ATOs were analyzed for expression of Class I MHC through surface staining of *hB2M* **(A)**. After 7 weeks of T cell differentiation, DKO+TCR PSC-derived ATOs were analyzed for maturation markers of conventional T cells (data representative of n=1 experiments)

3.3 Discussion

Here, we report the generation of Class I MHC-null, antigen-restricted, mature, naïve SP8 T cells from *RAG1*$^{-/-}$*/RAG2*$^{-/-}$*/B2M*$^{-/-}$ TKO+TCR PSCs in the ATO system by engineering the necessary components required for positive selection through the addition of an exogenous TCR in edited PSCs and introducing Class I MHC into MS5-hDLL4 stromal cells. While other groups have generated Class I MHC-null SP8 T cells from edited PSCs[56]**,** our system permitted induced positive selection of DP precursors to naïve, conventional CD3^{+}TCRαβ^{+}CD8α^{+}CD8β^{+} T cells without the need for activation or agonist-mediated selection.

Similar to the DKO+TCR experiments in Chapter 2, expression of the fully rearranged 1G4 was only sufficient for rescuing surface expression of TCRαβ and CD3 in TKO+TCR PSC-derived DP T precursors, in which surface human Class I MHCs are ablated; however, this presented a unique opportunity to determine if positive selection could be induced through T-stroma interactions **(Figures 3.10 and 3.11B)**. As positive selection is dependent on low affinity, “weak”, interactions between TCRs and non-specific pMHC[19], the murine-derived MS5-hDLL4 stromal cell line would have to be able to process broad repertoire of peptides that were also capable of being presented by the 1G4 TCR’s cognate MHC, HLA-A*0201.

Interestingly, we found that simply introducing HLA-A*0201 by itself was insufficient for generating SP8 T cells despite surface detection of HLA-A*0201 by antibody staining, which is indicative of proper folding and expression. In the absence of endogenously expressed cognate MHCs, however, SP8 T generation from TKO+TCR PSCs was dependent on the addition of *hB2M* in hDLL4-A02 cells (hDLL4-A02B)

(Figures 3.10 and 3.11C), indicating a species-specific effect of B2M on pMHC recognition by the exogenous 1G4 TCR during positive selection. Our results indicate that cross-species heterodimers of human Class I MHC and murine B2m alter TCR-pMHC interactions enough to prevent positive selection of DP T cell precursors.

Previous studies have shown that heterodimerization of murine Class I MHC and *hB2M* alters TCR-pMHC recognition significantly by preventing proper peptide presentation and decreasing CD8 binding[76,77]. While this study was not performed with our heterodimer combination (human Class I MHC and *mB2m*) or in the context of positive selection, our results demonstrate that these observations hold true. TCR signaling, in the context of human Class I MHC and *mB2m*, is likely to have decreased TCR-pMHC signaling below the threshold required to achieve positive selection of DP T precursors with the hDLL4-A02 stroma.

As positive selection was achieved when both human Class I MHC and *hB2M* were expressed, these results confirm that the murine MS5 cell line can inherently process and load a sufficiently diverse repertoire of peptides to induce positive selection signals through the 1G4 TCR. Furthermore, these results demonstrate that positive selection can be induced in MHC-null PSC-derived T cells without the need for activation or agonist selection of DP T precursors **(Figure 3.11C).**

Additionally, as we were able to induce positive selection through T-stroma interactions, we investigated if the murine MS5 stromal cell line could be further engineered to provide additional co-factors that could enhance positive selection. ICAM is one such molecule that has been reported to potentiate TCR activation and antigen sampling through LFA-1 interactions at low pMHC densities[73–75], which is an inherent

nature of positive selection when T cells are scanning for low affinity, “weak” peptides. It has also been shown that ICAM-LFA-1 signaling leads to cytoskeletal remodeling, increased TCR signal transduction, and survival gene expression[78]. While the direct mechanism of ICAM during ATO T cell development was not exhaustively characterized, its inclusion in murine MS5 stromal cells significantly increased maximum output of SP8 T cells per ATO aggregate, while having no observable effects on the ratios of developing T cells or the function of mature, naïve SP8 T cells **(Figures 3.11C)**. As our results were mainly focused on the major machinery required to induce positive selection, future studies could focus on determining additional signals and co-factors at the immune synapse that could enhance T cell development and function, similar to thymic epithelial cells during physiological thymopoiesis.

TCR sequencing of mature, naïve SP8 T cells generated from WT+TCR PSCs revealed a broad repertoire of endogenous TCRs in addition to the exogenous 1G4 TCR. Allelic exclusion of the endogenous TCR Vα locus by a functional, fully rearranged TCR was not observed, similar to a previous study of T cell differentiation from PSCs[57]. Additionally, sequencing revealed a diverse repertoire of endogenous TCR Vβ chains in addition to exogenous transcripts, indicating that allelic exclusion of endogenous TCR Vβ locus by a fully rearranged exogenous TCR was incomplete[18,60,79]. While we did not analyze endogenous TCR Vβ repertoire surface antibody staining, the low frequencies we observed from our sequencing indicate that flow cytometry may not have the sensitivity to detect these rare populations.

One caveat to our TCR repertoire analysis is that the WT+TCR SP8 T cells were derived from the HLA-A*0201^{neg} ESI017 parent line, which could explain the significant

amount of endogenous TCR rearrangements that we observed. *RAG*-competent HLA-A*0201^{neg} WT+TCR PSCs can rearrange their endogenous TCR loci as a mechanism for bypassing the MHC restriction of the 1G4 TCR. Additionally, this is supported by our experiments in Chapter 2, where HLA-A*0201^{neg} DKO+TCR PSC could not achieve positive selection in the absence *RAG* recombination machinery.

While positive selection was more efficient, SP8 T cell output from TKO+TCR PSC ATO cultures was still lower than WT+TCR PSCs, perhaps due to the antigen-specific nature of TKO+TCR DP precursors. In *RAG*-competent PSCs, mispairing between exogenously and endogenously rearranged TCR chains broadens the range of recognized epitopes[57], increasing the probability of finding a suitable pMHCs for positive selection. Logically, these mispaired TCRs could increase SP8 T cell output as it would expand the repertoire of pMHCs that could induce positive selection. Taken together, our results demonstrate that the mechanism for bypassing MHC-restriction is functionally dependent on *RAG* machinery, underscoring the need to eliminate *RAG*-recombination machinery in order to prevent alloreactive TCR development.

While mature, naïve SP8 T cells generated from TKO+TCR PSCs were functionally similar to WT+TCR PSC-derived SP8 T cells *in vitro,* they proved to be superior *in vivo*. Tetramer staining of WT+TCR SP8 T cells revealed significant TCR mispairing on the surface, confirming our sequencing results, and demonstrating its functional significance. While WT+TCR SP8 T cells functioned similarly *in vitro*, these assays are limited in demonstrating tumor control, and not subject to physiological requirements for tumor reduction, such as antigen scarcity or tumor homing. Reduction

in tumor control was not surprising as it has been reported that TCR mispairing decreases antigen specificity, which is compounded under physiological conditions[57,80,81].

RAG1-RAG2 deletion did not result in observable functional defects or decreased cytotoxicity, as TKO+TCR SP8 T cells outperformed their unedited controls. While T cells have been generated by *RAG*-knockout, other studies have neither characterized a complete gene ablation strategy of either protein, nor both at the same time[56,57]. Simple knockout strategies may be insufficient in preventing all endogenous TCR recombination, as clinical studies of *RAG* proteins have shown that residual activity can be retained despite truncation or frameshift mutations[35,58,59]. Furthermore, simple insertion, deletion, or frameshift of either *RAG* protein may be sufficient in preventing alloreactive TCR generation during activation or agonist DP T cell maturation; however, residual activity from either protein may be especially permissive to endogenous TCR recombination during positive selection, as it is a rate-limiting, stochastic step.

In summary, we have demonstrated the dynamic nature through which positive selection can be either spontaneously or artificially induced in the ATO system, all without the need for activation or agonist selection of DP T precursors. We found that positive selection of antigen-specific, Class I MHC-null SP8 T cells can be induced by engineering the ATO microenvironment to recapitulate the necessary signals that are lost when alloreactive mechanisms are disrupted. As a platform for generating MHC-deficient T cells, accessory cells within the ATO system can be readily engineered to express cognate MHC for TCR-mediated positive selection, as well as co-stimulation factors that could improve T cell function or specification. Due to their inherent self-renewal capacity, engineered PSCs are a replenishable source for engineered, ATO-derived T cells that

could be further modified with novel additional, gene editing strategies that augment T cell function, enhance immune-evasion, and prevent exhausted phenotypes. Taken together, these results demonstrate the versatility of the ATO as a platform for generating engineered, mature, naïve T cells from PSCs and other stem cell sources[31,32,34,35,82]. As naïve cells have been implicated in conveying superior antitumor immunity and persistence[47,48], the development of conventional, mature, naïve SP8 T cells without the need for activation or agonist mediated selection has broad implications for developing novel, engineered allogeneic approaches to T cell immunotherapy.

3.4 Materials and Methods

Cell Lines

The MS5-hDLL4 cell line was generated in our lab as previously described[32]. Briefly, MS5 cells[61] were transduced with a lentiviral vector encoding full-length human *DLL4*. The highest 5% DLL4-expressing cells were isolated by FACS using an anti-DLL4 antibody and passaged in DMEM with 10% fetal bovine serum (FBS). Stable expression was confirmed by flow cytometry for DLL4 expression after several weeks of culture, as well as qRT-PCR and DNA sequencing.

For the cell lines including Class I MHC and scaffolding proteins, the previously-derived MS5-hDLL4 line was transduced with varying combinations of individual lentiviruses encoding human HLA-A*0201, human B2M, and human ICAM. The highest 5% of transduced cells were isolated by FACS using antibodies detecting human HLA-A*0201, human B2M, and human ICAM and passaged in DMEM with 10% FBS for expansion and cryopreservation. Stable expression was also confirmed by flow cytometry for DLL4, human HLA-A*0201, human B2M, and human ICAM.

Artificial antigen presenting cells (aAPCs) were generated in our lab as previously described[32]. K562 cells (ATCC, Cat. CCL-243) were transduced with lentiviral vectors encoding full length human CD80, CD83, CD137L, and either HLA-A*0201/B2M/NYESO1$_{157\text{-}165}$ or MART1$_{26\text{-}35}$ single chain trimers (SCTs; gifts from Dr. David Baltimore, Caltech). Cytotoxicity assay target cells were created by transduction of K562 with either NYESO1 or MART1 SCTs alone.

Lentiviral vectors packaging

The full-length coding sequences of human DLL4, human HLA-A*0201, human B2M, and human ICAM1 were synthesized (Integrated DNA Technologies, Skokie, IL) and cloned into third-generation lentiviral vector backbone pCCL-c-MNDU3 (gift from Dr. Donald Kohn, UCLA). The mStrawberry fluorescent protein coding sequence was added downstream of HLA-A*0201, separated by a furin-SGSG-2A linker for polycistronic expression.

The codon optimized TCR Vα and Vβ (including Vβ13.1) chains of a TCR specific for HLA-A*0201/NYESO1$_{157\text{-}165}$ (derived from the 1G4 TCR[51]) is previously described[52] (gift from Dr. Antoni Ribas, UCLA). TCR coding sequences and the mTagBFP2 fluorescent protein[62], all separated by furin-SGSG-2A linkers, were subcloned into the third-generation pCCL lentiviral vector downstream of the ubiquitin C (UBC) promoter and intron 1.

Packaging and concentration of lentivirus particles was performed as previously described[31]. Briefly, 293T cells (ATCC) were co-transfected with a lentiviral vector plasmid, pCMV-DR8.9, and pCAGGS-VSVG using TransIT 293T (Mirus Bio, Madison, WI) for 17 hours followed by treatment with 20 mM sodium butyrate for 8 hours, followed by generation of cell supernatants in serum-free UltraCulture for 48 hours. Supernatants were concentrated by ultrafiltration using Amicon Ultra-15 100K filters (EMD Millipore, Billerica, MA) at 4000 x g for 40 minutes at 4C and stored as aliquots at -80C.

Human pluripotent cell lines

The human pluripotent stem cell (PSC) lines[49] (WiCell, Cat. WA01) and ESI017 [50] (ESI BIO, Cat. ES-700), were maintained and expanded on Matrigel-coated 6-well plates (Growth Factor reduced Matrigel matrix, BD Biosciences, Cat. 356231) in mTeSR™ Plus complete medium (mTeSR™ Plus Basal Medium + 5X Supplement, Stem Cell Technologies, Cat. 100-0276). Culture medium was changed daily. After reaching ~70% confluency, PSC cultures were dissociated with TrypLE™ Express (GIBCO Life Technologies, Cat. 12604-013) and seeded in single cell suspension at a density of 2 x 10^5 cells/well of a Matrigel-coated 6-well plate in mTeSR™ Plus complete medium and ROCK inhibitor Y-27632 dihydrochloride (10μM) (Tocris, Cat. 1254), which was removed from culture medium after 1 day.

Design and validation of CRISPR/Cas9 guide RNAs

Using published algorithms found on the Benchling web tool (https://benchling.com), 5 guide RNAs (gRNAs) with optimal *in silico* predicted on- and off-target scores (out of 100) were designed to target sequences near the start of *RAG1, RAG2,* and *B2M*[53–55,63–65]*.* On-target efficiency was assayed *in vitro* at each target locus by nucleofection of gRNA expressing pX459 plasmid (Zhang Lab, MIT; Addgene, Cat. 62988) into K562 erythroleukemia cells (ATCC, Cat. CCL-243).

Genomic DNA (gDNA) was harvest from nucleofected cells, and flanking regions of *RAG1, RAG2,* and *B2M* cleavage sites were amplified via PCR. Products were purified and on-target CRISPR/Cas9 cutting efficiency was determined by Sanger sequencing of the PCR products. Using the Tracking of Insertion or Deletion mutations (INDELs) by

Decomposition (TIDE) tool[66], the percentage of edited cells was calculated based on the INDELs produced as a result of double stranded breaks from CRISPR/Cas9.

For each gene target, the 2 gRNA candidates with the highest on-target *in vitro* cutting activity were chosen for off-target cleavage activity *in vitro* via the genome-wide, unbiased identification of DSBs enabled by sequencing (GUIDE-seq) [67].1 gRNA with high on- and low off-target cutting activity was chosen for each target gene to proceed with editing in PSC lines.

Gene editing of human pluripotent stem cell lines

CRISPR/Cas9 gene editing of PSCs was performed with ribonucleoprotein complexes [68,69] (RNPs) of purified spCas9-NLS (QB3 MacroLab, UC Berkeley, Berkeley, CA) and custom synthesized small guide RNAs (gRNAs) (Synthego, Mountain View, CA). spCas9-NLS and gRNAs were stored at -80C prior to use for gene editing of PSCs.

Briefly, PSCs were allowed to grow in wells of a Matrigel-coated 6-well plate until reaching ~70% confluency before being dissociated with TrypLE™ Express (GIBCO Life Technologies, Cat. 12604-013) and resuspended in single cell solution. Prior to nucleofection, 60pmol spCas9 and individual 84pmol gRNA were complexed together at a ratio of 1pmol spCas9:1.4pmol gRNA for 15m at room temperature. PSCs were resuspended at a concentration of 2 x 10^5 cells in 14µL of P4 Primary Cell Nucleofector® Solution (P4 Primary Cell 4D-Nucleofector™ X Kit S, Lonza, Cat. V4XP-4032).

For single gRNA reactions, fully complexed RNPs (60pmol spCas9:84pmol gRNA) were added to resuspended cells and the volume was brought up to 20µL using P4 Primary Cell Nucleofector® Solution. For dual gRNA reactions, RNPs were complexed

individually and then added (2 x 60pmol spCas9 total) into the cell suspension with a custom-synthesized single stranded oligo donor template (ssODN, 100bp, resuspended at 100μM) (Ultramer® DNA Oligo, Integrated DNA Technologies, Skokie, IA) to a final concentration of 3μM in solution. 20μL of combined PSC, RNP, and/or ssODN solutions were added into individual wells of the Lonza 16-well Nucleocuvette® Strip (Lonza). Nucleofection was performed on the Lonza 4D-Nucleofector® Core and X Unit (Lonza, Cat. AAF1003B and AAF-1003X) using pulse and frequency code CB-150. Cells were allowed to rest in the cuvette for 10m before transferring into 1.5mL mTeSR™ Plus and ROCK inhibitor Y-27632 dihydrochloride (10μM), and then plated in 1 well of a Matrigel-coated 12-well plate. Culture medium was changed daily, and ROCK inhibitor Y-27632 dihydrochloride (10μM) was removed from medium after 48hr. Edited PSCs were allowed to reach ~70% confluency before being expanded for single cell cloning and cryopreservation.

Knockout of *B2M* in DKO lines was achieved by introducing insertion deletion mutations (INDELs) at the beginning of its coding sequence with B2M gRNA #3 **(Figure 3.1C-E)**. Polyclonal knockout lines were purified via FACS.

Table 3.1 List of primers used genotyping *B2M*

Primer Name	Sequence (5'-3')	Sequence Amplified (length)
B2M FWD	tgaagtcctagaatgagcgccc	B2M Exon 1 (644bp)
B2M REV	taaactttgtcccgaccctccc	B2M Exon 1 (644bp)

Single cell cloning of edited human pluripotent stem cell lines

Single cell cloning was achieved with low density plating of expanded, edited PSCs as previously described[53]. Briefly, expanded, edited PSCs were dissociated into single cell solution with TrypLE™ Express (GIBCO Life Technologies, Cat. 12604-013) and then plated in Matrigel-coated 10cm dishes at a density of 0.5-1 x 10^4 cells/plate in mTeSR™

Plus complete culture medium with ROCK inhibitor Y-27632 dihydrochloride (10μM). Culture medium was changed daily, and ROCK inhibitor Y-27632 dihydrochloride (10μM) was removed from medium after 48hr. After colony formation, 24-48 individual colonies were scraped with a 200μL "P200" pipette tip under a microscope, and then transferred into individual wells of a Matrigel-coated 12-well plate with mTeSR™ Plus culture medium. Once cells reached 60-80% confluency, cells were passaged via scraping for expansion and genotyping PCRs to determine bi-allelic knockout of edited genes. Clones with bi-allelic knockouts were expanded, cleaned for differentiation and then genotyped once again before cryopreservation and karyotyping.

Transduction of human pluripotent stem cell lines

NYESO TCR-transduced PSC lines were generated by transduction of unedited or knockout H1 or ESI017 PSCs with a lentiviral vector encoding the 1G4 TCR (Class I MHC-restricted NYESO1 specific TCR, described below) and the fluorescent marker mTagBFP2. Briefly, PSCs were dissociated into single cell suspension and plated at a density of 2 x 10^5 cells/well of a Matrigel-coated 6-well plate in mTeSR™ Plus culture medium with ROCK inhibitor Y27632 dihydrochloride (10μM). The following day, culture medium was changed to 1mL of mTeSR™, and concentrated lentiviral supernatant was added directly into the wells. Medium was changed each day until cells reached ~70% confluency, when cells were dissociated with TypLE™ Express (GIBCO Life Technologies, Cat. 12604-013) and purified via FACS sorting using the following phenotype: TRA1-81$^+$mTagBFP2$^+$. Isolated cells were returned to culture on Matrigel-

coated 6-well plates and mTeSR™ Plus culture medium for expansion and cryopreservation.

Generation and isolation of human embryonic mesodermal progenitors (EMPs)

Mesodermal commitment was induced as previously described [32,33,70] with certain optimizations. Briefly, PSCs were maintained as single-cell cultures on Matrigel-coated 6-well plates in mTeSR™ Plus complete medium. PSCs were harvested as single cell suspension after TrypLE™ Express (GIBCO Life Technologies Ref 12604-013) treatment for 6 minutes at 37C, washed, and counted. Cells were resuspended directly in X-VIVO15 medium (Lonza, Cat. 04-418Q) supplemented with rhActivin A (10ng/mL) (R&D Systems, Cat. 338-AC-0101), rhBMP4 (10ng/mL) (R&D Systems, Cat. 314-BP-010), rhVEGF (10ng/mL) (R&D Systems, Cat. 298-VS-005), rhFGF (10ng/mL) (R&D Systems, Cat. 233-FB-025), and ROCK inhibitor Y-27632 dihydrochloride (10μM) (Tocris, Cat. 1254). Cells were plated on Matrigel coated 6-well plates at 3.3 x 10^6 cells per well in 3mL. Media was then changed daily with X-VIVO 15 supplemented with rhBMP4 (10ng/mL), rhVEGF (10ng/mL), and rhFGF (10ng/mL). At day 3.5, cells were washed 3 times with PBS and incubated with Accutase (Innovative Cell Technologies, Cat. AT-104), 1mL per well for 10m at 37C. Cells were harvested by dilution with MACS buffer (PBS, 0.5% bovine serum albumin, 2mM EDTA) followed by depletion of $CD326^+$ (EPCAM) cells by magnetic cell sorting (MACS) using CD326 (EPCAM) MicroBeads (Miltenyi, Auburn, CA, Cat. 130-061-101). In addition, EMPs derived from *RAG1*$^{-/-}$*RAG2*$^{-/-}$*B2M*$^{-/-}$ triple knockout (TKO) PSCs were stained with PE-conjugated B2M antibody and then depleted of $B2M^+$ cells by MACS using Anti-PE MicroBeads (Miltenyi, Auburn, CA, Cat. 130-048-801).

Human pluripotent stem cell-derived EMO and ATO cultures

EMOs and ATOs were generated as previously described[32]. Briefly, sequential generation of EMOs and then ATOs was accomplished in 3D aggregates through changing media **(Figure 1.2C-D**). EMOs were established by aggregating purified EMPs with MS5-hDLL4 cell. MS5-hDLL4 cells were harvested by trypsinization and resuspended in hematopoietic induction media comprised of EGM2 (Lonza, Cat. CC-4176) supplemented with fROCK inhibitor Y-27632 dihydrochloride (10μM) (Tocris Bioscience, Cat. 1254) and TGF-bRI inhibitor SB-431542 ("SB Blocker") (10μM) (Tocris Bioscience, Cat. 1614). At Day -14, 5 x 10^5 MS5-hDLL4 cells were combined with 5 x 10^4 (H1) or 1 x 10^5 (ESI017) purified EMPs per ATO in 1.5mL Eppendorf tubes and centrifugated at 300 x g for 5m at 4C in a swinging bucket centrifuge.

Multiple (up to 180) EMOs were prepared per tube. Supernatants were carefully removed and the cell pellet was resuspended by brief vortexing and resuspended in hematopoietic induction medium at a volume of 5mL per EMO. 3 EMOs were individually plated (5μL/EMO) on a 0.4mm Millicell transwell insert (EMD Millipore, Billerica, MA, Cat. PIMC0R5G50) and then placed in a 6-well plate containing 1mL of hematopoietic induction medium per well. Medium was changed every 2-3 days for 1 week with medium composed of EGM2 with SB Blocker (10mM). At Day 7, medium was changed to EGM2 + SB Blocker (10mM) with the hematopoietic cytokines, rhTPO 5ng/mL (R&D Systems, Cat. 288-TPN-025), rhFLT3L 5ng/mL (R&D Systems, Cat. 308-FK-025), and rhSCF 50ng/mL (R&D Systems, Cat. 255-SC-200). This medium was changed every 2-3 days for an additional 7 days. At Day 0, ATOs were initiated by simply changing the medium

to “RB27” (described above) supplemented with 10ng/mL rhSCF, 5ng/mL rhFLT3L, and 5ng/mL rhIL-7(R&D Systems, Cat. 207-IL-200). Medium was changed completely every 3-4 days.

For experiments involving the use of different stromal lines for ATO T cell differentiation (MS5-hDLL4-A*0201, MS5-hDLL4-A*0201-hB2M, MS5-hDLL4-A*0201-hB2M-ICAM), EMOs were harvested in bulk by adding 1mL MACS buffer (PBS, 0.5% bovine serum albumin, 2mM EDTA) to each filter, briefly disaggregating the ATO by scraping with a 1mL “P1000” pipette, and then passed through a 50μm nylon strainer. Harvested cells were counted, and then 2 x 10^4 cells were combined with 2.5 x 10^5 derivative MS5-hDLL4 stromal cells per ATO in 1.5mL Eppendorf tubes. Cell mixtures were centrifuged at 300 x g for 5m at 4C in a swinging bucket centrifuge prior to formation of 3D aggregates on 0.4mm Millicell transwell inserts (EMD Millipore, Billerica, MA, Cat. PIMC0R5G50) as described above.

Isolation of ATO-derived T cells

ATOs were harvested by adding MACS buffer (PBS, 0.5% bovine serum albumin, 2mM EDTA) to each filter, briefly disaggregating the ATO by pipetting with a 1mL “P1000” pipette, and then passed through a 50μm nylon strainer. For bulk-scale collection of ATOs, aggregates were harvested in a similar fashion; however, up to 150 aggregates were collected in a well filled with MACS buffer and then transferred onto a 50μm nylon filter, where aggregates were physically dissociated on top of the filter using the back end of a sterile 1mL syringe. After dissociation, the filter was washed with MACS buffer, and cell mixtures were centrifuged at 300 x g for 5m at 4C in a swinging bucket centrifuge.

Single cell RNA library preparation and sequencing

ATO-derived T cells were isolated as described above and then FACS-sorted for WT ($mCD29^{-}CD45^{+}CD8\alpha^{+}CD4^{-}$) and 1G4 TCR-transduced ($mCD29^{-}mTagBFP2^{+}CD45^{+}CD8\alpha^{+}CD4^{-}$) SP8 into PBS + 0.04% bovine serum albumin. Cells were counted and resuspended at a concentration of ~1000 cells/μL and provided to the Technology Center for Genomics and Bioinformatics (TCGB) core for unique molecular identifier (UMI) tagging and library generation using the 10X Chromium Next GEM Single Cell V(D)J Reagent Kit v1.1 (10X Genomics, Pleasanton, CA). Single cell RNA-sequencing (scRNA-seq) libraries were sequenced on the Illumina NovaSeq platform.

TCR repertoire analysis by single cell RNA-sequencing

Full, endogenous TCR Vα and Vβ contigs were aligned and assembled using the Cell Ranger (10X Genomics, Pleasanton, CA) pipeline. As the exogenous TCR was expressed using a codon optimized sequence, reads from the 5' Genomic Expression libraries were aligned using a human genome reference (GRCh38) that was customized to include the codon optimized sequence for the 1G4 TCR. After full reconstruction of TCRs and gene alignment, Cell Ranger outputs were filtered using the 10X Loupe Browser (10X Genomics, Pleasanton, CA) for quality control purposes.

Barcoded cells were filtered using Seurat (v4.1.0) to remove cells that did not have reads for genes specific to the SP8 phenotype ($CD8\alpha^{+}CD4^{-}CD3E^{+}$), high mitochondrial gene expression (likely due to cellular stress or loss of cytoplasmic RNA), and low number of expressed genes. For samples including the exogenous 1G4 TCR, barcoded cells were

also filtered for cells that expressed the exogenous transgene. Finally, remaining barcoded cells were exported as a list and used to filter VDJ sequencing outputs in R for TCR diversity calculations, using the number of barcoded cells remaining after quality control as a denominator, and calculations of percentages of cells expressing endogenous and/or exogenous TCR.

Expansion of ATO-derived T cells for functional proliferation assays

For functional and proliferation assays, ATO-derived SP8 T cells were isolated as described above and expanded *in vitro* using irradiated antigen-expressing K562 aAPCs (K562 CD80/83/137L/1073ESO) in a 1:3 aAPC:T cell ratio in AIM V (GIBCO Life Technologies, Cat. 12055083) supplemented with 5% human AB serum (Gemini Bio-Products, West Sacramento, CA, Cat. 100-512), 20ng/mL rhIL-2 (Peprotech, Rocky Hill, NJ, Cat. 200-02), and 5ng/mL rhIL-7 (R&D Systems). Fresh medium was added every 2-3 days, and cells were replated into larger wells as necessary. Restimulations for proliferation assays were performed every 5 days.

For CFSE proliferation assays, expanded SP8 T cells from ATOs were rested for an additional 2 days after the previous expansion cycle (7 days from aAPC stimulation) with reduced cytokines, 5ng/mL rhIL-2 (Peprotech) only, on the night prior to the assays. 5 x 10^5 rested SP* T cells were labeled with CFSE (Biolegend, San Diego, CA) at a final concentration of 5μM and co-cultured with irradiated K562 aAPCs expressing cognate (NYESO, HLA-A*0201/NYESO$1_{157-165}$) or irrelevant (MART1, HLA-A*0201/MART1_{26-35}) single chain trimers[32] at a 1:1 T cell:aAPC ratio in a 24-well plate and 3mL AIM V (GIBCO Life Technologies) with 5% human AB serum (Gemini) and 20ng/mL rhIL-2 (Peprotech).

On day 5, cells were washsed and stained for CD25 and 4-1BB (Biolegend, San Diego, CA) and analyzed by flow cytometry.

T cell cytokine assays

Expanded SP8 T cells from ATOs were rested as described above. 2 x 10^5 rested ATO-derived SP8 T cells co-cultured with K562 aAPCs expressing cognate (NYESO) or irrelevant (MART1) single chain trimers at a 2:1 T cell:aAPC ratio in 96-well U-bottom plates and 200μL AIM V (GIBCO Life Technologies) with 5% human AB serum (Gemini Bio-products) and protein transport inhibitor cocktail (eBioscience, San Diego, CA, Cat. 00-4980-03) for 6h. After 4 hours, CD107a-APC antibody (Biolegend, San Diego, CA) was added to wells at a 1:50 final dilution. Cells were washed and stained for CD3, CD4, and CD8α (Biolegend, San Diego, CA) and Zombie NIR Fixable Viability Dye (Biolegend, San Diego, CA) prior to fixation and permeabilization with an intracellular staining buffer kit (eBioscience, San Diego, CA, Cat. 88-8824-00), and intracellular staining with antibodies against IFNγ, TNFα, and IL-2 (Biolegend, San Diego, CA).

***In vitro* cytotoxicity assays**

Expanded SP8 T cells from ATOs were rested as described above. For cytotoxicity assays, 2-fold serial dilutions of rested SP8 T cells in 96-well U-bottom plates starting at 1 x 10^5 cells in 200μL AIM V (GIBCO Life Technologies) with 5% human AB serum (Gemini Bio-products). K562 aAPCs expressing cognate (NYESO) or irrelevant (MART1) single chain trimers were plated at 1 x 10^5 target cells per well. Apoptotic cell death of target cells was quantified by Apotracker™ Green (Biolegend, San Diego, CA) and DAPI

staining at 6h.Target cell death was calculated by subtracting percent Apotracker^{TM} Green^{+} target cells in wells receiving no T cells from wells that received T cells.

In vivo tumor assay

8–14-week-old NOD.Cg-Prkdcscid Il2rgtm1Wjl/SzJ (NSG) mice (Jackson Laboratory, Bar Harbor, Main) were intravenously injected (tail vein) with 5 x 10^5 NALM6 target cells transduced with a HLA-A*0201/NYESO1$_{157-165}$ single chain trimer and firefly luciferase. *In vivo* imaging was performed by intraperitoneal injection of luciferin (IVIS spectrum, Perkin Elmer) 5 days after tumor injection. Groups were randomized based on average luciferase signal activity. ATO-derived SP8 T cells expressing NYESO TCR (1 x 10^7 cells/mouse) were intravenously injected (retro-orbital) after mice were grouped on day 5; control mice received PBS injections. Mice were dosed intraperitoneally (I.P.) with 10,000 IU rhIL-2 (R&D Systems, Cat. 202-IL-500) on days 5-7 post tumor injection, and then every 3 days until euthanasia was necessary. Tumor bioluminescence was repeated twice a week (every 3-4 days) for at least 26 days, and mice were euthanized based on disease burden criteria.

Flow cytometry and antibodies

Staining for flow cytometry was performed in PBS with 0.5% BSA and 2mM EDTA for 15m at 4^{o}C in the dark. TruStain FcX (Biolegend, San Diego, CA) was added to all samples for 5m prior to antibody staining. Tetramer staining with the PE-conjugated HLA-A*0201/NYESO1$_{157-165}$ tetramer (MBL International, Woburn, MA) at a 1:50 final dilution

at room temperature for 20m prior to additional antibody staining for 15m at 4°C. DAPI was added to all samples prior to analysis.

Analysis was performed on a BD LSRII Fortessa, and FACS sorting on FACSARIA or FACSARIA-H instruments (BD Biosciences, San Jose, CA) at the UCLA Broad Stem Cell Research Center Flow Cytometry Core. For all analyses (except intracellular staining), DAPI+ cells were gated out, and doublets were removed through FSC-H vs. FSC-W and SSC-H vs SSC-W gating. Anti-human antibody clones for surface and intracellular staining were obtained from Biolegend (San Diego, CA): CD3 (UCHT1), CD4 (RPA-T4), CD5 (UCHT2), CD7 (CD7-6B7), CD8α (SK1), CD25 (BC96), CD27 (O323), CD28 (CD28.2), CD326 (EPCAM) (Clone 9C4), CD34 (581), CD45 (HI30), CD45RA (HI100), CD45RO (UCHL1), CD56 (HCD56), CD62L (DREG-56), CD107α (H4A3), B2M (2M2), CCR7 (G043H7), HLA-ABC (W6/32), IFNγ (4S.B3), IL-2 (MQ1-17H12), TCRαβ (IP26), TNFα (MAb11), Vβ13.1 (H131), 4-1BB (clone 4B4-1); and Miltenyi (San Jose, CA): CD8β (clone REA715). Anti-mouse CD29 (clone HMb1-1) was obtained from Biolegend (San Diego, CA). Flow cytometry data were analyzed with FlowJo software (Tree Star Inc.).

Quantification and statistical analysis

In all figures, n represents independent experiments and data are represented as mean ± standard error of the mean (SEM) as indicated. For all figures, statistical analysis was performed using GraphPad Prism software and p-values were calculated from the Wilcoxon rank sum test (Mann-Whitney U Test). The p-values are directly indicated on

the figure, above the corresponding graphs. *$p < 0.05$; **$p < 0.01$; and ***$p < 0.001$ were considered statistically significant.

Table 3.2 Key Resources

REAGENT or RESOURCE	SOURCE	IDENTIFIER
Antibodies		
Anti-human CD3	Biolegend	(clone UCHT1) RRID: AB_830754
Anti-human CD4	Biolegend	(clone RPA-T4) RRID: AB_2564392
Anti-human CD5	Biolegend	(clone UCHT2) RRID: AB_314098
Anti-human CD7	Biolegend	(clone CD7-6B7) RRID: AB_2632912
Anti-human CD8α	Biolegend	(clone SK1) RRID: AB_2565243
Anti-human CD8β	Miltenyi	(clone REA715) RRID: AB_2659522
Anti-human CD25	Biolegend	(clone BC96) RRID: AB_314276
Anti-human CD27	Biolegend	(clone O323) RRID: AB_2562086
Anti-human CD28	Biolegend	(clone CD28.2) RRID: AB_314310
Anti-human CD326 (EPCAM)	Biolegend	(Clone 9C4) RRID: AB_2098808
Anti-human CD34	Biolegend	(clone 581) RRID: AB_1731862
Anti-human CD45	Biolegend	(clone HI30) RRID: AB_2563129
Anti-human CD45RA	Biolegend	(clone HI100) RRID: AB_893357
Anti-human CD45RO	Biolegend	(clone UCHL1) RRID: AB_2563819
Anti-human CD56	Biolegend	(clone HCD56) RRID: AB_2561944
Anti-human CD62L	Biolegend	(clone DREG-56) RRID: AB_2562914
Anti-human CD107α	Biolegend	(clone H4A3) RRID: AB_1279055
Anti-human B2M	Biolegend	(clone 2M2) RRID: AB_492839
Anti-human CCR7	Biolegend	(clone G043H7) RRID: AB_10913813
Anti-human HLA-A,B,C	Biolegend	(clone W6/32) RRID: AB_314873
Anti-human IFNγ	Biolegend	(clone 4S.B3) RRID: AB_2563882
Anti-human IL-2	Biolegend	(clone MQ1-17H12) RRID: AB_2563877
Anti-human TCRαβ	Biolegend	(clone IP26) RRID: AB_10612569
Anti-human TNFα	Biolegend	(clone MAb11) RRID: AB_10960738
Anti-human Vβ13.1	Biolegend	(clone H131) RRID: AB_2564032
Anti-mouse CD29	Biolegend	(clone HMb1-1) RRID: AB_528790
Bacterial and Viral Strains		
pCCL-c-MNDU3-hDLL4 (lentivirus)	Montel-Hagen et al. 2019[32]	N/A
pCCL-c-MNDU3-A0201-mStrawberry (lentivirus)	This paper	N/A
pCCL-c-MNDU3-hB2M-wPRE (lentivirus)	This paper	N/A
pCCL-c-MNDU3-hICAM1-wPRE (lentivirus)	This paper	N/A
pCCL-UBC-opt1G4-mTagBFP2 (lentivirus)	Montel-Hagen et al. 2019[32]	N/A
Chemicals, Peptides, and Recombinant proteins		
rhIL-2	Peprotech	Cat. 200-02
rhIL-2	R&D Systems	Cat. 202-IL-500
rhBMP4	R&D Systems	Cat. 314-BP-010
rhVEGF	R&D Systems	Cat. 298-VS-005
rhFGF	R&D Systems	Cat. 233-FB-025
rhFLT3L	R&D Systems	Cat. 308-FK-025
rhIL-7	R&D Systems	Cat. 207-IL-200
rhTPO	R&D Systems	Cat. 288-TPN-025
rhSCF	R&D Systems	Cat. 255-SC-200
ROCK inhibitor Y-27632	Tocris Bioscience	Cat. 1254
TGF-bRI inhibitor SB-431542	Tocris Bioscience	Cat. 1614

Continued		
Chemicals, Peptides, and Recombinant proteins		
B27 Supplement	GIBCO	Cat. 17054-044
Accutase	Innovative Cell Technologies	Cat. AT-104
TrypLE™ Express	GIBCO Life technologies	Cat. 12604-013
TruStain FcX	Biolegend	Cat. 422302
DAPI	Life technologies	Cat. D1306
Critical Commercial Assays		
CD326 (EpCAM) MicroBeads, human	Miltenyi	Cat. 130-061-101
Anti-PE MicroBeads	Miltenyi	Cat. 130-048-801
iTAg Tetramer/PE-HLA-A*0201 NYESO1 (SLLMWITQC)	MBL International	Cat. T01064
Chromium Next GEM Single Cell 5' Library & Gel Bead Kit v1.1	10X Genomics	Cat. PN-1000165
Chromium Next GEM Single Cell V(D)J Reagent Kit, Human T Cell	10X Genomics	Cat. PN-1000005
Cell Stimulation Cocktail (plus protein transport eBioscience inhibitors)	eBioscience	Cat. 00-4975-03
Protein Transport Inhibitor Cocktail	eBioscience	Cat. 00-4980-03
Intracellular Fixation & Permeabilization Buffer Set	eBioscience	Cat. 88-8824-00
CFSE proliferation assay Biolegend	Biolegend	Cat. 423801
ApotrackerTM Green	Biolegend	Cat. 427403
Zombie Green Fixable Viability Kit	Biolegend	Cat. 423112
Zombie NIR Fixable Viability Kit	Biolegend	Cat. 423106
Zombie UV Fixable Viability Kit	Biolegend	Cat. 423107
Experimental Models: Cell Lines		
H1 hPSC Line	WiCell	Cat. WA01
ESI017 hPSC Line	ESI BIO	Cat. ES-700
H1-opt1G4-mTagBFP2 hESC line	Montel-Hagen et al. 2019[32]	N/A
H1 $RAG1^{-/-}RAG2^{-/-}$ DKO	This Paper	N/A
H1 $RAG1^{-/-}RAG2^{-/-}$ + opt1G4-mTagBFP2	This Paper	N/A
ESI017 $RAG1^{-/-}RAG2^{-/-}$ DKO	This Paper	N/A
ESI017 $RAG1^{-/-}RAG2^{-/-}$ DKO + opt1G4-mTagBFP2	This Paper	N/A
ESI017 $RAG1^{-/-}RAG2^{-/-}B2M^{-/-}$ TKO	This Paper	N/A
ESI017 $RAG1^{-/-}RAG2^{-/-}$ $B2M^{-/-}$ TKO + opt1G4-mTagBFP2	This Paper	N/A
MS5-hDLL4	Montel-Hagen et al. 2019[32]	N/A

Continued		
Experimental Models: Cell Lines		
MS5-hDLL4-A*0201 (hDLL4-A02)	This paper	N/A
MS5-hDLL4-A*0201-hB2M (hDLL4-A02B)	This paper	N/A
MS5-hDLL4-A*0201-hB2M-ICAM (hDLL4-A02BI)	This paper	N/A
K562-CD80/83/137L-HLA-A*0201/B2M/NYESO$_{157-165}$ aAPC	Montel-Hagen et al. 2019[32]	N/A
K562-HLA-A*0201/B2M/ NYESO$_{157-165}$ aAPC	Montel-Hagen et al. 2019[32]	N/A
K562-HLA-A*0201/B2M/ MART1$_{26-35}$ aAPC	Montel-Hagen et al. 2019[32]	N/A
MS5-hDLL4-mB2mKO-A*0201-hB2M (hDLL4-mKO-A02B)	This paper	N/A
MS5-hDLL4-mB2mKO-A*0201-hB2M-ICAM (hDLL4-mKO-A02BI)	This paper	N/A
MS5-hDLL4-mB2mKO-A*0201-hB2M-VCAM (hDLL4-mKO-A02B-VCAM)	This paper	N/A
MS5-hDLL4-mB2mKO-A*0201-hB2M-ICAM-VCAM (hDLL4-mKO-A02BI-VCAM)	This paper	N/A
Experimental Models: Organisms		
Mouse: NSG: NOD.Cg-Prkdcscid Il2rgtm1Wjl/SzJ	The Jackson Laboratory	JAX: 005557
Software and Algorithms		
Flowjo	Tree Star Inc.	https://www.flowjo.com/solutions/flowjo
Benchling	Benchling	https://benchling.com
GraphPad Prism	GraphPad Software	https://www.graphpad.com/scientific-software/prism/
Cell Ranger v.6.0.2	10X Genomics	https://support.10xgenomics.com/single-cell-vdj/software/
Seurat v 4.1.0	Satija Lab	https://satijalab.org/seurat/
R	R	https://www.R-project.org/
Experimental Models: Organisms		
Mouse: NSG: NOD.Cg-Prkdcscid Il2rgtm1Wjl/SzJ	The Jackson Laboratory	JAX: 005557

REFERENCES

1. Shah, D. K. & Zúñiga-Pflücker, J. C. An overview of the intrathymic intricacies of T cell development. *Journal of immunology (Baltimore, Md. : 1950)* 192, 4017–4023 (2014).

2. Rothenberg, E. V., Ungerbäck, J. & Champhekar, A. Forging T-Lymphocyte Identity: Intersecting Networks of Transcriptional Control. *Advances in immunology* 129, 109–174 (2016).

3. Hao, Q.-L. *et al.* Human intrathymic lineage commitment is marked by differential CD7 expression: identification of CD7- lympho-myeloid thymic progenitors. *Blood* 111, 1318–1326 (2008).

4. Casero, D. *et al.* Long non-coding RNA profiling of human lymphoid progenitor cells reveals transcriptional divergence of B cell and T cell lineages. *Nat Immunol* 16, 1282–1291 (2015).

5. Spits, H. Development of alphabeta T cells in the human thymus. *Nat. Rev. Immunol.* 2, 760–772 (2002).

6. Han, J. & Zúñiga-Pflücker, J. C. A 2020 View of Thymus Stromal Cells in T Cell Development. *J Immunol* 206, 249–256 (2021).

7. Hozumi, K. *et al.* Delta-like 4 is indispensable in thymic environment specific for T cell development. *The Journal of experimental medicine* 205, 2507–2513 (2008).

8. Koch, U. *et al.* Delta-like 4 is the essential, nonredundant ligand for Notch1 during thymic T cell lineage commitment. *The Journal of experimental medicine* 205, 2515–2523 (2008).

9. Walle, I. V. de, Davids, K. & Taghon, T. Characterization and Isolation of Human T Cell Progenitors. *Methods Mol Biol* 1323, 221–237 (2016).

10. Schatz, D. G. & Ji, Y. Recombination centres and the orchestration of V(D)J recombination. *Nat. Rev. Immunol.* 11, 251–263 (2011).

11. Oettinger, M. A. *et al.* The recombination activating genes, RAG 1 and RAG 2, are on chromosome 11p in humans and chromosome 2p in mice. *Immunogenetics* 35, 97–101 (1992).

12. Shinkai, Y. *et al.* RAG-2-deficient mice lack mature lymphocytes owing to inability to initiate V(D)J rearrangement. *Cell* 68, 855–867 (1992).

13. Mombaerts, P. *et al.* RAG-1-deficient mice have no mature B and T lymphocytes. *Cell* 68, 869–877 (1992).

14. Brauer, P. M. *et al.* Modeling altered T-cell development with induced pluripotent stem cells from patients with RAG1-dependent immune deficiencies. *Blood* 128, 783–793 (2016).

15. Lee, Y. N. *et al.* Characterization of T and B cell repertoire diversity in patients with RAG deficiency. *Sci Immunol* 1, (2016).

16. Xu, Y., Davidson, L., Alt, F. W. & Baltimore, D. Function of the pre-T-cell receptor alpha chain in T-cell development and allelic exclusion at the T-cell receptor beta locus. *Proc National Acad Sci* 93, 2169–2173 (1996).

17. Biro, J. *et al.* Regulation of T cell receptor (TCR) β gene expression by CD3 complex signaling in immature thymocytes: Implications for TCRβ allelic exclusion. *Proc National Acad Sci* 96, 3882–3887 (1999).

18. Giannoni, F. *et al.* Allelic exclusion and peripheral reconstitution by TCR transgenic T cells arising from transduced human hematopoietic stem/progenitor cells. *Mol. Ther.* 21, 1044–1054 (2013).

19. Klein, L., Kyewski, B., Allen, P. M. & Hogquist, K. A. Positive and negative selection of the T cell repertoire: what thymocytes see (and don't see). *Nat. Rev. Immunol.* 14, 377–391 (2014).

20. Anderson, G. & Takahama, Y. Thymic epithelial cells: working class heroes for T cell development and repertoire selection. *Trends Immunol* 33, 256–263 (2012).

21. Stritesky, G. L., Jameson, S. C. & Hogquist, K. A. Selection of Self-Reactive T Cells in the Thymus. *Annu Rev Immunol* 30, 95–114 (2012).

22. Lambolez, F., Kronenberg, M. & Cheroutre, H. Thymic differentiation of TCRαβ+ CD8αα+ IELs. *Immunol Rev* 215, 178–188 (2007).

23. Plum, J., Smedt, M. D., Defresne, M., Leclercq, G. & Vandekerckhove, B. Human CD34+ fetal liver stem cells differentiate to T cells in a mouse thymic microenvironment. *Blood* 84, 1587–1593 (1994).

24. Seach, N., Hammett, M. & Chidgey, A. Epithelial Cell Culture Protocols, Second Edition. *Methods Mol Biology* 945, 251–272 (2012).

25. Chung, B. *et al.* Engineering the Human Thymic Microenvironment to Support Thymopoiesis In Vivo. *Stem Cells* 32, 2386–2396 (2014).

26. Schmitt, T. M. & Zúñiga-Pflücker, J. C. Induction of T Cell Development from Hematopoietic Progenitor Cells by Delta-like-1 In Vitro. *Immunity* 17, 749–756 (2002).

27. Motte-Mohs, R. N. L., Herer, E. & Zúñiga-Pflücker, J. C. Induction of T-cell development from human cord blood hematopoietic stem cells by Delta-like 1 in vitro. *Blood* 105, 1431–1439 (2005).

28. Mohtashami, M., Shah, D. K., Kianizad, K., Awong, G. & Zúñiga-Pflücker, J. C. Induction of T-cell development by Delta-like 4-expressing fibroblasts. *Int Immunol* 25, 601–611 (2013).

29. Snauwaert, S. *et al.* In vitro generation of mature, naive antigen-specific CD8+ T cells with a single T-cell receptor by agonist selection. *Leukemia* 28, 830–841 (2014).

30. Trotman-Grant, A. C. *et al.* DL4-µbeads induce T cell lineage differentiation from stem cells in a stromal cell-free system. *Nat Commun* 12, 5023 (2021).

31. Seet, C. S. *et al.* Generation of mature T cells from human hematopoietic stem and progenitor cells in artificial thymic organoids. *Nat. Methods* 14, 521–530 (2017).

32. Montel-Hagen, A. *et al.* Organoid-Induced Differentiation of Conventional T Cells from Human Pluripotent Stem Cells. *Cell stem cell* 24, 376-389.e8 (2019).

33. Evseenko, D. *et al.* Mapping the first stages of mesoderm commitment during differentiation of human embryonic stem cells. *Proceedings of the National Academy of Sciences of the United States of America* 107, 13742–13747 (2010).

34. Wang, Z. *et al.* 3D-organoid culture supports differentiation of human CAR+ iPSCs into highly functional CAR T cells. *Cell stem cell* 29, 515-527.e8 (2022).

35. Bosticardo, M. *et al.* Artificial thymic organoids represent a reliable tool to study T-cell differentiation in patients with severe T-cell lymphopenia. *Blood Adv* 4, 2611–2616 (2020).

36. Hinrichs, C. S. & Rosenberg, S. A. Exploiting the curative potential of adoptive T-cell therapy for cancer. *Immunol Rev* 257, 56–71 (2014).

37. June, C. H., Riddell, S. R. & Schumacher, T. N. Adoptive cellular therapy: a race to the finish line. *Sci Transl Med* 7, 280ps7 (2015).

38. Eyquem, J. *et al.* Targeting a CAR to the TRAC locus with CRISPR/Cas9 enhances tumour rejection. *Nature* 543, 113–117 (2017).

39. Poirot, L. *et al.* Multiplex Genome-Edited T-cell Manufacturing Platform for “Off-the-Shelf” Adoptive T-cell Immunotherapies. *Cancer Res.* 75, 3853–3864 (2015).

40. MacLeod, D. T. *et al.* Integration of a CD19 CAR into the TCR Alpha Chain Locus Streamlines Production of Allogeneic Gene-Edited CAR T Cells. *Mol. Ther.* 25, 949–961 (2017).

41. Fraietta, J. A. *et al.* Determinants of response and resistance to CD19 chimeric antigen receptor (CAR) T cell therapy of chronic lymphocytic leukemia. *Nature medicine* 24, 563–571 (2018).

42. Sommermeyer, D. *et al.* Chimeric antigen receptor-modified T cells derived from defined CD8+ and CD4+ subsets confer superior antitumor reactivity in vivo. *Leukemia* 30, 492–500 (2016).

43. Bendle, G. M. *et al.* Lethal graft-versus-host disease in mouse models of T cell receptor gene therapy. *Nat Med* 16, 565–570 (2010).

44. Themeli, M., Rivière, I. & Sadelain, M. New Cell Sources for T Cell Engineering and Adoptive Immunotherapy. *Cell Stem Cell* 16, 357–366 (2015).

45. Qasim, W. *et al.* Molecular remission of infant B-ALL after infusion of universal TALEN gene-edited CAR T cells. *Sci Transl Med* 9, (2017).

46. Palmer, D. B. The Effect of Age on Thymic Function. *Front Immunol* 4, 316 (2013).

47. Hinrichs, C. S. *et al.* Adoptively transferred effector cells derived from naïve rather than central memory CD8+ T cells mediate superior antitumor immunity. *Proc National Acad Sci* 106, 17469–17474 (2009).

48. Arcangeli, S. *et al.* CAR T-cell manufacturing from naive/stem memory T-lymphocytes enhances antitumor responses while curtailing cytokine release syndrome. *J Clin Invest* (2022) doi:10.1172/jci150807.

49. Thomson, J. A. *et al.* Embryonic stem cell lines derived from human blastocysts. *Science* 282, 1145–1147 (1998).

50. Crook, J. M. *et al.* The generation of six clinical-grade human embryonic stem cell lines. *Cell stem cell* 1, 490–494 (2007).

51. Robbins, P. F. *et al.* Single and dual amino acid substitutions in TCR CDRs can enhance antigen-specific T cell functions. *Journal of immunology (Baltimore, Md. : 1950)* 180, 6116–6131 (2008).

52. Gschweng, E. H. *et al.* HSV-sr39TK positron emission tomography and suicide gene elimination of human hematopoietic stem cells and their progeny in humanized mice. *Cancer Res.* 74, 5173–5183 (2014).

53. Young, C. S. *et al.* A Single CRISPR-Cas9 Deletion Strategy that Targets the Majority of DMD Patients Restores Dystrophin Function in hiPSC-Derived Muscle Cells. *Cell stem cell* 18, 533–540 (2016).

54. Doench, J. G. *et al.* Rational design of highly active sgRNAs for CRISPR-Cas9-mediated gene inactivation. *Nat. Biotechnol.* 32, 1262–1267 (2014).

55. Doench, J. G. *et al.* Optimized sgRNA design to maximize activity and minimize off-target effects of CRISPR-Cas9. *Nat. Biotechnol.* 34, 184–191 (2016).

56. Wang, B. *et al.* Generation of hypoimmunogenic T cells from genetically engineered allogeneic human induced pluripotent stem cells. *Nat Biomed Eng* 5, 429–440 (2021).

57. Minagawa, A. *et al.* Enhancing T Cell Receptor Stability in Rejuvenated iPSC-Derived T Cells Improves Their Use in Cancer Immunotherapy. *Cell stem cell* 23, 850-858.e4 (2018).

58. lJspeert, H. *et al.* Similar recombination-activating gene (RAG) mutations result in similar immunobiological effects but in different clinical phenotypes. *J Allergy Clin Immunol* 133, 1124-1133.e1 (2014).

59. Santagata, S. *et al.* N-terminal RAG1 frameshift mutations in Omenn's syndrome: Internal methionine usage leads to partial V(D)J recombination activity and reveals a fundamental role in vivo for the N-terminal domains. *Proc National Acad Sci* 97, 14572–14577 (2000).

60. Gschweng, E., Oliveira, S. D. & Kohn, D. B. Hematopoietic stem cells for cancer immunotherapy. *Immunol Rev* 257, 237–249 (2014).

61. Itoh, K. *et al.* Reproducible establishment of hemopoietic supportive stromal cell lines from murine bone marrow. *Experimental hematology* 17, 145–153 (1989).

62. Subach, O. M., Cranfill, P. J., Davidson, M. W. & Verkhusha, V. V. An enhanced monomeric blue fluorescent protein with the high chemical stability of the chromophore. *PloS one* 6, e28674 (2011).

63. Ran, F. A. *et al.* Genome engineering using the CRISPR-Cas9 system. *Nat Protoc* 8, 2281–2308 (2013).

64. Shalem, O. *et al.* Genome-scale CRISPR-Cas9 knockout screening in human cells. *Science* 343, 84–87 (2014).

65. Hsu, P. D. *et al.* DNA targeting specificity of RNA-guided Cas9 nucleases. *Nat. Biotechnol.* 31, 827–832 (2013).

66. Brinkman, E. K., Chen, T., Amendola, M. & Steensel, B. van. Easy quantitative assessment of genome editing by sequence trace decomposition. *Nucleic Acids Res* 42, e168 (2014).

67. Tsai, S. Q. *et al.* GUIDE-seq enables genome-wide profiling of off-target cleavage by CRISPR-Cas nucleases. *Nat. Biotechnol.* 33, 187–197 (2015).

68. Liang, X. *et al.* Rapid and highly efficient mammalian cell engineering via Cas9 protein transfection. *J. Biotechnol.* 208, 44–53 (2015).

69. Roth, T. L. *et al.* Reprogramming human T cell function and specificity with non-viral genome targeting. *Nature* 559, 405–409 (2018).

70. Chin, C. J. *et al.* Genetic Tagging During Human Mesoderm Differentiation Reveals Tripotent Lateral Plate Mesodermal Progenitors. *Stem Cells* 34, 1239–1250 (2016).

71. Mandal, P. K. *et al.* Efficient ablation of genes in human hematopoietic stem and effector cells using CRISPR/Cas9. *Cell stem cell* 15, 643–652 (2014).

72. Shultz, L. D. *et al.* Generation of functional human T-cell subsets with HLA-restricted immune responses in HLA class I expressing NOD/SCID/IL2r gamma(null) humanized mice. *Proceedings of the National Academy of Sciences of the United States of America* 107, 13022–13027 (2010).

73. O'Rourke, A. M., Shao, H. & Kaye, J. A role for p21ras/MAP kinase in TCR-mediated activation of LFA-1. *Journal of immunology (Baltimore, Md. : 1950)* 161, 5800–5803 (1998).

74. Evans, R., Lellouch, A. C., Svensson, L., McDowall, A. & Hogg, N. The integrin LFA-1 signals through ZAP-70 to regulate expression of high-affinity LFA-1 on T lymphocytes. *Blood* 117, 3331–3342 (2011).

75. Ma, V. P.-Y. *et al.* The magnitude of LFA-1/ICAM-1 forces fine-tune TCR-triggered T cell activation. *Sci Adv* 8, eabg4485 (2022).

76. Mitsuki, M., Matsumoto, N. & Yamamoto, K. A species-specific determinant on beta2-microglobulin required for Ly49A recognition of its MHC class I ligand. *Int Immunol* 16, 197–204 (2004).

77. Achour, A. *et al.* Structural basis of the differential stability and receptor specificity of H-2Db in complex with murine versus human beta2-microglobulin. *J Mol Biol* 356, 382–396 (2006).

78. Verma, N. K. & Kelleher, D. Not Just an Adhesion Molecule: LFA-1 Contact Tunes the T Lymphocyte Program. *Journal of immunology (Baltimore, Md. : 1950)* 199, 1213–1221 (2017).

79. Najima, Y. *et al.* Induction of WT1-specific human CD8+ T cells from human HSCs in HLA class I Tg NOD/SCID/IL2rgKO mice. *Blood* 127, 722–734 (2016).

80. Bethune, M. T. *et al.* Isolation and characterization of NY-ESO-1–specific T cell receptors restricted on various MHC molecules. *Proc National Acad Sci* 115, E10702–E10711 (2018).

81. Cohen, C. J., Zhao, Y., Zheng, Z., Rosenberg, S. A. & Morgan, R. A. Enhanced Antitumor Activity of Murine-Human Hybrid T-Cell Receptor (TCR) in Human Lymphocytes Is Associated with Improved Pairing and TCR/CD3 Stability. *Cancer Res* 66, 8878–8886 (2006).

82. Montel-Hagen, A. *et al.* In Vitro Recapitulation of Murine Thymopoiesis from Single Hematopoietic Stem Cells. *Cell Reports* 33, 108320 (2020).